Molecular Characterization of Polymer Networks

Scott P. O. Danielsen,[*,†,‡,¶] Haley K. Beech,[†,§] Shu Wang,[†,‖] Bassil M. El-Zaatari,[†,⊥] Xiaodi Wang,[†,⊥] Liel Sapir,[†,‡] Tetsu Ouchi,[†] Zi Wang,[†,‖] Patricia N. Johnson,[†,‖] Yixin Hu,[†,‖] David J. Lundberg,[§] Georgi Stoychev,[¶] Stephen L. Craig,[*,†,‖] Jeremiah A. Johnson,[*,†,#] Julia A. Kalow,[*,†,⊥] Bradley D. Olsen,[*,†,§] and Michael Rubinstein[*,†,‡,‖,@,¶,△]

†*NSF Center for the Chemistry of Molecularly Optimized Networks*
‡*Thomas Lord Department of Mechanical Engineering and Materials Science, Duke University, Durham, NC 27708, United States*
¶*Marsico Lung Institute, University of North Carolina, Chapel Hill, NC 27599, United States*
§*Department of Chemical Engineering, Massachusetts Institute of Technology, 77 Massachusetts Avenue, Cambridge, MA 02139, United States*
‖*Department of Chemistry, Duke University, Durham, NC 27708, United States*
⊥*Department of Chemistry, Northwestern University, Evanston, IL 60208, United States*
#*Department of Chemistry, Massachusetts Institute of Technology, 77 Massachusetts Avenue, Cambridge, MA 02139, United States*
@*Departments of Biomedical Engineering and Physics, Duke University, Durham, NC 27708, United States*
△*World Primer Institute for Chemical Reaction Design and Discovery (WPI-ICReDD), Hokkaido University, Kita 21 Nishi 10, Kita-ku, Sapporo, Hokkaido, 001-0021, Japan*

E-mail: scott.danielsen@duke.edu; stephen.craig@duke.edu; jaj2109@mit.edu; jkalow@northwestern.edu; bdolsen@mit.edu; michael.rubinstein@duke.edu

Abstract

Polymer networks are complex systems of molecular components. Whereas the properties of the individual components are typically well understood by most chemists, translating that chemical insight to polymer networks themselves is limited by the statistical and poorly defined nature of network structures. As a result, it is challenging, if not currently impossible, to extrapolate from the molecular behavior of components to the full range of performance and properties of the entire polymer network. Polymer networks therefore present an unrealized, important, and interdisciplinary opportunity to exert molecular-level, chemical control on material macroscopic properties. A barrier to sophisticated molecular approaches to polymer networks is that the techniques for characterizing the molecular structure of networks is often unfamiliar to chemists. Here, we present a critical overview of the current characterization techniques available to understand the relation between the molecular properties and the resulting performance and behavior of polymer networks, in the absence of added fillers. We highlight the methods available to characterize the chemistry and molecular-level properties of individual polymer strands and junctions, the gelation process by which strands form net-

works, the structure of the resulting network, and the dynamics and mechanics of the final material. The purpose is not to serve as a detailed manual for conducting these measurements, but rather to unify the underlying principles, point out remaining challenges, and provide a concise overview by which chemists can plan characterization strategies that suit their research objectives. Because polymer networks cannot often be sufficiently characterized with a single method, strategic combinations of multiple techniques are typically required for their molecular characterization.

Contents

1 Introduction

Through synthesis, chemists can now program remarkable properties and function into individual polymer molecules, including precise conformational behavior, unusual extensional profiles, and covalent chemical responses. The level of molecular control of individual macromolecules, however, has yet to be replicated at the level of polymer networks. The challenge in translating from single macromolecular to network behavior originates from the fact that the details of molecular design have been hidden by statistical chemistry and poorly defined structures, limiting the ability to bring chemical knowledge to bear on challenges in polymer network performance and properties. Thus, there currently exists no direct and quantitative method to extrapolate from the molecular behavior of the individual components of a polymer network to the full range of physical behaviors of that network. Polymer networks therefore present an unrealized, important, and interdisciplinary opportunity for chemists of different sub-fields to exert molecular-level, chemical control of on material macroscopic properties. If polymer networks could be treated as complex chemical systems, the full power of synthetic, physical, and theoretical chemistry might be rationally directed toward overarching challenges in de novo molecular network design.

As synthetic techniques provide increasing control over a greater range of molecular structure space, an overarching challenge to realizing this vision is that of characterization. Polymer networks are not amenable to the characterization techniques commonly applied to small molecules, and even the language necessary to describe statistical distributions of connectivity is unfamiliar to most chemists. These barriers limit the ability of chemists to connect the creativity possible in molecular structure and function to the resulting structure and function of polymer networks. In this review, we survey techniques available for extracting molecular-level details of polymer network structure. Some of these techniques are well established over decades of use but are still rarely employed by chemists; others have been developed only recently and offer more direct and precise measures of quantities and distributions that historically have been inferred indirectly.

The focus of the review is to survey the current characterization toolkit available for extracting molecular information relevant to polymer network behavior. A comprehensive review of every instance in which a given characterization technique has been used is neither possible nor useful. Instead, we emphasize the key considerations and limits of the various techniques and provide representative examples of their use. While we cannot walk through the detailed steps required to execute each technique, we highlight key technical considerations, and we encourage the reader to seek technical details for implementation in the primary literature we cite. Our goal is that the chemist can use this review to identify techniques that are suitable to a given molecular characterization question, and in so doing address major knowledge gaps in the field. By combining contemporary characterization tools with ongoing advances in polymer chemistry, the field is now poised to update existing theories of network behavior and uncover molecular strategies to control network properties that are presently obscured.

Here, we review the methods in characterizing polymer networks. The polymer networks can be neat materials, like thermosets or elastomers, or can be gels, swollen in mobile solvent. We will refer to macromolecules that are connected to network junctions as strands. The strands can be connected as bridges be-

tween different junctions, as dangling loops that connect different sites of the strand to the same junction, or as dangling ends that retain unreacted groups (Figure 1). The junctions connecting the polymer strands can be either permanent in the case of covalent bonds and trapped entanglements, or reversible in the case of supramolecular interactions, dynamic covalent associations, or transient entanglements. We will focus our attention on amorphous networks with flexible strands (persistence length smaller than the strand length between cross-links) and without fillers.

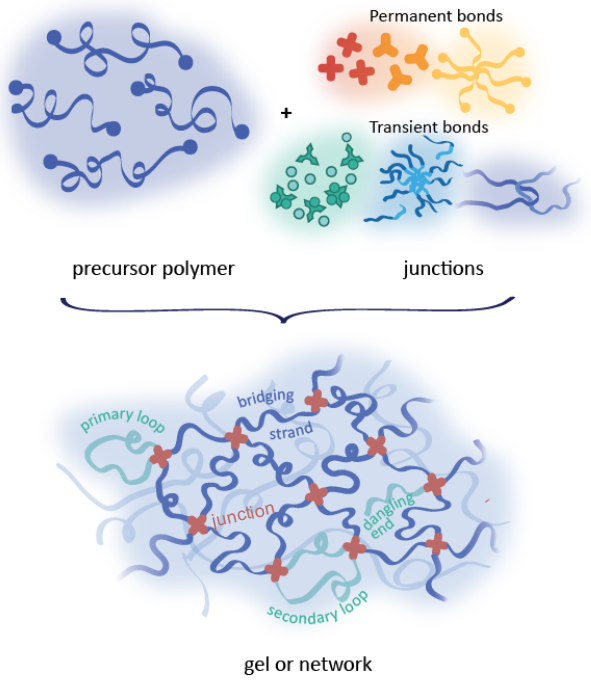

Figure 1: Structural motifs common to polymer networks: strands are connected to junctions by permanent or transient bonds as elastically effective bridging strands (including higher order loops) and defects such as dangling ends and primary loops, which are unable to support stress.

Typically, only partial information can be obtained from individual methods; a combination of several techniques is always necessary for complete characterization of polymer networks. First, the methods available to characterize the chemistry and molecular-level properties of strands and junctions are discussed in Section 2. These methods are largely similar to traditional characterization of polymers and so we focus on only the salient techniques for comparison and connection to the analysis of cross-linked materials. We then survey analysis of the gelation process, separation of the sol and gel components, and basic molecular characterization of the sol in Section 3. We outline the main methods for characterizing the structure of the network in Section 4, particularly focusing on classical approaches for the determination of mesh size and modern methods to tease out the fraction of dangling ends and other defects. In Section 5, we thoroughly explore the main characterization techniques for describing the mechanics and dynamics of the polymer networks, with particular emphasis on the rheology and molecular spectroscopy. We highlight in Section 6 the utility of computer simulations in explaining experimental data, testing theories, and providing predictions for network structure and properties. Finally, in Section 7, the current state of polymer network characterization is summarized, best practices are discussed, and a prognosis for the future is offered.

2 Polymer Strands

Polymer networks can be formed from a mixture of bi- and multi-functional monomers or by cross-linking precursor chains. These precursor strands, also known as pre-polymers, are polymer chains containing reactive side chains or end groups that can form macroscopic networks under appropriate conditions, by end-linking with a multi-functional junction or by random cross-linking (i.e., vulcanization). As the basic building block, thorough physical and chemical characterization of precursor strands is vital to predictably and reproducibly form polymer networks with desirable properties. Below we discuss characterization methods applicable to the molecular and macromolecular levels. Many of these techniques are applicable before and after cross-linking; comparison of the results from these techniques before and after network formation thus provides useful information regarding the cross-links.

2.1 Chemical Analysis

2.1.1 Nuclear Magnetic Resonance

Nuclear magnetic resonance (NMR) spectroscopy is a highly versatile and powerful technique that has expanded into nearly all subdisciplines of chemistry and materials science. Commonly, an NMR spectrum presents peaks at different chemical shifts corresponding to nuclei of different chemical environments, allowing structural analysis and compositional characterization. More sophisticated and multidimensional NMR techniques connect NMR parameters such as chemical shift, line width, couplings, and relaxation rates to the structure and dynamics of the polymer chains at the atomic level.[1]

Common one-dimensional (1D) NMR techniques (e.g., ^{1}H and ^{13}C) are often used to provide information on reaction conversion, functionalization, product purity, and monomer content. 1D NMR is particularly useful in elucidating the composition of copolymers, where recent advances of quantitative NMR measurements coupled to high-resolution mass spectrometry have enabled sequence-level characterization.[2]

2.1.2 Infrared/Raman Spectroscopy

Infrared spectroscopy (IR) exploits the absorption of light by molecules at frequencies that match their characteristic vibrational frequencies. Specifically, Fourier-transform infrared (FTIR) and Raman are two well-established spectroscopic techniques that detect activities related to the symmetry of the molecules. A change in the dipole moment of a bond provides IR signal while a change in polarizability causes it to be Raman active. The vibrational spectra of complex molecules, such as polymers, which consist of many atoms and bonds, are correspondingly complex. However, the absorption maxima for many chemical groups have already been tabulated and enable rapid determination of the presence or absence of specific functional groups, such as carbonyls, azides, and alcohols.[3,4] Since FTIR and Raman spectroscopies are complementary to each other, these techniques collect information on the vibrational states associated with different chemical bonds.[5] Thus, IR spectroscopy to be used as a quick and low-cost (compared to NMR) method to confirm the chemical structure of a polymer by confirming the presence of the expected functional groups.[6]

Common uses of FTIR and Raman spectroscopy in polymer science center around functional group determination via comparison between peaks of interest with databases. The area under a characteristic region can be translated to a molar quantity using a Beer's Law type analysis.[7] This information can then be used to determine the degree of polymerization, degree of functionalization, as well as the presence of contaminants and the morphology of polymer crystals.[8–11] In addition to the conventional bulk sampling techniques, IR has been coupled with atomic force microscopy (AFM). The combination allows high spatial resolution on a nanoscale that can hardly be achieved previously due to the optical diffraction limit on conventional IR.[12] Other molecular spectroscopies such as ultraviolet/visible absorption (UV-Vis) or fluorescence spectroscopies can also be used to identify molecular subgroups, and are particularly useful for quantifying the concentration and states of chromophores such as those necessary for optical-based network characterization methods (Sections 4.4, 5.4.3, and 5.9).

2.2 Physical Properties Analysis

There are a variety of experimental methods available for determining different average molecular-weights (e.g., number-average $\overline{M}_{\mathrm{n}}$ and weight-average $\overline{M}_{\mathrm{w}}$), molecular-weight distributions, as well as the interactions between precursor polymers and a given solvent (e.g., second virial coefficient A_2), which will be discussed later in this section. These methods typically utilize dilute solutions, and often require measurements at several concentrations to extrapolate to the limit of zero concentration. Different methods are applicable to different ranges of polymer molecular weights, as summarized in Table 1.

Table 1: Summary of characterization techniques used to determine different types of polymer molecular weights.[13–15]

Method	Absolute	Relative	$\overline{M}_\mathrm{n}$	$\overline{M}_\mathrm{w}$	A_2	Range ($\mathrm{g\,mol^{-1}}$)
NMR (end-group analysis)	×		×			$\overline{M}_\mathrm{n} < 10000$
Mass Spectrometry (MALDI-TOF-MS)	×		×	×		$M < 10000$
Membrane Osmometry (MO)	×		×		×	$20000 < \overline{M}_\mathrm{n}$
Vapor Pressure Osmometry (VPO)	×		×		×	$\overline{M}_\mathrm{n} < 10000$
Intrinsic Viscosity (IV)		×				$M < 10^6$
Light Scattering (LS)	×			×	×	$10^4 < \overline{M}_\mathrm{w} < 10^6$
SEC with dRI detector		×	×	×		$10^3 < M < 10^7$
SEC with dRI and LS detectors	×			×		$10^4 < M < 10^7$
SEC with dRI and IV detectors		×	×	×		$10^3 < M < 10^6$

2.2.1 Nuclear Magnetic Resonance

Beyond quantifying the chemical composition (Section 2.1.1), for polymers with distinct chain-end functionalities, NMR end-group analysis provides the number-average molecular weight ($\overline{M}_\mathrm{n}$) of the polymer, by molar ratio of the integrated peaks from the chain-end moieties and the main-chain units.[16] However, the sensitivity of modern NMR machines is typically only sufficient to determine $\overline{M}_\mathrm{n}$ of relatively short polymers with degree of polymerization $N < 100$.[1] Further, other properties of the polymer are also accessible by advanced and multi-dimensional NMR techniques, such as 2D and 3D NMR.[1,17]

Two-dimensional (2D) NMR techniques, which provide correlation between two parameters by plotting in the space over two frequency axes, have become increasingly popular in polymer characterization.[18,19] Through-bond correlation methods, both homonuclear (e.g., correlation spectroscopy (COSY)) and heteronuclear (e.g., heteronuclear single-quantum correlation spectroscopy (HSQC) and heteronuclear multiple-bond correlation spectroscopy (HMBC)) permit characterization of the bonded structure and are useful for polymers with complex architectures. Through-space correlation methods (e.g., nuclear Overhauser effect spectroscopy (NOESY)) are useful in identifying stereochemistry and describing chain configurations. One advanced NMR method is particularly useful in polymer characterization: diffusion ordered spectroscopy (DOSY) enables the determination of size and size distribution of polymers difficult to characterize via other methods by measuring their distribution of diffusion coefficients, but only provides an estimated average molecular weight upon calibration.[19,20] NMR experiments can be performed in solution or solid-state, depending on sample solubility and information of interest, permitting complete characterization of the precursor strands prior to network formation.[21–24]

2.2.2 Mass Spectrometry

Mass spectrometry (MS) measures the mass-to-charge ratio (m/z) of a molecule by passing the sample through the following processes: ionization, separation, and detection.[25,26] Gas/liquid chromatography can be installed prior to the spectrometer to provide physical separation of molecules before their masses are measured. Owing to the discovery of soft-ionization protocols such as electrospray ionization (ESI) and matrix-assisted laser desorption/ionization (MALDI), MS has gained more popularity among the polymer chemistry community.[27]

During MALDI, the polymer sample and matrix solutions are mixed and dried. The solid crystals are ionized with a laser beam, causing the polymer strands desorb into the gas phase.[28,29] The sample is then passed through a time-of-flight analyzer where ions of different m/z are dispersed while they fly through

the compartment, and eventually detected at the detector. Despite its ability to produce intact molecular ions of polymers well above 10^4 g mol^{-1}, MALDI demonstrates best performance on polymers with low dispersity as higher-mass species could be underrepresented in the analysis.[28,29] Frequently, matrix selection plays an important role in the success of MALDI characterization; strategies on sample preparation can be found in the literature.[30]

One of the most common properties obtained from a MALDI experiment is the average molecular weight and is commonly compared with results obtained from classical methods such as SEC.[31] A MALDI spectrum, however, further provides a distribution of molecular weights from which $\overline{M}_\mathrm{n}$, $\overline{M}_\mathrm{w}$, and $Đ$ can be directly calculated provided that molecular ions ionize similarly across the distribution.[25] However, because higher-mass species are potentially underrepresented in the spectrum, MALDI can return biased distributions and shifted averages for polydisperse, high molar-mass samples.

In addition to providing the molecular-mass distribution, advancements such as deconvolution mass spectrometry enable finer separation. In this technique, a low molar-mass spectrometer is used to measure and deconvolute a high m/z spectrum by coupling two mass spectrometers such that analyte ions separated by m/z are then fragmented and detected again.[32] Detailed structural information can be extracted by comparing parent ions and cleaved end-groups such as shown in Figure 2 for poly(methylacrylates).[33]

2.2.3 Osmometry

Osmotic pressure is a thermodynamic colligative property (that is, sensitive to the number of molecules present) that measures the free-energy difference between a polymer solution and a pure solvent. While osmometry determines the number-average molecular weight ($\overline{M}_\mathrm{n}$) of the material, other information like molecular distribution cannot be evaluated, which, with the advent of methods such as size-exclusion chromatography, has resulted in a decrease in the use of osmometry in polymer analysis.[34,35]

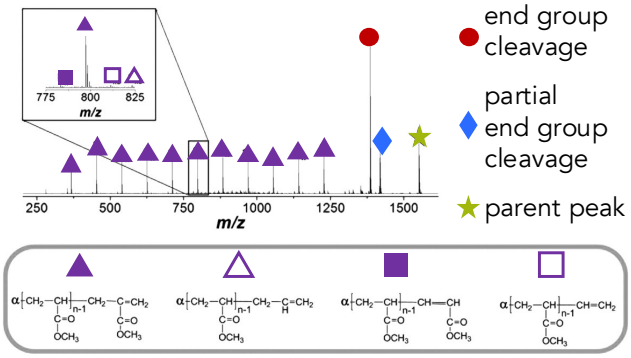

Figure 2: Fragmentation behavior of poly(methylacrylates) in the lower molar-mass range: assigned ESI-TOF spectrum (left), comparison plot of multiple polymer conditions (right), and proposed main fragment series (bottom). Figure reproduced with permission from Ref. 33. Copyright © 2013 Wiley Periodicals, Inc.

There are two main types of osmometry techniques: membrane osmometry (MO) and vapor pressure osmometry (VPO).[36] In MO, a semi-permeable membrane separates pure solvent from a polymer solution in the same solvent. The pressure difference between the solvent and polymer solution is called the osmotic pressure Π:

$$\frac{\Pi}{RT} = \frac{c}{\overline{M}_\mathrm{n}} + A_{2,\mathrm{w}}c^2 + \cdots \qquad (2.1)$$

where c is the concentration, $R = N_\mathrm{A}k_\mathrm{B} = 8.314\ \mathrm{J\,mol^{-1}\,K^{-1}}$ is the universal gas constant, $N_\mathrm{A} = 6.022 \times 10^{23}\ \mathrm{mol^{-1}}$ is Avogadro's number, $k_\mathrm{B} = 1.38 \times 10^{-23}\ \mathrm{J\,K^{-1}}$ is Boltzmann's constant, and T is the absolute temperature, permitting calculation of the polymer's number-average molecular weight $\overline{M}_\mathrm{n}$ and the weight-average second virial coefficient $A_{2,\mathrm{w}}$, a measure of the interaction between the dissolved polymers in solution.[15] The osmotic pressure at sufficiently dilute concentrations is then directly correlated to molecular weight according to the van't Hoff law:[36]

$$\lim_{c\to 0}\frac{\Pi}{c} = \frac{N_\mathrm{A}k_\mathrm{B}T}{\overline{M}_\mathrm{n}} = \frac{RT}{\overline{M}_\mathrm{n}}. \qquad (2.2)$$

VPO, on the other hand, is dependent on the equilibrium thermodynamics of vapor pressure, by measuring the difference in temperature (ΔT) between the two thermistor beads (which in practice is measured as a resistance difference ΔR).[35,37,38] Similar to MO, VPO directly correlates to the number-average molecular weight; unlike MO, however, VPO gives no information about absolute yield. The main advantage of VPO lies in its accuracy in determining the $\overline{M}_\mathrm{n}$ of lower molecular-weight polymers ($< 10^4$ g mol^{-1}).[36]

2.2.4 Viscometry

Viscometry is another classic technique that has been utilized in polymer science and characterization. It takes advantage of a change in the viscosity of a dilute polymer solution η in comparison to a pure solvent η_s. In its simplest form, with Ubbelohde viscometers, successive measurements of the time that it takes for this dilute solution to pass between two different viscometer marks are compared to that of the pure solvent.[15,36,39] These measurements give information about the intrinsic ability of a certain polymer to increase the viscosity of a solution, which enables the calculation of its intrinsic viscosity:

$$[\eta] = \lim_{c \to 0} \frac{\eta/\eta_s - 1}{c} \tag{2.3}$$

where c is the polymer concentration. The Flory–Fox equation relates intrinsic viscosity to the hydrodynamic size R and viscosity-average molecular weight, $\overline{M}_\mathrm{v}$, of the suspended polymer,

$$[\eta] = \Phi \frac{R^3}{\overline{M}_\mathrm{v}} \tag{2.4}$$

where $\Phi = 0.425 N_\mathrm{A} = 2.5 \times 10^{23}\,\mathrm{mol}^{-1}$ is a universal constant, in conjunction with the Mark–Houwink–Sakurada equation,

$$[\eta] = K \overline{M}_\mathrm{v}^a \tag{2.5}$$

where K and a are Mark–Houwink parameters, which are tabulated for nearly all common linear polymer–solvent combinations.[15] Typically, the $\overline{M}_\mathrm{v}$ value lies between $\overline{M}_\mathrm{n}$ and $\overline{M}_\mathrm{w}$.[36]

Many other viscometric measurement geometries exist in addition to the Ubbelohde viscometer mentioned previously. Most common in polymer science are falling ball (or rising bubble) viscometers where the viscosity is proportional to the rate at which a ball falls (or a bubble rises) through the fluid. Rotational viscometers, which obtain viscosity from the torque needed to shear the fluid between rotating boundaries, are also common. The main advantage of viscometry is its simplicity, speed, and superior precision over a wide range of molecular weights. In order to increase the accuracy of molecular weight detection in polymer precursors, size-exclusion chromatography (below) can be combined with online viscosity detection.[40–42]

2.2.5 Size-Exclusion Chromatography

Size-exclusion chromatography (SEC), including gel-permeation chromatography (GPC), is a commonly utilized characterization technique to measure polymer molecular-weight distributions (including number-average molecular weight $\overline{M}_\mathrm{n}$, weight-averaged molecular weight $\overline{M}_\mathrm{w}$, and dispersity $Đ$).[36,43] During this process, a dilute polymer solution is injected into a solvent stream and flows through a separation column packed with porous beads, resulting in an exit stream fractionated according to the pervaded volume of the material, $[\eta]M$, where $[\eta]$ is the intrinsic viscosity and M is the molar mass. Detectors, most commonly differential refractometry (dRI) and ultraviolet (UV) absorption, log the separation with elution time, differentiating between different polymeric components and providing the molecular-weight distribution of the polymer when calibrated to known polymer standards such as polystyrene.

One approach to overcome the limitation of calibration to a known standard is to combine SEC with viscometry (Section 2.2.4), as the absolute molecular weight of the polymer can be elucidated from its hydrodynamic size (obtained from SEC) by knowing its intrinsic viscosity, according to the Flory–Fox equation.[44] This relationship is the basis of the so-called universal SEC calibration. In a typical calibration process, the intrinsic viscos-

ity is replaced by the Mark–Houwink relationship, $[\eta] = K_1 M_1^{a_1} = K_2 M_2^{a_2}$. Knowing the Mark–Houwink relations for two different polymer–solvent pairs, the molecular weight of one polymer eluting at a particular volume can be calculated in terms of the other polymer, provided its elution-volume–molecular-weight relation is known.[45] The intrinsic viscosity can be measured either separately, for example, by capillary or rotary viscometry; or the SEC systems can be equipped with an online differential viscometer.

Incorporating an in-line light-scattering detector (SEC-LS) can be useful for novel systems (e.g., biopolymers and proteins) in which reference standards are unavailable and Mark–Houwink parameters are unknown.[46,47] To complement the aforementioned techniques, researchers have recently coupled SEC with Nuclear Magnetic Resonance Spectroscopy (NMR)[48–50] and Mass Spectrometry (MS)[51] in an effort to provide additional structural resolution and selectivity. Characterizing polymer precursors and strands prior to network formation using SEC can be extremely useful in planning the synthetic strategy of subsequent network formation[52] and accurate depiction of strand mass in subsequent gel characterization.

However, it should be noted that precise characterization of structural properties, composition, and purity of network strands, particularly of complex architectures, can be challenging and the results need to be analyzed with caution.[53] Finally, the determination of molecular weight distributions by SEC is not a suitable approach for many reversible network systems. Specifically, in supramolecular polymers, significant tailing in the distribution is normally observed due to the reversible nature of the chemical or physical bonds.[54] However, SEC also offers a significant opportunity to better understand association/dissociation kinetics in dynamic networks, by measuring the mass distribution as a function of temperature or another stimulus.[55–57]

2.2.6 Light Scattering

In polymer solutions, light scattering occurs due to the difference in refractive indices between the polymer n and the solvent n_s. There are two major modes of light scattering experiments—static (SLS) and dynamic (DLS) light scattering. The technique is dependent on the relationship between the intensity of incident light of wavelength λ that is scattered by a molecule (in this case the polymer chains) and the molecular weight and size of these molecules:[36,58]

$$\frac{Kc}{R_\theta} \simeq \frac{1}{\overline{M}_\mathrm{w}} \left(1 + \frac{R_\mathrm{g}^2 q^2}{3} + \cdots\right) (1 + A_{2,z} c + \cdots) \tag{2.6}$$

where $K = 4\pi^2 n_s^2 (dn/dc)^2/(N_\mathrm{A}\lambda^4)$ is an optical constant, $\mathrm{d}n/\mathrm{d}c$ is the refractive-index increment, and R_θ is the Rayleigh ratio. Structural information regarding the size and shape of the chains can be obtained by Guinier ($\ln R_\theta$ vs. q^2) or Kratky ($q^2 R_\theta$ vs. q) analyses with light intensity data measured at a single (dilute) concentration as a function of angle θ (or scattering vector $q = 4\pi n_s \sin(\theta/2)/\lambda$). Static light-scattering data from a series of angles and concentrations allows calculation of the weight-average molecular weight $\overline{M}_\mathrm{w}$, z-average radius of gyration R_g, and z-average of the second virial coefficient $A_{2,z}$. A corresponding Zimm plot analysis and a schematic of the technique is shown in Figure 3. Light scattering is accurate for determination of the molecular weight in a range of $\sim 10^4 - 10^6$ g mol^{-1}.[36]

In dynamic light scattering (DLS, discussed more in depth in Section 5.5.1), the change in the instantaneous scattering intensity on a time scale of the molecular motion is recorded. The scattering intensity fluctuates due to local fluctuations in concentration caused by the thermal motion (diffusion) of the polymer chains. By analyzing the time-resolved scattering intensity the diffusion coefficient D of the macromolecules can be calculated. The hydrodynamic size of the polymer can be estimated from the diffusion coefficient through

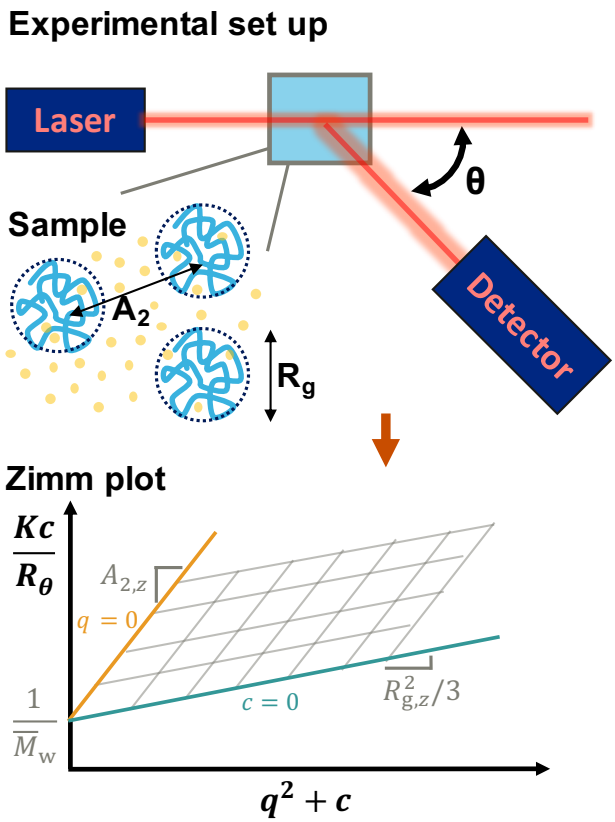

Figure 3: Schematic of a typical light-scattering experiment as a function of angle θ (top) and Zimm analysis (bottom) for polymers of weight-average molecular weight $\overline{M}_{\mathrm{w}}$, z-average radius of gyration R_{g}, and interaction between pairs of polymer molecules in a given solvent characterized by second virial coefficient A_2.

the Stokes–Einstein equation:

$$R_{\mathrm{h}} = \frac{k_{\mathrm{B}}T}{6\pi\eta_s D} \tag{2.7}$$

where $k_{\mathrm{B}}T$ is the thermal energy and η_s is the viscosity of the solvent. Both SLS and DLS detectors can be integrated with a SEC system, completely freeing it from the necessity of calibration.[59]

2.2.7 Thermogravimetric Analysis

Thermogravimetric analysis (TGA) is a thermal analysis technique that measures mass changes of the material in response to a change in temperature. TGA is often carried out in a well-controlled atmosphere such as a vacuum or an inert gas filled environment to control the nature of the thermal decomposition by preventing oxidation. The measurements can be presented in plots that are either temperature-dependent or time-dependent where changes in mass can usually be attributed to material volatility or degradation.[60] Assessing the thermal stability of polymers is the predominant application of TGA. These data are especially valuable for polymer strands before or after formation of the network as it provides a temperature range in which the material can ultimately operate.[61] For example, a typical TGA curve is shown in Figure 4 and is used to confirm thermal stability of a solid polymer electrolyte at the operating conditions of a lithium ion battery.[62] Finally, TGA coupled to a mass spectrometer, can be useful for monitoring cross-linking that occurs by thermolysis with the loss of small molecules.[63]

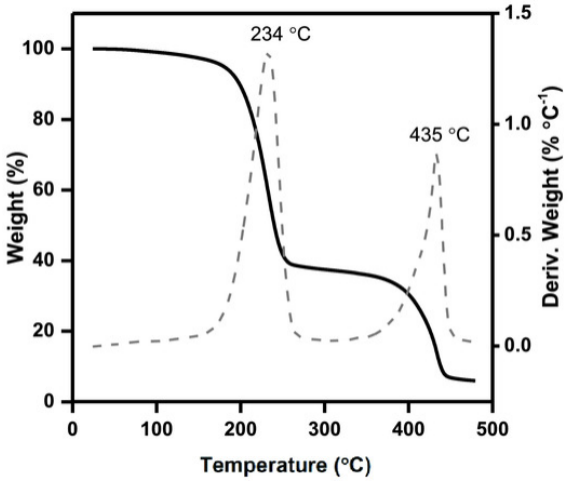

Figure 4: TGA curve of cross-linked poly(tetrahydrofuran) with LiTFSI for use as a solid polymer electrolyte indicating thermal stability. The decomposition temperatures at low and high temperatures correspond to polymer and salt degradation, respectively. Decomposition temperatures were higher than the corresponding non-cross-linked polymers. Figure reproduced with permission from Ref. 62. Copyright © 2018 Wiley-VCH Verlag GmbH & Co. KGaA, Weinheim.

2.2.8 Differential Scanning Calorimetry

Differential Scanning Calorimetry (DSC) is an analytical technique that is effective at de-

termining physical and chemical properties of polymers undergoing glass transitions and thermodynamic phase transformations.[14,36,64] DSC works by monitoring temperature differences between two samples, the polymer sample and a reference. The rate of change in the temperature will differ between the two samples based on compositional and physical phase changes, yielding a difference in heat flow as a function of temperature that correlates to the specific heat, C_p, of the material.[65] Thus, DSC is routinely used to determine glass-transition temperatures of polymers and to evaluate melting and crystallization enthalpies. DSC has been furthermore used to study monomer[66] reactivity and precursor polymerization kinetics.[67]

2.2.9 Single-Molecule Force Spectroscopy

Single-Molecule Force Spectroscopy (SMFS) enables quantitative investigation into the intra-molecular interactions of macromolecules, including the mechanics of proteins and other biopolymers,[68–70] the elastic properties and conformational changes of single polymer chains,[71–73] and mechanochemical structure–activity relationships.[74,75] Recently, SMFS has been used to characterize the mechanics of macromolecules from forces as low as a few pN and as high as several nN, and with a dynamic range of ≥ 1 µs.[76–78] Molecular properties and behaviors that have been quantified using SMFS include the force–extension relationship of a random-coiled polymer,[72,79,80] the chair-to-boat conformational transition of polysaccharides corresponding to a plateau in the force–extension curves,[71,72,81] and correlation of mechanochemical reactions with molecular structure of synthetic polymers, for which model fitting unveils reaction pathways.[75,82,83]

A popular manifestation of SMFS is based on an atomic force microscope (AFM) setup (Figure 5). Polymer chains are mounted on a solid substrate, which is moved upwards until the polymer sample is brought into contact with the tip, allowing polymers to bridge the cantilever tip and the substrate through physical interactions or covalent bonding. After equilibration, the piezoelectric stage is moved downward to stretch the polymer. The deflection of the laser reflection from the cantilever is recorded with the stage translation as the force–extension relationship. Low-force regimes (usually < 200 pN) are dominated by a reduction in the chain conformational degrees of freedom, and this is often referred to as the "entropic" regime. Extensions at higher forces come with increasing contributions from so-called "enthalpic" deformations, including the extension of bond lengths and bond angles, that eventually dominate the extensional behavior.[84]

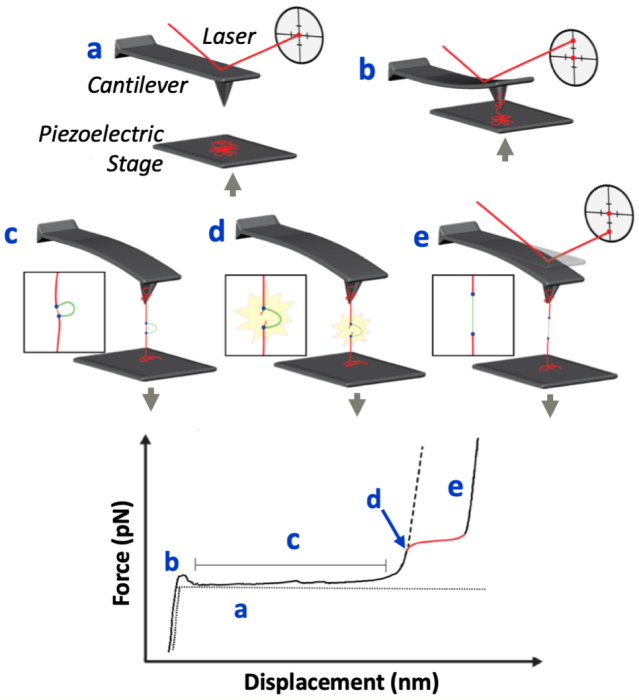

Figure 5: Schematics of AFM-based SMFS setup and a single-molecule experiment of a synthetic polymer with stored length released. Coiled polymer chains (red) are absorbed onto a solid piezoelectric stage moving vertically. The reflected laser beam is well aligned between the cantilever tip and the center of photodiode in (a). In the force–displacement curve, the dotted line represents the process from (a) to (b) as the piezoelectric stage approaches the cantilever tip. The solid line represents the process from (b) to (e) as the piezoelectric stage retracts away from the tip. Specifically, the red plateau represents the scissions of relatively weak bonds and the releases of stored length.

While AFM-based SMFS provides high-

resolution imaging at high-force regimes ($10 - 10^4$) pN, optical ($10^{-1} - 10^2$) pN and magnetic ($10^{-3} - 10^2$) pN tweezers-based SMFS show advantages for low-force-range measurements.[85] Created by focusing a laser to a diffraction-limited spot, optical tweezers are ideal for the 3D manipulation of targeted molecules due to its low-noise and low-drift dumbbell geometry.[70,86,87] Manipulating magnetic particles ranging 0.5−5 µm by an external magnetic field, magnetic tweezers combine force-clamp properties with the ability to impose rotation.[88,89]

A particularly useful strategy to engineer molecular responses into polymer extensional behavior is to incorporate mechanophores, chemical moieties that undergo force-coupled covalent transformations,[90,91] into the polymer strands. For example, as shown schematically in Figure 5, the scission of relatively weak bonds incorporated into the backbone occurs at low to moderate force extension (typically 400 pN 4000 nN), resulting in the release of the stored-length and enhanced single-chain toughness. SMFS enables the quantification of such mechanochemistry on a single-chain level.[92] The mechanochemical reaction rate as a function of force can be obtained from a "constant-velocity" experiment (described above and in Figure 5), in which the polymer chain is stretched at a constant velocity (usually several hundreds of $\mathrm{nm\,s^{-1}}$), but also from the "force clamp" methodology, in which the polymer is kept under a constant force. "Force clamp" experiments yield kinetic rate data from the analysis of the polymer elongation as a function of time and have been used to study polyproteins and synthetic polymers with multi-mechanophores.[93–95]

3 Gelation

Below the gel point, all species are soluble (in the appropriate solvent) allowing the standard dilute solution characterization methods to be utilized. Above the gel point, there is an insoluble gel fraction and a soluble sol fraction. Characterization of the sol fraction both below and above the gel point is important in understanding the gelation process and the properties of the formed gels. The sol fraction typically consists of randomly branched polymers of various sizes and non-cross-linked precursor chains not connected to the gel, together with solvent and any other low-molecular weight reagents, catalysts, or byproducts that might be present in the reaction mixture. Of particular interest are the chemical composition of the polymer species in the sol fraction, as well as their molecular characteristics, such as molecular weight and molecular weight distribution, chain size, branching, etc.[45,96]

3.1 Sol Extraction and Characterization

When immersed in an excess of the appropriate solvent, the gel fraction will swell, and the sol fraction will slowly diffuse or flow out of the swollen gel into the excess solvent. A major experimental concern in any study of polymers beyond the gel point is the question of perfect separation of this sol from the gel. Soxhlet extraction, shown schematically in Figure 6, is a convenient method for complete separation of the sol and gel fractions. Solvent is boiled in the bottom flask and condenses at the top of the apparatus, dripping down on to the gel in a paper or glass thimble. The solvent carrying the sol fraction siphons back to the bottom flask, where only solvent boils. Eventually the Soxhlet extractor has all of the sol fraction in the boiling solvent and all of the gel fraction in the thimble. The swollen gel can then be dried under vacuum and weighed to determine the gel fraction, defined as the fraction of all monomers belonging to the gel. Every monomer must be either part of the sol or part of the gel, so the sum of the sol and gel fractions is unity:

$$P_{\mathrm{gel}} + P_{\mathrm{sol}} = 1 \tag{3.1}$$

The properties of the gel and sol fractions can then be characterized separately. The sol fraction can be characterized with many of the same solution techniques used below the gel point. Molecular spectroscopies, particularly Nuclear Magnetic Resonance (NMR, Section 2.1.1) and

Infrared (IR, Section 2.1.2) spectroscopies, can be applied in the same manner as analyzing the precursor strands to determine the chemical composition of the sample. Discussion of the characterization of the gel point follows below, while much of the remainder of this review will focus on characterization of the gel phase.

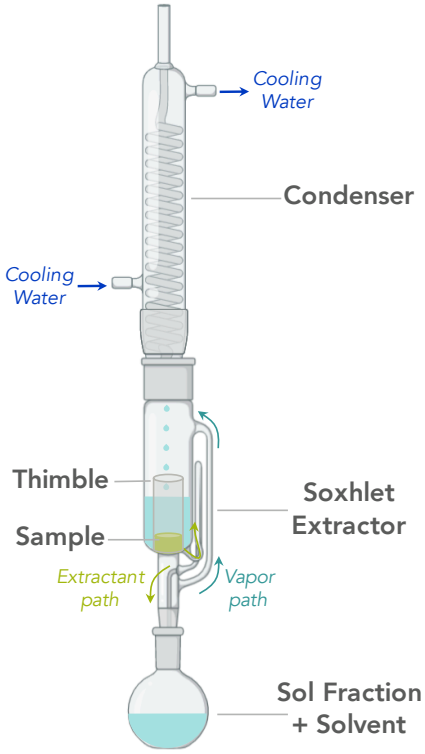

Figure 6: Schematic of a Soxhlet extraction apparatus used to separate the sol from the gel.

3.2 Gel Point Determination

Owing to the very broad molar mass distributions associated with branching as the gel point is approached, one primary characterization tool is size-exclusion chromatography (Section 2.2.5). Low-angle light-scattering detectors enhance the capability to determine the molecular-weight distribution of the sol. In the sol there is a very small amount of the largest species, but they dominate the light scattering. The light-scattering intensity corresponds to the product $c_i M_i$, which corresponds to a special self-similar distribution of molecular weights of all branched or cross-linked species (Figure 7a) with fraction of N-mers $P(N) \sim N^{-\tau}$ up to the characteristic degree of polymerization N^*. The critical exponent τ (also called the Fisher exponent) is between 2 and 3 assuring that number-average degree of polymerization ($\overline{M}_\mathrm{n}$) is finite at the gel point, while the weight-average degree of polymerization ($\overline{M}_\mathrm{w}$) and dispersity index $Đ = \overline{M}_\mathrm{w}/\overline{M}_\mathrm{n}$ diverges. The z-average degree of polymerization $\overline{M}_\mathrm{z}$ is proportional to N^* and diverges faster than $\overline{M}_\mathrm{w}$. The Fisher exponent $\tau = 2.5$ in the mean-field theory (Flory–Stockmayer) and is close to 2.2 in 3D critical percolation. Most experimental situations are in the cross-over between mean-field and critical percolation limits.[45,97,98] A universal molar-mass distribution plot, such as Figure 7a, can then be constructed from the concentration, intrinsic viscosity, and weight-average molar mass using appropriate detectors.

The extent of reaction p can, in principle, be measured by molecular spectroscopy methods such as FTIR and NMR (Sections 2.1.1 and 2.1.2). These molecular spectroscopies further allow calculation of the distribution of reacted cross-linkers (i.e., mono-, bi-, tri-, tetra-reacted) and end-group analysis. However, even with small relative error, the relative extent of reaction (i.e., distance from the gel point p_c: $\epsilon = (p - p_\mathrm{c})/p_\mathrm{c}$) goes to zero at the gel point and the error diverges. While this poses a problem for evaluation of the critical exponents (e.g., Fisher exponent τ), it typically is sufficient to measure the extent of reaction and empirically find the gel point over a relatively narrow window. Figure 7b shows the determination of the gel point by plotting the measured weight-average molecular weight from SEC against the extent of reaction measured by NMR for both solutions before the gel point and the sol fraction after the gel point. The estimated window of the gel point is shaded in grey, highlighting difficulties in accurately measuring the gel point. Since the weight-average molecular weight ($\overline{M}_\mathrm{w}$) diverges rapidly at the gel point, it is easy to find the approximate gel point in this fashion, although due to the large inherent error in measuring the extent of reaction, it is often more accurate to plot the size R or weight-average molecular weight as a function of N^*. As such, the gel point is bet-

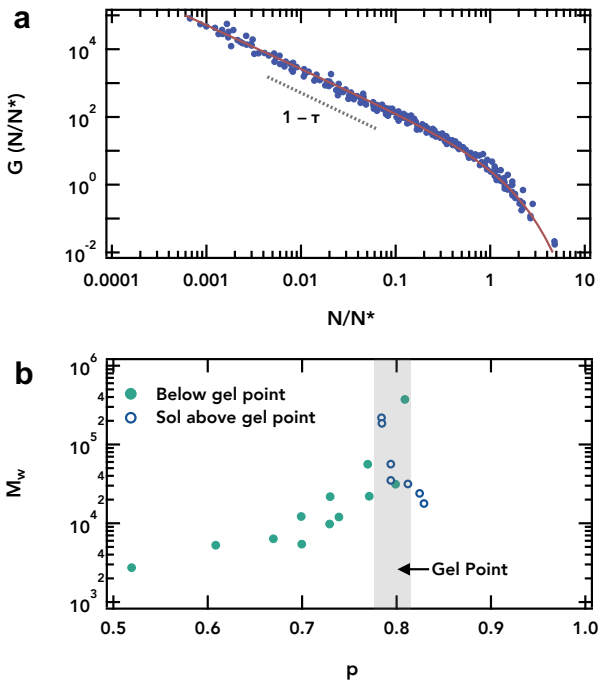

Figure 7: (a) Universal molar-mass distribution G of branched polyesters below the gel point as a function of size N relative to the characteristic size N^*. Figure adapted with permission from Ref. 96. Copyright © 1989 American Chemical Society. (b) Weight-average molecular weight ($\overline{M}_w$ as a function of extent of reaction p determined by NMR for polyesters below the gel point and in the sol fraction above the gel point. Figure adapted with permission from Ref. 45. Copyright © 1992 American Chemical Society.

ter determined by rheology, as will be discussed below.

Although crude, many chemists rely on the oft-used "inversion test" where a gel is identified as a sample that supports its own weight and does not flow when the vial is inverted. It is emblematic, however, of the facts that rheology (Section 5.1) is the most common manner to identify the gel point and that in many situations, most chemists care that their gel is well formed, so that they can continue to further applications and testing but are unconcerned with the exact gel point. If the reader is interested in questions such as how molecular structure influences properties in the vicinity of the gel point, then absolute characterization of the gel point or extent of network formation is likely necessary. It is also useful to know if the materials of interest are near the gel point, as very small differences in reactivity can cause small changes in the extent of reaction and thus large changes in macroscopic properties. In this situation, precise characterization of the relative extent of reaction is also necessary to appropriately compare data. In many cases, however, polymer chemists are primarily interested in whether a majority, percolating network is formed and how much material is in the network, before continuing with measurements on the isolated gel. Measurements of the gel point from oscillatory rheology (Section 5.1.4) and dynamic light scattering (Section 5.5.1) will be discussed more in depth later in this review; we will refer the interested reader to the references of this section and proceed to discuss characterization of the network structure, dynamics, and mechanical properties.

4 Network Structure

The properties of polymer networks are largely dictated by the underlying chemical and topological structure of junctions and strands. Whereas the primary chemical structure of a strand is relatively intuitive to most chemists, the statistics and topology of how strands are connected within a network is unique to polymer network chemistry relative to other synthetic targets.[99] The topological structure of networks is related to the connectivity of network sub-components, and because it is determined by synthetic methodology it presents an opportunity for chemical control and the molecular optimization of network structure for specific purposes. Characterization of topological structure (and its relationship to synthetic method), however, is in a more nascent stage than the characterization of individual strands. Polymer networks, in general, as shown schematically in Figure 8, are characterized at the molecular scale by the connectivity of components and defined by parameters such as branch functionality, percent functional group conversion, and loop identity and population. At larger length scales, polymer network

topology is characterized by features such as molecular entanglements and inhomogeneities in network density (due to quenched concentration fluctuations present at gelation).[100,101]

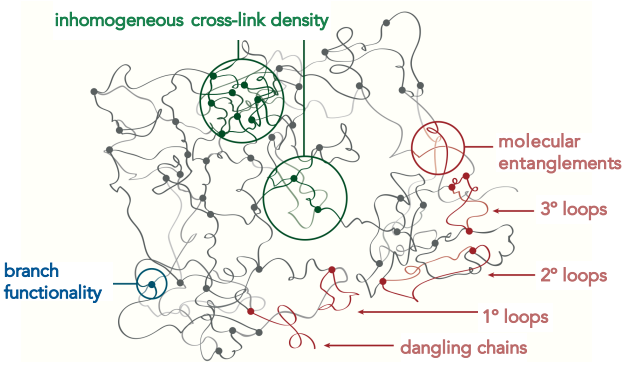

Figure 8: Schematic illustration of a network structure with network strands connected to junctions of a specified branch functionality. The network topology consists of a tree structure with loops of various orders. Primary loops and dangling ends serve as defects in the network due to their inability to support stress (i.e., are elastically ineffective). Figure reproduced with permission from Ref. 100. Copyright © 2019 Elsevier, Inc.

Conventional scattering, microscopy, and other spectroscopic techniques are useful tools in elucidating the topology of polymer networks but lack molecular-level precision or contrast. In many cases, topological features of polymer networks (loops, dangling ends) are often teased out by fitting theoretical models to swelling experiments and other mechanical tests. However, advances such as advanced solid-state NMR and network disassembly spectroscopy are creating opportunities for probing the molecular details of the network structure directly and quantitatively. These nascent techniques can aid in the verification of existing methods and improvement of our understanding of polymer network structure and topology on their resultant properties.

4.1 Swelling

The measurement of the equilibrium swelling of the polymer network in a particular solvent allows estimation of important network characteristics.[45] Characterization methods of network swelling can be divided into two major categories — gravimetric and size measurements. The networks need to sustain the stress induced by the swelling process without catastrophic failure. Typically, with these methods, the volume of equilibrium swelling state V_{eq} and the volume of the dry state V_{dry} can be obtained. Therefore, the equilibrium swelling ratio $Q \equiv V_{\mathrm{eq}}/V_{\mathrm{dry}}$, and the linear deformation factors $\lambda = L_{\mathrm{eq}}/L_{\mathrm{dry}}$ in different macroscopic directions can be calculated (L_{eq} and L_{dry} are the length of equilibrium and dry state in the direction of measurement). However, estimation of molecular-level quantities, such as the average molecular-weight between cross-links $\overline{M}_{\mathrm{x}}$ and the number density of elastically effective chains ν_{eff}, requires further assumptions and experimental details. The classical Flory–Rehner model[102,103] is based on the affine network elasticity model[104] with Gaussian chains and the Flory–Huggins solution theory:[105,106]

$$\begin{aligned} &\ln\left(1-Q^{-1}\right)+Q^{-1}+\chi Q^{-2} \\ &= \frac{\nu_{\mathrm{eff}}\hat{v}_s}{N_{\mathrm{A}}}\left(\frac{1}{2Q}-Q^{-1/3}\right) \\ &= \frac{\rho}{\overline{M}_{\mathrm{x}}}\left(1-\frac{2\overline{M}_{\mathrm{x}}}{M}\right)\left(\frac{1}{2Q}-Q^{-1/3}\right) \end{aligned} \tag{4.1}$$

where $\hat{v}_s$ is the molar volume of the solvent and χ is the Flory–Huggins interaction parameter between the polymer and swelling solvent. Although this model is widely used to relate Q measured experimentally to ν_{eff} and $\overline{M}_{\mathrm{x}}$,[107] many modified interaction and network elasticity models have been developed,[108–113] which can replace the original components in the Flory–Rehner model to correct for deficiencies.[114]

Another challenge is that models typically assume both the elastic part of the free energy restricting swelling and the mixing part of free energy driving swelling are determined by the same elastically active parts of the network. However, in many cases there is a significant elastically ineffective part of the network (defects such as dangling ends and dangling loops)

that contributes to the mixing component, but not to the elastic component of the free energy. This unknown fraction of elastically ineffective part of network that can be as large as 50% in some cases even far from gel point and makes determination of network properties from swelling much more difficult. So, instead of delving into the details of particular physical models, we herein focus on the technical details of operations for both gravimetric and size measurements; the approaches that probe the molecular details of the equilibrium swelling are discussed afterwards.

4.1.1 Gravimetry

Both equilibrium swelling and swelling kinetics (if the process is slow enough) can be measured by simply weighing the gel. In a typical experiment, a network with a known mass is placed in a solvent, and then at certain time intervals, the sample is taken out and weighed. Typically, cylindrical samples with heights and diameters in the centimeter range are prepared and the swelling times range from hours to days or even weeks,[115] rendering the method convenient and low-cost, albeit slow. The gel reaches equilibrium swelling when the weight has saturated to a constant value. The method can be extended to thin gel films provided they are firmly attached to a solid, non-swellable substrate such as a glass slide. The total weight of the system (glass slide and attached gel) is usually smaller than 100 g and can be measured on standard balances with an accuracy of 0.1 mg.

Although gravimetry is arguably one of the easiest methods for studying gel swelling, several important experimental steps should be followed to ensure accurate results. Care should be taken to remove any excess solvent from the gel surface, usually by gentle patting with a paper tissue. After the solvent removal, however, the gel might start to dry immediately, potentially skewing the results. Thus, the weight of the gel should be large enough to allow the drying to introduce only a minor error in the weight measurements. For example, under ambient conditions (25 °C and 40% relative humidity) the evaporation rate of water from hydrogels can be as high as $1\,\mathrm{mg\,min^{-1}\,cm^{-2}}$,[116] which could result in significant weight loss in the case of thin gel films with large surface-to-volume ratio. Another limitation of the gravimetric approach is that it only gives an average swelling for the whole sample, regardless of whether the swelling is homogeneous in all directions or not.

4.1.2 Size Measurements

The physical dimensions of macroscopic, centimeter-sized gels are also easily measurable by a ruler or caliper.[117] Size measurements are especially valuable when the gel exhibits different swelling in different directions.[118,119] Size measurements, however, of gels very small in one or more dimension (e.g., thin films, microgels), require more sophisticated treatment. Direct size measurement of microgels or thin films with dimensions on the order of micrometers or larger, is usually achieved with optical microscopy.[120] One challenge with this approach, however, is the timeframe of the experiment as swelling rates increase with decreasing sample size, necessitating fast image acquisition for small samples. Optical microscopy has also been applied to measure the swelling kinetics of thin-film gels with a small number of fluorescent micrometer-sized particles trapped in them.[121] The swelling of reversible thin-film gels can also be studied by confocal microscopy[122,123] using a more complicated experimental setup. Further, network particles with dimensions smaller than micrometers are inaccessible to measurement with optical microscopy, and dynamic light scattering (DLS, Section 5.5.1) is used instead.[124] However, DLS is only suitable for the measurement of the equilibrium swelling because of limitations in time resolution and the accuracy. Nevertheless, DLS is a popular technique to study the effect of environmental factors, such as temperature and pH, on the equilibrium swelling of microgels.

4.1.3 Equilibrium Swelling

Equilibrium swelling results from the balance of the elastic free energy change of the gel due to swelling of the network, ΔF_{el}, and the free

energy of the gel due to mixing between the network and solvent molecules, ΔF_{mix}.[102] The osmotic pressure of the gel Π_{gel} against the swelling solvent is zero at equilibrium swelling and positive for as prepared, neat, and partially swollen networks. The elastic component of the gel $\Pi_{\text{gel}}^{\text{el}}$ is proportional to the modulus G at corresponding concentration, which can be determined by mechanical testing (Section 5.1). The mixing contribution to the osmotic pressure of the gel $\Pi_{\text{gel}}^{\text{mix}}$ is usually considered to be equal to the osmotic pressure $\Pi_{\text{sol'n}}$ of a semidilute solution of non-cross-linked chains at the same concentration;[15] an estimation of $\Pi_{\text{gel}}^{\text{mix}}$ can be obtained by measuring $\Pi_{\text{sol'n}}$ with osmometry (Section 2.2.3). Therefore, comparison of the pressure of the gel Π_{gel} with the independently measured modulus $G \propto \Pi_{\text{gel}}^{\text{el}}$ and semidilute solution osmotic pressure $\Pi_{\text{sol'n}} \approx \Pi_{\text{gel}}^{\text{osm}}$ can provide an estimate of the relative contributions of tension in elastically effective strands and free energy of mixing of all chains in the swelling solvent.[15]

Other than investigating the swelling behavior of gels in pure solvent, the swelling behavior of gels can be studied in media that can exert osmotic pressure on the gels as well. Experimentally, this approach is achieved by placing a network into a particle or polymer solution with known osmotic pressure and letting it swell to equilibrium against the osmotic pressure of solution.[121,125] The size of the solute particle/polymer should be much larger than the mesh size of the gel so that solutes cannot penetrate the gel, and the equilibrium swelling of the gel is suppressed in comparison to that in pure solvent. With this method, both elastic and mixing components of network free energy can be characterized. At equilibrium swelling, the sum of the mixing and elastic components of the swollen gel ($\Pi_{\text{gel}}^{\text{mix}}$ and $\Pi_{\text{gel}}^{\text{el}}$ respectively) should equal the osmotic pressure of the swelling media Π_{ext}:

$$\Pi_{\text{gel}} = \Pi_{\text{gel}}^{\text{mix}} + \Pi_{\text{gel}}^{\text{el}} = \Pi_{\text{ext}} \qquad (4.2)$$

Furthermore, in principle, this method can be operated together with the probe penetration method— by placing networks into solutions with both dilute labeled probes, which can diffuse into the network, and large solutes, which are excluded by the network, the average mesh size of partially swollen gels can be measured while measuring Π_{ext}.

4.1.4 Mesh Size Characterization

The mesh size ξ_{mesh} of polymer network is an important parameter that is related to the osmotic pressure and network swelling; molecularly, it is related to the correlation length ξ, which is defined as the average distance between the closest polymer segments of neighboring polymers. It is important to distinguish the mesh size (correlation length) from the size of the network strand between two neighboring cross-links. The former is usually smaller than the latter in a gel since polymer chains are overlapping.[15]

In principle, the mesh size of a polymer network can be obtained from the modulus and the swelling of the polymer network.[126–128] Albeit very accessible, the analysis of these two methods is based on the choice of specific network elasticity and solution models and knowledge of the interaction parameters between polymer and solvent at the relevant gel concentration. Further, the exact mesh size of a network cannot be easily obtained without major assumption, since the mesh size of a polymer network usually has a wide distribution[123,126] and direct measurement is experimentally challenging, as explored elsewhere in this review (Sections 4.3 and 4.7). Finally, it would be useful for future studies to compare the mesh size obtained by multiple techniques, both to corroborate the experimental methodologies, but also to refine theoretical understanding of characteristic network length scales: correlation length ξ, mesh size ξ_{mesh}, size of an elastically effective strand, distance between cross-links, etc.[129]

4.2 Microscopy

4.2.1 Electron Microscopy

Electron microscopy (EM) has found widespread use as a characterization tool for soft materials, where it is able to offer precise real-space identification of local structural

features. In particular, transmission electron microscopy (TEM) has proven invaluable for characterizing the morphology and interfacial properties of semi-crystalline polymers,[130–132] polymer nanocomposites,[133–138] and block copolymers including thermoplastic elastomers (Figure 9b), but historically has been less useful for amorphous polymer networks.[139–142]

Although the spatial resolution of electron microscopy techniques is theoretically smaller than length scales of structural/topological features in polymer networks, lack of electron density contrast in a homogeneous material makes it only suitable for polymer networks consisting of large mesh sizes and relatively stiff chains.[123] For example, EM techniques have imaged the supramolecular fibrillar structure of gels made from polysaccharides including gelatin, guar, and pectin (Figure 9a) to visualize structural features of $\sim$ 10 nm.[143,145,146] Radial integration of the Fourier transform of the obtained EM images can produce simulated scattering curves which can be compared against experimentally obtained data from small-angle X-ray or neutron scattering (Section 4.3). In the case of pectin networks (Figure 9a), the two methods were found to be broadly consistent on scales above 20 nm.[143] Another challenge is that EM images are 2D projections of a 3D sample; this issue can be partially mitigated by use of ultramicrotomy to prepare ultra-thin samples with thickness $\lesssim$ 100 nm.[147] This issue can also be addressed through the use of electron tomography, in which a series of 2D EM images are taken at different tilt angles to reconstruct the 3D sample.[148]

Inhomogeneous materials can be more readily imaged by preparation techniques to enhance contrast between different regions. Staining with heavy-elements (e.g., ruthenium and osmium tetroxide) is one of the most common methods in polymers due to its transferability and ease of use (although its safety hazards must be noted).[149] Other methods, such as freeze-fracture scanning electron microscopy (FF-SEM), fracture the flash-frozen sample along weak portions of the sample (i.e., membranes, interfaces or surfaces) and have been used to image biological samples and polyelectrolyte microgels (Figure 9c).[144,150] Additionally, the absence of appreciable contrast can be useful in some cases, such as confirming the absence of precipitated iron nanoparticles in metallo-cross-linked polymer networks.[151]

However, the accuracy of these methods is usually limited by fixation and staining artifacts, which prevents direct imaging of mesh size, heterogeneities, and network defects for many samples.[147] It needs to be stressed that the combination of complex samples, elaborate preparation procedures, and highly specialized techniques can lead to flaws in the final data. It is of utmost importance to distinguish genuine micrographs from artifacts. Finally, it is interesting to note the potential future of single-molecule super-resolution microscopy, which has hitherto been focused in biological research,[152] but could be realized in reversible gels and would add a significant tool to molecularly characterize polymer networks.[153]

4.2.2 Polarized Optical Microscopy

Birefringence is a property of optically anisotropic materials whose refractive index, n, depends on the polarization and direction of propagating light.[154] Birefringence of a material, Δn, is typically measured as the difference in refractive index of the material for light polarized in two orthogonal directions. Individual polymer molecules have a polarizability anisotropy due to their three-dimensional structure, but because all of the molecules in a completely amorphous polymer material are randomly oriented, the material itself is optically isotropic. In the case of materials with some anisotropic orientation, such as in crystalline regions of a material or due to chain extension in the direction of strain, birefringence can be observed using an optical microscope containing two polarizers that are 90° to each other on either side of the sample and is closely related to the stress–optic effect to be discussed in Section 5.4. In this way, the birefringence measured through polarized optical microscopy (POM) can provide information about the strain-induced crystallization in vulcanized natural rubber, crystallinity in melt-blown or

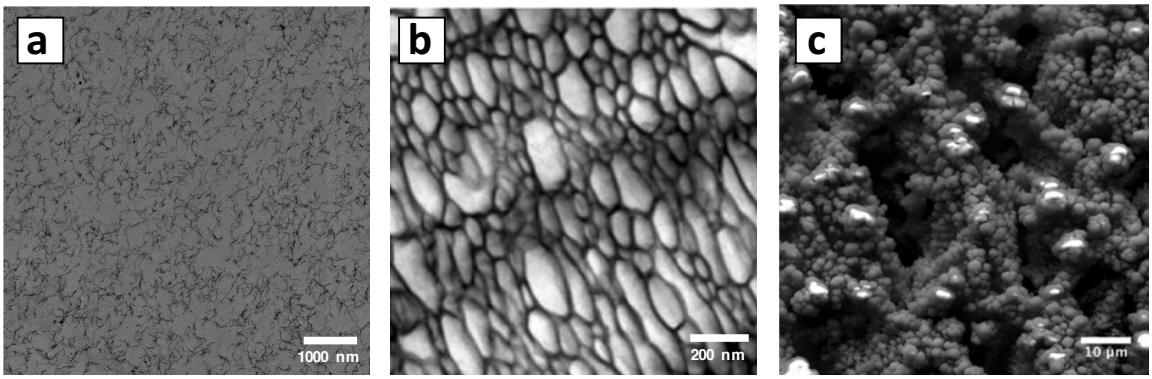

Figure 9: (a) TEM images of (a) a pectin network and (b) an aperiodic "bricks and mortar" mesophase thermoplastic elastomer composed of a miktoarm copolymer and homopolymer binary blend. (c) Freeze-fracture SEM image of a polyelectrolyte hydrogel exhibiting a heterogeneous, jammed microgel structure. Figures reproduced from (a) Ref. 143 (Copyright © 2018 American Chemical Society), (b) Ref. 139 (Copyright © 2015 American Chemical Society), and (c) Ref. 144 (Copyright © 2018 American Chemical Society).

electro-spun fibers, and molecular strain and orientation during processing.[155–157] Further, birefringence is commonly quantified in oriented polymeric systems, especially as a signature of networks under mechanical stress and self-assembled materials such as block copolymers.[156,158–161]

4.3 Scattering

A classical technique for characterizing the structural and topological features of polymer networks is scattering, which involves exposure of a sample to incident radiation and measurement of the intensity of scattered radiation as a function of the scattering wavevector q defined as

$$q = \frac{4\pi}{\lambda} \sin(\theta/2) \tag{4.3}$$

where, λ is the wavelength of incident radiation and θ is the angle between the incident radiation and the detector measuring the scattered intensity. The same basic principles apply to scattering of different forms of radiation. Sufficient scattering contrast between the background (solvent or matrix) and structures of interest is necessary to identify key features in scattering patterns. Typical forms of radiation used for studying polymers include X-rays where the scattering contrast arises from electron density differences, neutrons where the scattering contrast comes from differences in atomic nuclei, and light where the scattering contrast relies on differences in refractive index (i.e., differences in polarization of electron clouds).

Small-angle scattering (SAS), including static or small-angle light scattering (SLS/SALS, $0.0003 < q < 0.002$ Å^{-1}) small-angle X-ray scattering (SAXS, $0.003 < q < 0.2$ Å^{-1}), and small-angle neutron scattering (SANS, $0.001 < q < 0.5$ Å^{-1}), is particularly suited to studying the structure of polymer networks on the order of $1 - 1000$ nm. SANS is particularly relevant to studying the most widely used types of polymer networks, due to the ability to impart contrast through the use of deuterated solvent in the case of gels or preparation with deuterated strands in the case of elastomers.

Representative SANS patterns obtained for gels typically lack peaks corresponding to strong correlations between strands or junctions due to the lack of long-range order and amorphous character of the network (Figure 10).[162–169] Although, it should be noted that scattering curves from charged gels typically do have a feature called the "polyelectrolyte peak", which corresponds to the correlation length ξ resulting from the like-charge repulsion of neighboring charged strands.[170–178] SANS curves are usually fit with physical

models to extrapolate structural parameters, similar to other techniques discussed in this review. Broadly, the high-q region characterizes polymer chains and the low-q region highlights larger length-scale network inhomogeneities. Very- (VSANS) or ultra-small-angle neutron scattering (USANS) or SALS can be further used to extend the accessible wavevector (and associated length scales) to lower-q (longer length scales). An empirical correlation-length model describes features from both such high- and low-q region:

$$I(q) = \frac{\alpha}{q^n} + \frac{\beta}{1 + (q\xi)^m} + I_{\text{inc}} \qquad (4.4)$$

where the power-law term describes Porod scattering from larger network inhomogeneities and the Lorentzian function describes scattering from smaller, mesh-scale structures. α and β are constants of proportionality indicative of the relative contrast and concentration, I_{inc} is the q-invariant incoherent background, n is the Porod exponent that reflects the degree of large length scale homogeneity (i.e., disorder due to concentration fluctuations present at gelation), m is the Lorentzian exponent reflective of the polymer–solvent interactions, and ξ is the correlation length. This Lorentzian component of the empirical correlation-length model is related to the Ornstein–Zernike scattering function, which characterizes the correlation length ξ of semidilute polymer solutions, and is the same mathematical form of an exact theoretical structure factor derived from the random phase approximation (RPA) for gels in theta solvents.[179] Fitting the scattering to this scattering function, the average mesh size ξ_{mesh} of a polymer network can be obtained (at the mean-field level).[15,180,181]

Further, SAXS has been recently used to further analyze networks with is especially useful where network structural features of interest have high X-ray scattering contrast (e.g., metal-containing junctions or counter-ions condensed on polyelectrolyte strands). The scattered intensity $I(q)$ obtained from SAXS (but generally from any scattering technique) can be expressed as $P(q) \cdot S(q)$, where $P(q)$ is the form factor describing the size and shape of the network sub-components (i.e., junctions or strands) and $S(q)$ is the structure factor describing the spatial arrangement of the sub-components. For example, in one study on metallo-cross-linked elastomers, the size and distribution of iron cross-link clusters could be identified in this manner.[151,182] This approach has significant potential in the characterization of molecularly optimized networks of defined structure and topology.

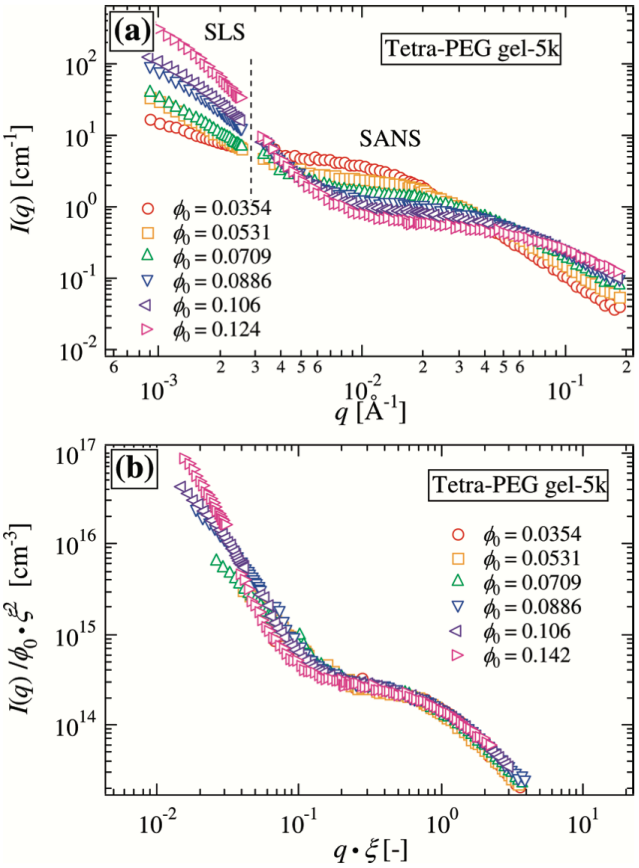

Figure 10: (a) SANS and SLS intensity curves for 5kDa Tetra-PEG gels prepared at various concentrations, φ_0. The missing q region is indicated by the vertical dashed line. (b) Scaled plots, $I(q)/(\varphi_0 \cdot \xi^2)$ and $q\xi$. Figure reproduced with permission from Ref. 166. Copyright © 2009 American Chemical Society.

Once formed, (i.e., after gelation or vulcanization) a polymer network is characterized by an inhomogeneous monomer density profile, which depends on temperature, solvent quality, overall polymer concentration, and externally imposed deformation fields. This bonded-in inho-

mogeneity of the structure of the gel is determined by the density of cross-links in the state of preparation and in turn, dominates the structure factor.[179] Figure 10 shows SANS curves superimposed with static light scattering data at low-q as measured at different preparation conditions and after collapsing the data according to the correlation length ξ and preparation volume fraction φ_0, confirming such expected behavior.[166]

Small-angle scattering further provides an opportunity to connect macroscopic mechanical deformation and swelling of polymer networks to the microscopic structure. Ex situ SANS measurements on deformed (either stretching or swelling) have shown the formation of "butterfly" patterns in the 2D SANS curves, as shown in Figure 11.[183–198] This butterfly effect has been described theoretically as the existence of inhomogeneities in the equilibrium deformed state and related to the inherent anisotropy of the elastic restoring forces in the stretched network. As such, these butterfly patterns highlight the quenched disorder in the network. Further, thermal fluctuations (as observed by dynamic light scattering (DLS, Section 5.5.1 or other scattering spectroscopies) about this anisotropic equilibrium configuration are also anisotropic, but rotated 90°.[179,197] In a related protocol, the small-angle scattering can be decomposed into contributions from thermal and quenched fluctuations, as the thermal contribution is equivalent to the scattering of a polymer solution at the same concentration and the quenched contribution results from the excess scattering of swollen gels.[184] This is analogous to the procedure discussed in Section 4.1 whereby comparing the modulus of a gel and the osmotic pressure of the non-cross-linked polymers at the same concentration, the osmotic and elastic components to the swelling could be estimated.

Recently, scattering coupled with in situ rheological measurements have become more popular to aid in the development of structure–property relationships.[200–204] Rheo-small-angle-neutron scattering (rheo-SANS) is most common in polymer networks due to the contrast selectivity as mentioned for static

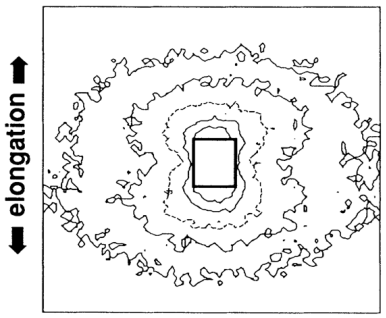

Figure 11: Experimental iso-intensity 2D SANS curves for a gel stretched uniaxially to an elongation factor $\lambda = 1.5$. The rectangle in the center indicates the limits of the beam-stop. Range of scattering wavevector: $0.006\,\text{Å}^{-1} < q < 0.044\,\text{Å}^{-1}$. Figure reproduced with permission from Ref. 199. Copyright © 1991 American Physical Society.

SANS, and provides a direct correlation between the structure and the macroscopic rheological response. There are a number of flow devices compatible with in situ neutron scattering measurements (flow-SANS or rheo-SANS), most notably, Couette cells, capillary flow cells, $1-2$ shear cells, and even entire oscillatory rheometers.[200] Capillary[205] and microfluidic flow devices,[206,207] for low sample volume experiments under arbitrary deformation fields, are also available. Such rheo-SANS experiments have given insights into the interplay of chain branching and alignment with the formation/breakage of reversible cross-links under different shear conditions.[200–203] Further, rheo-SAXS has shown that the glassy styrene domains (within a microphase-separated poly(styrene-*b*-ethylene-*co*-butylene-*b*-styrene) (SEBS) triblock thermoplastic elastomer) change shape, spacing, and ordering while undergoing uniaxial or biaxial stretching.[204]

4.4 Network Disassembly Spectroscopy

Some specific topological features of polymer networks can be quantified through network disassembly spectrometry (NDS) which precisely analyzes the proportion of vari-

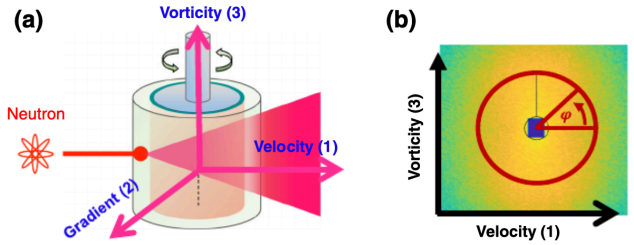

Figure 12: Flow- or Rheo-SANS. (a) $1-3$ (velocity–vorticity) and $1-2$ (velocity–velocity gradient) plane setups are exploited to monitor microstructural evolution with a Couette geometry. (b) A 2D SANS pattern overlaid with the azimuthal angle $\varphi = 0 - 360°$. Figure reproduced with permission from Ref. 203. Copyright © 2019 American Institute of Chemical Engineers.

ous network degradation products. Initially, Johnson and coworkers were able to quantify the primary loop fraction in end-linked A_2B_3 PEG gels through analysis of chromophore-labeled network degradation products via liquid-chromatography–mass-spectrometry (LC-MS).[208] A general schematic for an NDS experiment is shown in Figure 13. The concept of NDS could be extended to measure the primary loop fraction in networks with higher branch functionality ($f > 3$) or a dispersity in junction functionality. Further development of NDS focused on increasing ease of use and accuracy through the preparation of network precursors with isotopic or methyl group mass labels.[209,210] The quantification of secondary loops in end-linked networks, and primary loops in vulcanized networks has also been achieved with NDS.[211,212] Importantly, the direct quantification of loop defects in polymer networks through NDS has facilitated the development and validation of kinetic models to predict the topology of polymer networks as a function of their composition and synthesis conditions, as well as new theories to predict the impact of defects on polymer network elasticity.[113,213–215]

4.5 Solid-State Nuclear Magnetic Resonance

Solid-state NMR is a useful spectroscopic tool to investigate the chemical structure of the gel, particularly for unique chemical environments contained in cross-links. This specificity and quantitative manner allow one to differentiate between dangling vs. elastically active cross-links and determine the average number of repeat units between cross-links.

4.5.1 ^{1}H, ^{13}C NMR

Common one-dimensional (typically ^{1}H or ^{13}C, but other NMR-active nuclei are possible) NMR measurements in the solid-state can yield useful information regarding the network, beyond its chemical composition. In particular, in addition to the overall extent of reaction, the ratio of tetra-, tri-, bi-, and mono-reacted cross-link junctions, was quantified by NMR in the gelation of polyesters.[45,96]

4.5.2 Multiple-Quantum NMR

Multiple-quantum NMR (MQ-NMR) has become one of the versatile approaches for probing the structures and dynamics of polymer networks.[216] This technique is able to distinguish between elastically active chains and elastically inactive dangling ends due to differences in their relaxation dynamics.[216–220] Due to the presence of constraints (e.g., cross-links, entanglements), polymer segmental motion (at temperatures above their glass-transition temperature T_g) is anisotropic. The ^{1}H–^{1}H dipolar coupling cannot be averaged out by fast molecular motions, leading to a residual proton dipolar coupling. If the time scale of the experiment is long enough, the dipolar orientation autocorrelation function for dangling ends will eventually decay to zero, whereas that for elastically active chains will not. Therefore, the residual anisotropic ^{1}H–^{1}H dipolar coupling can be used as a probe to extract quantitative information about the constraints in polymer network. This information can further be used to determine the cross-linking density[221,222] and structural heterogeneity[218,223,224] of the polymer network.

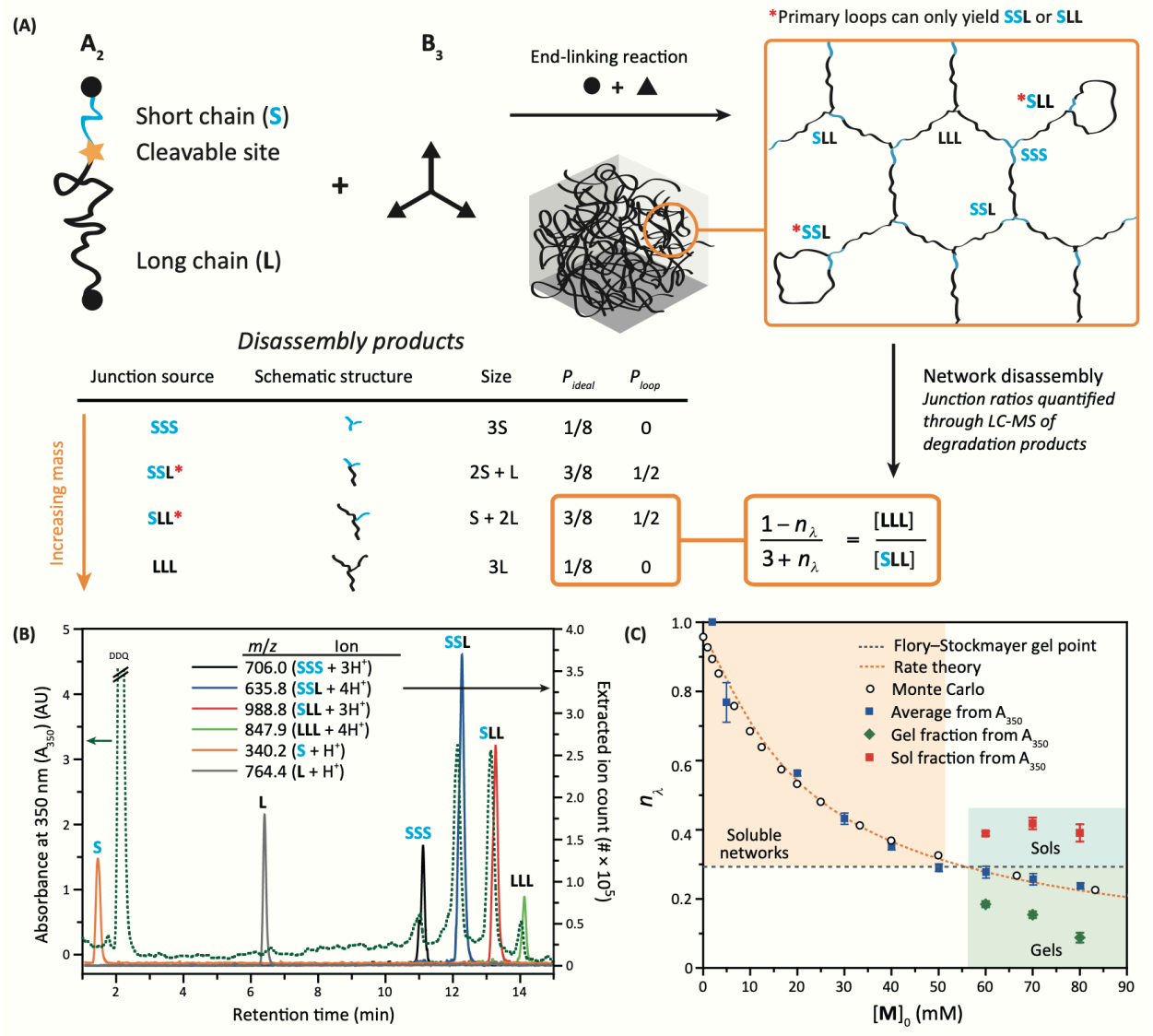

Figure 13: Network Disassembly Spectroscopy. (a) Schematic depiction of a degradable polymer network strand (A_2) with a degradable group (orange star) at a non-central position, which leads to a short chain (S, blue) and a long chain (L, black) after cleavage. End-linking of these strands with a tri-functional linker (B_3) yields a network in which each network junction is unique in terms of the orientation of S and L chains. Primary loops (red asterisks) cannot reside at SSS or LLL junctions. Disassembly of the network yields products whose masses depend on the junction source of that product. The probabilities for formation of each tri-functional product at ideal or loop junctions are listed as p_{ideal} and p_{loop}. The number of primary loops is captured in the ratio [LLL]:[SLL]. (b) Junction ratios quantified through LC-MS of degradation products. (c) Fraction of loop junctions, n_λ, for a tri-functional network. Figure reproduced with permission from Ref. 100. Copyright © 2019 Elsevier, Inc.

Experiments performed on too short of time scales can under-estimate the number of dangling ends, as dangling ends may exhibit slow isotropic motion, however swelling the network can increase chain mobility and lead to a more accurate measurement. Moreover, in the case of polymer networks with extremely homogeneous structures, MQ-NMR has enough resolution to distinguish higher order loop defects and their relative proportions can be distinguished through fitting procedures, as shown in Figure 14.[218] In a similar manner, MQ-NMR can

also provide information about network structural heterogeneities and molecular weight between cross-links.[217,219,221,225] While more accessible and versatile than network disassembly spectroscopy for measuring the fraction of elastically effective strands, MQ-NMR is typically unable to quantify higher-order loops and more complicated defects. It would be useful to compare the results obtained from the two different techniques.

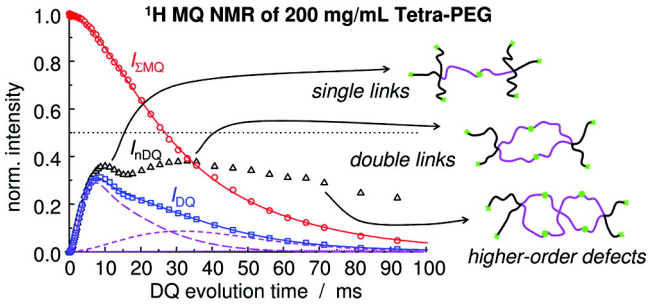

Figure 14: MQ-NMR experimental data of a tetra-PEG gel. The double-quantum buildup I_{DQ} (squares) and the decay of the total multiple-quantum magnetization $I_{\Sigma\mathrm{MQ}}$ (circles) are measured. The normalized double-quantum intensity I_{nDQ} (triangles) has been calculated. Through fitting, individual components to the I_{DQ} can be separated, quantifying the proportions of different topological structures. Figure reproduced with permission from Ref. 218. Copyright © 2011 American Chemical Society.

4.6 Solvent Permeability

The measurement of Darcy permeability of polymer gels in a solvent is another strategy for mesh size (characteristic pore size) characterization.[226] This can be achieved by enclosing the gel in a chamber and connect it to a tube or pipe with solvent flowing through, as shown in Figure 15. By measuring the pressure difference on both sides of the gel, the Darcy permeability can be obtained by Darcy's law,[227] which relates the low Reynold's number flow of a fluid through a porous medium, such a polymer gel:

$$Q = \frac{kA}{\eta_s L}\Delta P \tag{4.5}$$

where Q is the volumetric flow rate of fluid with a viscosity η_s, induced by a difference in pressure, ΔP, over a porous medium of cross-sectional area A, with thickness L, which defines a material property known as the Darcy permeability, k.[228] For flow through polymer gels, often a friction coefficient, f, is defined:

$$f = \frac{\Delta P}{vL} \tag{4.6}$$

where v is fluid superficial velocity.[229] For Darcian flow, f is the ratio of fluid viscosity to medium permeability, $f = \eta/k$. The value of f can be calculated through simple permeation experiments by measuring the rate of fluid flow driven by a hydrostatic pressure through a gel of known thickness, and an average value of mesh size can be estimated.[226]

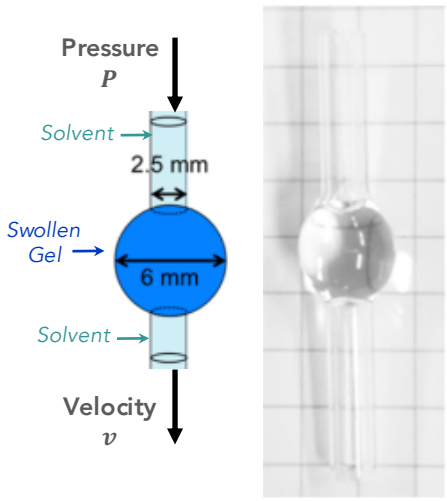

Figure 15: Schematic illustration of a water permeation apparatus for measuring the friction coefficient between a gel and water. Figure adapted with permission from Ref. 229. Copyright © 2017 American Chemical Society.

The swelling of a gel in situ or compression of a gel under applied pressures may interfere with measurements and should be considered carefully when interpreting experimental data. However, physical confinement of gels can enable characterization of gels swollen to below their equilibrium-swollen state or under large applied pressures.[229–231] The picture that fluid permeates a gel by passing through microscopic pores with a width proportional to

the correlation length, $\xi_{\text{mesh}} \simeq \xi$, predicts $f \simeq \eta/\xi^2$.[114] Recent SANS measurements of ξ and subsequent permeation experiments by Sakai et al. have confirmed this scaling argument for tetra-PEG hydrogels with homogeneous network structures.[229] Similar scaling arguments predict $f \sim \phi^{3/2}$ for equilibrium swollen gels in good solvents, confirming the expected concentration (volume fraction, ϕ) dependence of correlation length $\xi \sim \phi^{-3/4}$.[114,232] This scaling has been commonly observed in multiple techniques including SANS (Section 4.3), pulsed-field-gradient NMR (PFG-NMR, Section 5.7.2), and Darcy solvent permeability experiments using tetra-functional poly(ethylene oxide) networks cross-linked in various manners,[231,233–235] although high polymer volume fraction, degree of cross-linking or gel compression can lead to deviations.[229,230] Such comparisons can be used to compare the numerical coefficients of the scaling relation and help differentiate between closely related metrics like the correlation length, hydrodynamic screening length, and mesh size.

4.7 Probe Permeability

Another relatively direct method for characterizing the mesh size and structure of the network is called probe penetration (or probe diffusion).[123,236,237] The average mesh size of a polymer network can be obtained by using tracer-labeled particles, polymers, or small molecules with different sizes as probes and measuring their permeability from dilute solution into a polymer network. The sizes of the probes should be comparable to the average mesh size of the network (typically ranges from several nanometers to tens of nanometers.)[237,238] At the equilibrium permeation, an average mesh size of the network can be obtained by plotting partition coefficients of different probes against their sizes.[123] The partition coefficient of the probe is defined as the ratio of the probe concentrations between the gel and the dilute solution outside. Note that the probes and networks used in this method should not have significant inter-molecular interactions (such as hydrogen bonding or ionic bonding). Other than the partition coefficient, similarly, the relative diffusivity of the probe is also frequently used for mesh size characterization, but the data analysis depends on specific models that are used.[238] Furthermore, in principle, this method can be operated together with experiments of swelling in media that exert osmotic pressure on the gel (i.e., large solutes). By placing networks into solutions with both labeled probes (dilute), which can diffuse into the network, and large solutes, which are excluded by the network, the average mesh size can be measured while measuring Π_{ext}.

Finally, the diffusive behavior of probe particles or molecules within a polymer network can be used to characterize network structure on length scales determined by the probe size, R, and its mean-square displacement (MSD) on the time scale of the experiment. Within polymer gels, measuring the diffusion of small-molecule or polymeric probes can provide information relating to hydrodynamic interactions and obstruction effects between probe and polymer and reduction in free volume within the gel. Probe diffusion is commonly monitored using a variety of techniques including pulsed-field-gradient NMR (PFG-NMR, Section 5.7.2), diffusion-ordered NMR (DOSY, Section 5.7.3), or forced-Rayleigh scattering (FRS, Section 5.9) as discussed elsewhere in this review. NMR-based techniques have been used to measure the diffusion of small-molecule or polymeric probes on millisecond time scales, where network heterogeneity causes the observation of multiple diffusion coefficients, typically corresponding to diffusion in high-density and low-density regions of the gel.[239,240] The length-scale of structural heterogeneities can be estimated then by identifying the experimental time scale, and corresponding probe MSD, at which homogeneous diffusion behavior is observed. Finally, particle tracking experiments of probe diffusion can be used to analyze the viscoelastic properties of a network,[241,242] which is discussed in more detail in Sections 5.3, 5.5, and 5.6.

5 Network Mechanics and Dynamics

5.1 Viscoelasticity

Polymers, including gels and elastomers, are viscoelastic, exhibiting both viscous and elastic mechanical response upon deformation, which varies with the time scale and frequency of the deformation. To characterize this viscoelasticity with respect to tensile, compressive, or shear deformation, several types of experimental measurements are commonly applied, such as stress relaxation measurements, creep experiments, and oscillatory rheology.

Here, we will largely focus on linear viscoelasticity, a regime of linear response at sufficiently small values of applied strain, where the relaxation modulus is independent of strain (Figure 16). In the linear viscoelasticity regime, the elastic and viscous components of material response to deformation are independent and Boltzmann superposition states that the stress (strain) responses to successive strain (stress) stimuli are additive. All linear rheological methods (e.g., step-strain, creep, oscillatory) are equivalent and produce identical information from linear transformations.[15,36] Further, all materials have a region of linear response at sufficiently small values of applied strain; to confirm linearity one needs to check that the result is independent of the amplitude of oscillations (i.e., the measured modulus is strain-independent). Elastomers and gels have larger strain limits (typically $\gamma \lesssim 5$ %) to the linear viscoelastic regime than brittle glasses or tough plastics (typically $\gamma \ll 1$ %).

Taking a step back, simple toy models of viscoelasticity can be constructed using a spring of modulus G_0 obeying Hooke's law to describe the elastic component and a dashpot of viscosity η obeying Newton's law to describe the viscous component of the deformation behavior (Figure 17).[15] The Maxwell model places the spring and dashpot in series, while the Kelvin–Voigt model places the spring and dashpot in parallel.[36] However, this only describes a single relaxation mode; complex material behavior, especially over many time scales, can

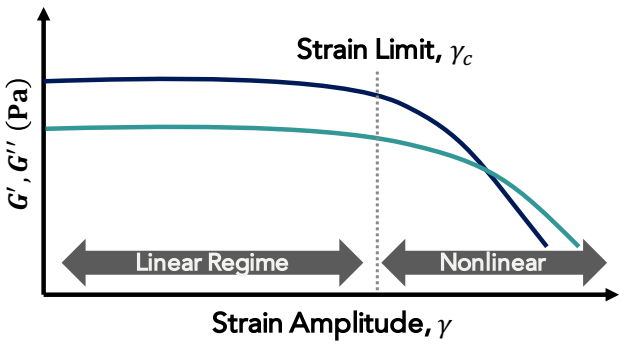

Figure 16: Schematic illustration of a strain amplitude sweep at a fixed frequency in oscillatory rheology. This experimental test is used to verify future rheological measurements are done within the linear viscoelastic regime, at strain amplitudes smaller than the strain limit.

be described by combining many such spring and dashpot elements in Maxwell ladders or Kelvin chains. It is important to emphasize that polymers are composed of many segments, contain many of such relaxation modes, and therefore display a spectrum of relaxation times τ.[15] Finally, it should be noted that the nonlinear mechanics regime is also of high interest to the study of polymer networks, particularly reversible networks, and can be probed using the same techniques discussed below, albeit at higher strains or higher strain rates $\dot{\gamma}$ (for reversible networks).[243–256]

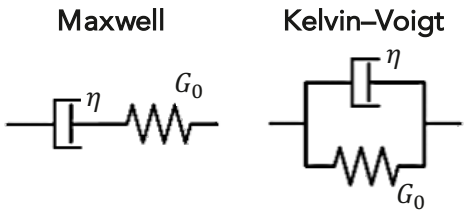

Figure 17: Maxwell and Kelvin–Voigt models for describing a single relaxation mode as a combination of a spring of modulus G_0 and a dashpot of viscosity η.

5.1.1 Tensile, Compressive, and Shear Tests

Tensile (or compressive) tests, in which uniaxial force is applied to elongate (or compress) mate-

rials, are commonly used to determine the mechanical properties of polymers and polymeric networks by recording the stress σ as a function of imposed strain γ. Several intrinsic material properties can be obtained from the resulting stress–strain curve (Figure 18a), including: (i) the Young's modulus, E, which is the slope at small strain;[257] (ii) the tensile strength, which is the stress at failure;[258] and, (iii) the toughness, which is the area under the curve from initial state to failure.[259] Similarly, shear tests, in which force is applied to shear materials, provide the shear modulus G,[260] which is related to Young's modulus through Poisson's ratio as

$$G \equiv \frac{\sigma}{\gamma} = \frac{1}{2(1+\mu)} E \tag{5.1}$$

where σ is the shear stress, and γ is the shear strain, and the Poisson's ratio μ is given by

$$\mu \equiv -\frac{\gamma_{yy}}{\gamma_{xx}} \tag{5.2}$$

where γ_{xx} and γ_{yy} are strains in the x and y directions. Poisson's ratios of elastomers and gels at short times (without a change in volume) are typically approximately 1/2, while Poisson's ratios for swollen gels is smaller (around 1/3) and depends on solvent quality.

Two simple and common models are widely used to extract molecular details of polymer networks from the elastic behavior of unentangled gels and elastomers. One is the affine network model, so called because it relies on the primary assumption of affine deformation: specifically, that both ends (cross-link junctions) of each elastically active network strand displace identically to the macroscopic deformation of the whole network.[15] Under this assumption, molecular details such as the number density of elastically active strands[261] (ν_{eff}) and the number-average molecular weight of a network strand (M_{s}) can be related to the measured shear modulus as

$$G = \nu k_{\text{B}} T = \frac{\rho RT}{M_{\text{s}}} \tag{5.3}$$

where ρ is the network mass density and R is the gas constant. Since the moduli are usually obtained from tensile tests (which provide the Young's modulus), the molecular properties are obtained by first converting the Young's modulus to the shear modulus when the Poisson's ratio is known.

The other common model is the phantom network model. Unlike the affine model, which assumes the ends of each network strands are directly pinned to the elastic non-fluctuating background, the phantom network assumes the network strands are joined at fluctuating cross-links. The phantom network model gives the shear modulus:

$$G = \left(\frac{f-2}{f}\right) \nu k_{\text{B}} T = \left(1 - \frac{2}{f}\right) \frac{\rho RT}{M_{\text{s}}} \tag{5.4}$$

where f is the functionality, i.e., the number of polymer arms that are connected to a cross-linking junction. In comparison to the affine network model, the phantom network model provides a lower modulus at the same number density of elastically active strands. This difference is due to the inclusion of cross-link fluctuation, such that the distance between average positions of junctions varies by smaller factor than in affine model (i.e., changes non-affinely). While the functionality f should be fixed and known a priori according to the chemistry of the network, polymer networks have defects including topological loops and dangling chains, which are elastically ineffective and do not contribute to the elasticity of the network. When the fraction of these defects is low, as in networks prepared in the melt far above gel point, and the polymer strands are unentangled, the measured modulus is well predicted by the phantom model but over-predicts the modulus for other preparation conditions.[113]

More recently, the real elastic network theory (RENT), was established by Olsen and Johnson to expand beyond the tree structure of the phantom network model by including the effects of loops and other topological structures on the bulk elasticity.[113] The initial RENT model treated loops of differing orders as independent without any interactions or correlations. Subsequent refinements have considered other details, such as dangling ends, pre-

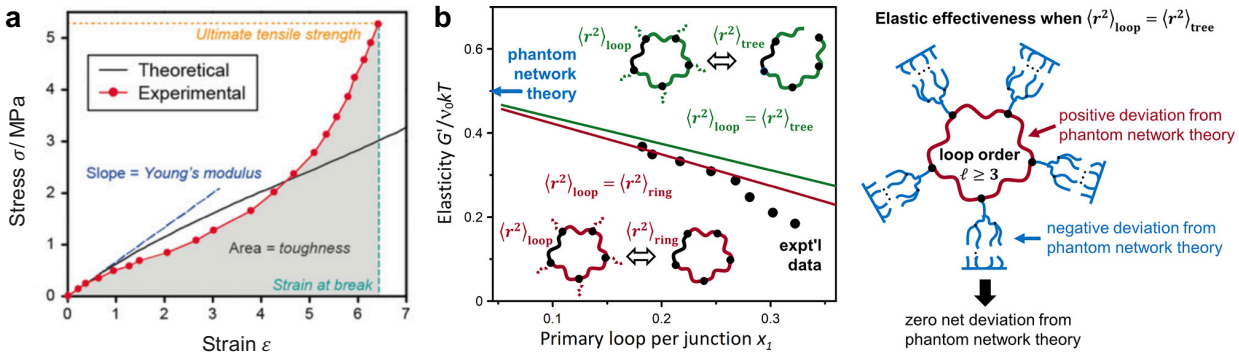

Figure 18: Basic features of polymer network elasticity. (a) Experimental stress–strain curve (red) for a cross-linked elastomer under a uniaxial tensile force. The black curve is the classical form fit to the small deformation data. Figure reproduced with permission from Ref. 101. (b) RENT was developed to predict the effects of loops of various orders on network elasticity. The experimentally determined values (black markers), where ν_0 is the total strand density (including both elastically effective and defective strands), were compared to predictions of phantom network theory (blue arrow), RENT without correction for strand pre-strain (green line), and RENT accounting for pre-strain of strands (red line). Figure reproduced with permission from Ref. 214 with data reproduced from Ref. 113. Copyright © 2019 American Chemical Society.

strain within the strands, and excluded volume interactions.[214,262–266] RENT and associated models significantly improve the connection between molecular-level and bulk properties and correspondingly improve the agreement with experimental data (Figure 18b). However, more advances in characterization of loops, dangling ends, and the tree structure of polymer networks are needed to quantify these defects for regular networks and develop correlations such that RENT could be applied for an arbitrary unentangled network obtained by random cross-linking or end-linking without measurement of these defects by NDS (Section 4.4) on each sample.

Further, in order to capture more features of stress–strain curves, the curve can be fit with the phenomenological Mooney–Rivlin model,[15,267,268]

$$f^* = \frac{\sigma_{\text{true}}}{\lambda^2 - 1/\lambda} = \frac{\sigma_{\text{eng}}}{\lambda - 1/\lambda^2} = 2C_1 + \frac{2C_2}{\lambda}, \tag{5.5}$$

where f^* is the Mooney–Rivlin function, λ is the stretch, σ_{true} is the true stress, and $\sigma_{\text{eng}} = \sigma_{\text{true}}/\lambda$ is the engineering stress, to obtain the Mooney–Rivlin coefficients C_1 and C_2. For classical models (e.g., affine or phantom networks), the Mooney–Rivlin coefficients are $2C_1 = G$ and $C_2 = 0$. Many stress-strain curves, however, have $C_2 > 0$, and they cannot be accommodated by classical models. A value of $C_2 > 0$ corresponds to a stress–strain curve that exhibits strain softening behavior, which is attributed to the contributions of non-affine entanglement tubes in polymer networks.[269]

In order to extract a greater level of molecular detail from stress–strain curves with non-classical behaviors (e.g., strain softening), the curves can be fit by using the Rubinstein–Panyukov relation[15,112,270]

$$\frac{\sigma_{\text{true}}}{\lambda^2 - 1/\lambda} = \frac{\sigma_{\text{eng}}}{\lambda - 1/\lambda^2} = G_{\text{x}} + \frac{G_{\text{e}}}{0.74\lambda + 0.61\lambda^{-1/2} - 0.35} \tag{5.6}$$

to obtain the contributions from entanglements and cross-links to the modulus, G_{e} and G_{x}, from which the apparent molar mass between cross-links $\overline{M}_{\text{x}}$ and the entanglement molar mass $\overline{M}_{\text{e}}$ can be calculated.[271] The universal uniaxial deformation curve is shown in Figure 19, which shows the relationship between Mooney–Rivlin function f^* and phantom modulus G_{x} and entanglement modulus G_{e} with respect to the

stretch λ.

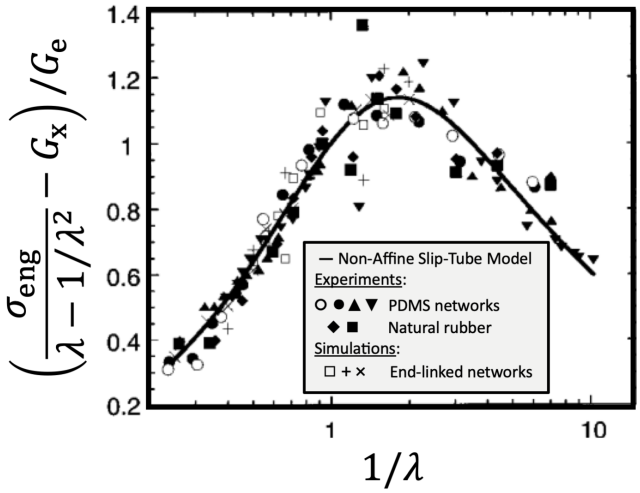

Figure 19: Universal curve extension and compression in a polymer network. Figure adapted with permission from Ref. 112 (Copyright 2002 American Chemical Society) and data reproduced from Refs. 272–274.

5.1.2 Stress Relaxation

Stress relaxation experiments impose an instantaneous step-strain of magnitude γ at time $t = 0$ and measure the stress remaining at time t. The ratio of this stress at time t to the constant strain γ is known as the stress relaxation modulus, $G(t)$,[15,36]

$$G(t) = \frac{\sigma(t)}{\gamma} \tag{5.7}$$

Viscoelastic liquids, such as polymer melts or solutions and reversible networks, can completely relax their stress. For viscoelastic solids, such as covalent networks, however, $G(t)$ relaxes to a finite value, the equilibrium shear modulus:

$$G_{eq} = \lim_{t\to\infty} G(t) \tag{5.8}$$

In broad terms, G_{eq} is determined by the permanent molecular scaffolding within a network (e.g., covalent cross-links), whereas the time-dependent portion of the moduli $(G(0) - G_{eq})$ is determined by the short-time-scale relaxation of network strands between cross-links, relaxation of defects (dangling strands or loops), and dynamic molecular scaffolding, such as reversible cross-linking or the slippage of physically entangled polymer strands.

Thus, stress relaxation testing can be useful in investigating the molecular-level processes of relaxation under load.[275] Since the sample is kept under a constant deformation due to the imposed step strain, molecular-level movement rather than macroscopic change dominates stress relaxation processes. Information about entanglement, chain alignment, cross-linker exchange, and, under more extreme conditions, chain scission under strain can be gleaned from stress relaxation experiments.[276,277] Additionally, stress relaxation experiments are industrially important in determining whether stress can be dissipated over accessible time scales in materials for applications that require repetitive strain or in molding and curing processes of polymers and composites.[278] This helps determine the best processing conditions and the working lifetime of a material.

Stress relaxation experiments are particularly useful in characterizing reversible networks, both ordinary reversible networks with a dissociative exchange mechanism and vitrimers, also known as covalent adaptable networks, which are a relatively new class of polymeric networks with an associative exchange mechanism of cross-linkers.[276,279] There is much discussion in the literature about the differences between these two classes of reversible networks and the impact of the cross-link exchange mechanism on the resulting mechanical properties.

Figure 20 showcases a typical stress relaxation curve of a reversible network, an ionomer with ionic clustering serving as physical transient cross-links.[280] Further, plotting observed relaxation time versus temperature can be used to calculate the activation energy of cross-link exchange in reversible networks.[281] Stress relaxation experiments are also useful in determining the topology freezing transition temperature T_V in vitrimers,[279] revealing differing network structures,[282] and quantifying the effects of exchange catalyst concentration,[283] chemical structure, and (in polymeric ionic liquids) counter-ion identity.[284]

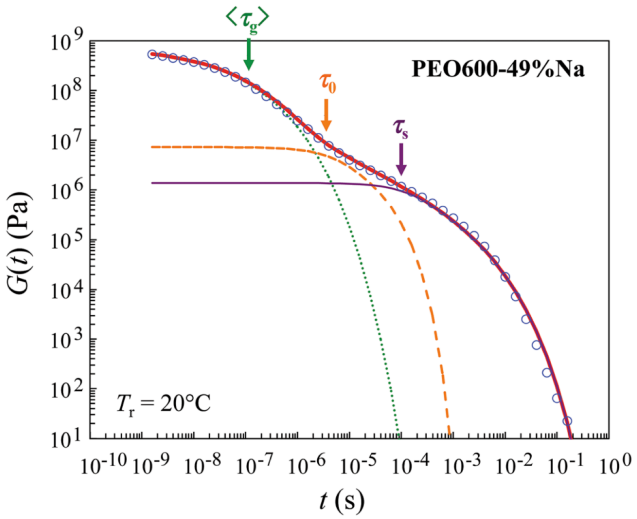

Figure 20: Stress relaxation modulus $G(t)$ for an ionomer (PEO600-49%Na). The green dotted, orange dashed, and purple thin solid curves correspond to fits of glassy, free Rouse, and the sticky Rouse parts of the modulus. The red thick solid curve represents a sum of the three parts. The solid arrows show the characteristic times of these three parts, average glassy relaxation time $\langle\tau_g\rangle$, elementary Rouse time of the segment τ_0, and the association lifetime of the sticky Rouse segment τ_s. Figure reproduced with permission from Ref. 280. Copyright © 2013 Society of Rheology.

5.1.3 Creep

Stress relaxation at a fixed strain and creep at a fixed stress are simple mechanical tests. Creep experiments impose a constant step-stress of magnitude σ at time $t = 0$ and measure the strain as a function of time t.[15] Such experiments enable the measurement of the creep compliance $J(t)$,

$$J(t) = \frac{\gamma(t)}{\sigma} \tag{5.9}$$

which is the ratio of the time-dependent strain $\gamma(t)$ to the constant stress σ.[36]

Over a time longer than the relaxation time, the strain γ and creep compliance $J(t)$ of viscoelastic materials will increase until they reach a steady state, which for solid materials becomes time-independent at an equilibrium strain $\gamma = \sigma J_{eq} = \sigma/G_{eq}$ and for liquid materials becomes linearly dependent on time, $\sim t/\eta$. J_{eq} and $G_{eq} = 1/J_{eq}$ are the equilibrium creep compliance and modulus and η is the viscosity. Upon reaching this steady state in an experiment, the stress can be removed completely ($\sigma = 0$), and the material's creep recovery can then be monitored. This part of an experiment in the linear regime gives rise to the recoverable compliance $J_R(t)$, which is the ratio of the time-dependent recovery strain $\gamma_R(t)$ and the stress σ. At the moment that stress is removed, $\gamma_R(t)$ is defined to be zero. For samples in which the steady-state creep compliance is time-dependent, only the elastic part of the compliance will contribute to the recoverable compliance,[15]

$$\lim_{t\to\infty} J_R(t) = \lim_{t\to\infty}\left[J(t) - \frac{t}{\eta}\right] = J_{eq} \tag{5.10}$$

Creep testing at very low stress values (within the linear viscoelastic limit) can be used to determine the zero-shear viscosity,[285] compare relative length or branching of polymer chains,,[286–288] and infer other important molecular information about a polymeric material, just as any other linear rheological function ($G(t)$, etc.). Creep testing, however, is typically most relevant and easiest to utilize for measuring the long-time relaxation of viscoelastic liquids. For example, experiments under long time scale (or low frequency conditions) are important for characterizing samples with very long relaxation times, such as hydrogels with reversible protein-based cross-links.[289] These experiments can also aid in and expedite creation of rheological master curves (to be discussed below) by extending the low-frequency data from oscillatory rheology (Section 5.1.4) to include long-time data from creep.[290] In fact, creep experiments on the order of months have been used to measure rheological behavior near the gel point (where the relaxation time diverges, Section 3.2).[291,292]

Both stress relaxation and creep testing can be performed using DMA, tensile testing, and rotational rheometers; specific, commercial creep-testing instruments are also available. A comparison of stress relaxation, creep, and os-

cillatory rheology is shown schematically in Figure 21. Nanoindentation and AFM experiments (Section 5.1.5) to study stress relaxation and creep are also sometimes designed for particularly small samples or to study nanoscale spatial heterogeneity in material properties.[293]

5.1.4 Oscillatory Rheology

Dynamic mechanical analysis (DMA) and oscillatory shear rheology are two of the most common and powerful techniques for analyzing the mechanical behavior of viscoelastic materials.[294–299] DMA and oscillatory shear rheology rely on the same fundamental concepts, but there are notable differences in suitability (Figure 22a). In typical DMA measurements, a thin sample (typically with thickness $(0.02 - 1)$ mm, width $(2 - 5)$ mm, and length $(5 - 10)$ mm) is placed between two clamps, and the mechanical response of the sample under oscillatory stretching is analyzed. Therefore, this technique is suitable for solid samples, such as glassy polymers, rubbers, and stiff gels. Oscillatory shear rheology, however, accommodates both solid and liquid samples, which are typically placed either between two flat plates or between a cone and a flat plate, and the mechanical response under oscillatory shear is analyzed. Although this method can be used for samples in a glassy state, glassy samples potentially cause slipping between the sample and the plates. Thus, this method is more suitable for soft materials, such as rubbers, gels, and liquids.

During experiments, an oscillatory stress, typically tensile for DMA and shear for oscillatory shear rheology, is imposed, and the strain in the material is measured, allowing the calculation of the dynamic moduli (E^* for DMA or G^* for oscillatory shear rheology) at various strain amplitudes, frequencies, and temperatures. Strain-controlled instruments with applied strain and measured resulting stress are less common but also available. Cone and plate geometries in oscillatory shear rheology are most common and useful for viscoelastic samples due to the uniform shear throughout the sample. Parallel plates can also be useful, particularly for more elastic samples, if the sample thickness needs to be uniform or if high shear rates are needed, although a correction factor needs to be applied to convert the measured force into true rather than engineering stress. DMA has a similar problem, and samples need to be uniform and aligned correctly for accurate measurements. The respective advantages and challenges of different measuring geometries in rheometry are discussed in polymer rheology texts.[301,302]

The dynamic or complex modulus G^*, related to the complex viscosity η^*, can be separated into storage (G') and loss (G'') components:[15]

$$G^*(\omega) = i\omega\eta^*(\omega) = G'(\omega) + iG''(\omega) \quad (5.11)$$

The loss tangent is defined as

$$\tan(\delta) = \frac{G''(\omega)}{G'(\omega)} \quad (5.12)$$

where δ is the phase shift between stress and strain responses. These storage and loss moduli characterize how much of the energy that goes into deforming the sample at a given frequency is stored as elastic energy or dissipated as heat. These moduli, as a function of frequency, are the key outputs of DMA and oscillatory shear rheology, and it is through an analysis of them that structural (e.g., molecular weight between cross-links) and dynamic (e.g., Rouse or sticker times) molecular properties can be inferred. Again, recall that the the linear viscoelastic functions ($G(t)$, $J(t)$, $G^*(\omega)$) are related and contain the same microstructural information; the choice of rheological method depends on convenience for the property and material of interest. Noteworthy examples of extracting molecular information in this way include the lifetime of "sticky" associations in linear ionomers from the frequency dependence[303] and the use of measured plateau modulus to characterize molecular weight between entanglements ($\overline{M}_e$) in linear entangled polymers.[304]

A common use of these techniques is a temperature sweep at constant frequency; a representative temperature–modulus curve at a single frequency is presented in Figure 22b for polymers of various cross-linking densities and

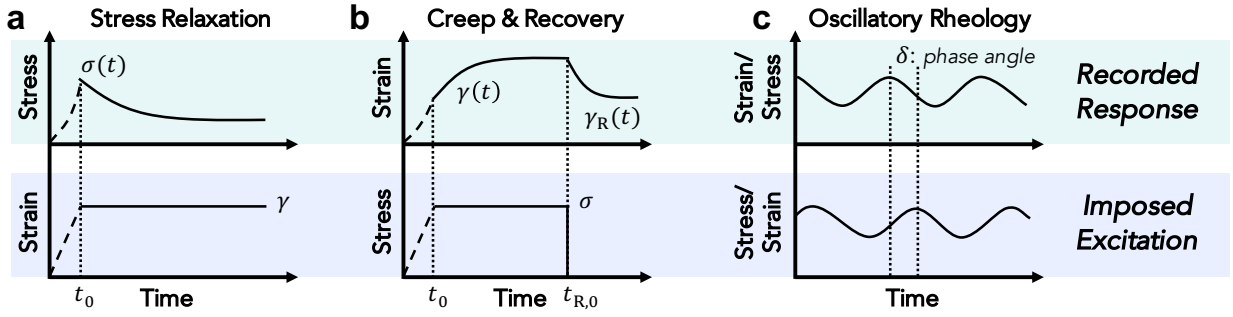

Figure 21: All linear viscoelastic functions are related by linear transformations and the choice of technique depends on the sample and properties of interest. Common experiments for measuring time-dependent mechanical properties of polymer networks: (a) Stress relaxation measures the temporal evolution of stress under application of a constant strain. (b) Creep measures the temporal evolution of strain under application of a constant stress. Creep recovery measures the temporal evolution of strain upon removal of the initial stress. (c) Oscillatory rheology characterizes the viscoelastic properties of materials by application of a sinusoidal stress (or strain) and monitoring the strain (or stress) response.

molecular weights. The resulting curves are frequency-dependent and shift with frequency, which is the basis of time–superposition and the creation of master curves, described below. At temperatures lower than the glass transition temperature (T_g), all polymer types show similar glassy behavior: constant high modulus on the order of GPa. As the temperature increases towards T_g, the moduli drop significantly as the glass transition is approached. For temperatures $T > T_g$, the chemically cross-linked polymers (i.e., conventional covalent networks) maintain nearly constant moduli that indicate a rubbery plateau regime on the order of MPa. All non-cross-linked polymers will eventually show a decrease in modulus that is related to their so-called terminal relaxation. For linear entangled polymers, however, this terminal relaxation at high temperatures will be preceded by a rubbery plateau modulus on the order of 100 kPa due to entanglements acting as physical cross-links.

Furthermore, DMA and oscillatory shear rheology can be used to characterize the relaxation behaviors of polymer materials throughout a wide range of frequencies by employing time–temperature superposition (TTS) (i.e., a master curve, Figure 22c).[15,305,306] The key concept behind TTS is that most dynamic processes have a temperature dependence; the same relaxation occurs more quickly at higher temperatures. Thus, linear rheological response data collected as frequency sweeps at a range of temperatures can be shifted to predict behavior corresponding to immeasurable frequencies. Often, the temperature dependence can be characterized as a single, Williams–Landel–Ferry (WLF) or Arrhenius-like activated process that is quantified through a so-called shift factor, a_T, and a much smaller modulus scale shift factor, b_T:

$$G^*(\omega, T) = b_T G^*(a_T \omega, T_0) \tag{5.13}$$

where ω is the angular frequency and T_0 is the reference temperature, which can be chosen to be any convenient temperature. However, TTS relies on several assumptions for validity and can fail if these assumptions are not met. The structure of the material must be homogeneous, amorphous, isotropic and not change over the temperatures used. Further, the material must be thermorheologically simple, that is, the contributing relaxation mechanisms must have the same temperature dependence. The former can be confirmed by techniques in Section 4; the latter can be detected by generating a Cole–Cole (G'' versus G') or wicket plot ($\tan(\delta)$ versus G') and identifying the characteristic semi-circle curve shape. Finally, the

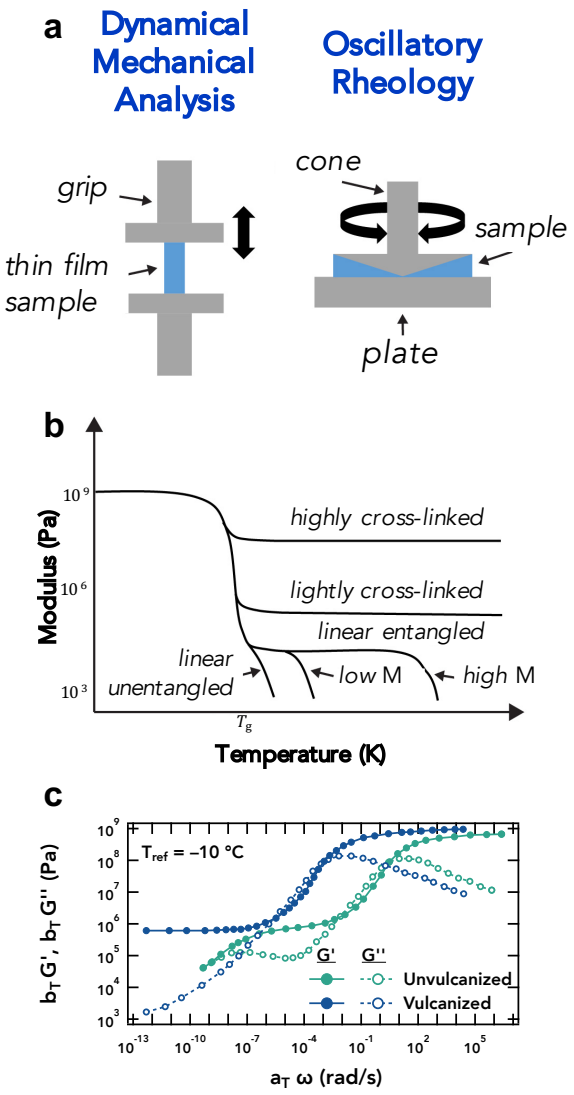

Figure 22: (a) Typical setups for DMA and oscillatory shear rheology, (b) representative storage modulus responses of chemically cross-linked polymers and linear polymers at a fixed frequency and as a function of temperature with semi- logarithmic axes, and (c) representative master curve for styrene-butadiene rubber (SBR) with double logarithmix axes. SBR master curve data in panel (c) reproduced with permission from Ref. 300. Copyright © 2014 American Chemical Society.

shift factor versus temperature can be analyzed to fit an Arrhenius or WLF-like process. TTS often fails in reversible networks when the gelation process affects the phase, structure, or extent of reaction.

As shown in the master curve of Figure 22c, at high frequency, there are sharp increases in modulus due to the glass transition. A rubbery plateau regime exists at intermediate frequencies for entangled or cross-linked samples. In entangled polymers this occurs at frequencies corresponding to times intermediate to the entanglement (τ_e) and reptation times (τ_{rep}), providing a plateau modulus (G_e) and thus an estimate of the molecular weight between entanglements ($\overline{M}_e$) and the chain density of effective strands. For cross-linked polymers without entanglements, the plateau region provides a plateau modulus G_x and an estimate of a molecular weight between cross-links $\overline{M}_x$. However, due to the statistical nature of cross-linking, there is a large distribution of distances between cross-linking junctions and many defects such as loops and dangling ends, so this is only an estimate and an ensemble average. For cross-linked polymers with entanglements, the plateau region provides a plateau modulus that contains contributions from both entanglements and chemical cross-links. Entanglements can become trapped when occurring on a strand between a pair of cross-links, but their relative contribution to the modulus is diminished as the molecular weight between cross-links becomes much smaller than the molecular weight between entanglements or for networks near the gel point with many dangling ends that do not trap entanglements.[307–313] Transient networks with physical cross-links can show a single plateau modulus that has contributions from entanglements and cross-links (as for covalent networks with trapped entanglements), or two plateaus if the reptation time is longer than the typical lifetime of the physical cross-links. At the lowest frequencies (i.e., at times longer than the longest relaxation time) is the terminal flow regime, in which both storage and loss moduli depend on frequency: $G' \simeq \Psi_{1,0}\omega^2$ and $G'' \simeq \eta\omega$. Thus, in the terminal regime, the loss modulus is proportional to the viscosity and the elastic modulus related to the zero-shear first normal-stress coefficient, $\Psi_{1,0}$.[15,36] However, local microphase separation can alter the expected terminal frequency scaling of the moduli if the sample is in an ordered state and can provide insight into samples' mesophase structure.[244,314,315] Further, for

microphase-separated polymer networks, the applied stress can affect and orient the microphase.[316–320]

Looking specifically at the loss modulus G'' in the plateau region of cross-linked networks, the Curro–Pincus method can be used to understand the contributions of dangling ends, which are elastically ineffective but contribute to the viscous dissipation. The amplitude of G'' corresponds to the total number density of defects in the network, while the power law of $G'' \sim \omega^{\alpha}$ where $\alpha \approx \overline{M}_{\mathrm{x}}/M - 1$ indicates the average molar mass of the defects (M) relative to an elastically active strand ($\overline{M}_{\mathrm{x}}$).[321–323]

Moreover, oscillatory shear rheology is particularly useful for analysis of network formation (i.e., gelation). Typical covalent networks are composed of non-reversible covalent bonds formed by chemical reactions. Reversible bonds induced by associative or "sticky" interactions, such as hydrogen bonding or ionic associations, lead to the formation of transient networks. The network formation kinetics for both networks can be studied by monitoring moduli and $\tan(\delta)$ during the gelation (e.g., G', G'', and $\tan(\delta)$ versus time), which helps to associate the developments of the network structures with their mechanical responses.[324–328] In principle, these can be done as kinetic or time-dependent measurements, but only the relaxation modes faster than the gelation itself can be measured and thus are unable to access the slowest relaxation modes related to large clusters near the gel point. This limits such kinetic experiments to a certain distance from the gel point. The correct manner to measure these slow modes is to quench the system (i.e., stop the cross-linking reaction) at various points and then measure the full range of relaxation times for each sample.[291,292]

As such, the gel point or gelation time can be determined by oscillatory shear measurements.[294,326–328] Although the criterion $G' = G''$ is commonly cited, this does not rigorously correspond to the gel point. The proper identification of the gel point is when $G' \sim G'' \sim \omega^{u}$ and $\tan(\delta) = \tan(u\pi/2)$ is frequency-independent, where u is the dynamic scaling exponent with a value of $0.5 - 0.8$ for unentangled gels.[291,326–329] For entangled gels, the relaxation exponent u is lower ($u \approx 0.3$), as predicted by theory and measured by experiments.[307–309] This criterion to determine the gelation time requires multiple measurements. Several frequency sweeps of the samples can be conducted at different curing times, and then the gel point is found when $G' \sim G'' \sim \omega^{u}$. Alternatively, aging experiments (i.e., $\tan(\delta)$ versus time t) can be conducted at several frequencies, followed by determining the gelation time as the cross point of all curves, which represent a frequency-independent $\tan(\delta) = \tan(u\pi/2)$.

Oscillatory shear rheology is also sensitive to and thus useful to studies of reversible gelation in associating polymers. Careful rheological studies have shown that ionomers exhibit a sol–gel transition as the average number of ionic groups (i.e., functionality for potential cross-linking) per chain is increased. Below, but close to the gel point, there is a power-law relaxation of the complex modulus similar to that of chemical cross-linking.[291,313] Very close to the gel point, the power-law relaxation of the complex modulus shifts from high frequency to low frequency, suggesting a transition from mean-field to critical percolation, as discussed in Section 3. However, even further above the gel point, terminal relaxation is observed in ionomers (and associating polymers or reversible networks more generally) as the dissociation of transient, physical cross-links occurs.[330] The rheological and dynamic properties of these associating polymers and reversible networks agrees well with previous theoretical predictions for gelation with effective breakup of clusters.[331–333] Finally, it is important to highlight that away from the gel point, these "sticky" or associative interactions form the basis of the sticky Rouse and sticky reptation models.[280,332,334–338]

5.1.5 Contact Mechanics

Nanoindentation provides a method to probe mechanical properties of materials on submicron length scales that are small enough to resolve spatial heterogeneities, providing nanoscale equivalents of bulk materials test-

ing. Originally developed as an extension of depth-sensing indentation techniques that measure the hardness of materials,[339] nanoindentation has been adapted to small-scale metal, ceramic, and polymer samples. During an experiment, an indenter with a tip of known geometry is vertically pressed into a sample starting from as low of a contact force as possible (typically $\sim 5\mu$N) and subsequently retracted. A load–displacement curve is recorded during both loading and unloading within a load range of $50-500$ mN, from which the material properties of the sample can be calculated, most commonly hardness and Young's modulus.[340]

Commercial nanoindentation instruments have indenters composed of diamond with tips of radius $50 - 100$ nm of precise geometry that move only in the z-direction. Berkovich indenters,[341] three-sided pyramid shapes with a face angle of 65.27°, are most common, but spherical, conical, and cube corner indenters are also used.[340] Determination of precise tip geometry and thus the projected contact area with the surface (which can be measured by microscopy) is an important consideration for any nanoindentation experiment.[342]

In order to bring the spatial resolution of the measurements closer to truly molecular length scales, atomic force microscopes (AFMs) can be used for nanoindentation in lieu of commercial nanoindenters. The mechanical measurements by AFM typically have lower force-resolution relative to designated nanoindenters, however, due to the large compliance of the cantilever, possible tip movement in the x–y plane, and lack of well-defined geometry of conventional silicon tips.[339] Nonetheless, in addition to higher spatial resolution, AFMs provide access to lower force ranges (sub-pN), which are advantageous for the characterization of very soft polymers and gels, and it is possible to precisely characterize the real shape of the indenter-tip contact area through imaging. As a result, there is ongoing development of AFM for use in nanoindentation.[342,343]

Nanoindentation characterization of polymeric materials requires the consideration of several major hurdles: (a) pile-up, viscoelasticity, and (c) adhesion.[340,344] When the indenter contact induces plastic deformation (as is more common in brittle networks, glasses, and semi-crystalline polymers), the sample material can either pile up or sink in at the edges of the contact area, changing the contact depth h_c in relation to the total indentation depth h_{max}, where with material pile-up, $h_c/h_{max} > 1$, and with material sink-in, $h_c/h_{max} < 1$. As such, the calculated contact area of the indenter is not accurate[340] resulting in an overestimation or underestimation of the material stiffness by up to 60%.[345] AFM or SEM can be used to observe the actual shape of the indenter contact area for fully plastic samples or more generally, numerical finite-element simulation can account for pile-up effects as well as sample adherence to the tip.[340,344,345] Spherical indenters, in particular, are occasionally used to reduce pile-up and for samples that require a small penetration depth;[346] corrections to the standard analysis procedure[341] for use with a spherical indenter are readily available.[347]

Viscoelasticity further complicates nanoindentation data collection and analysis,[344,348] since the measured hardness and modulus are loading-rate dependent.[293,349] Various models have been developed to analyze the load–displacement data under both load-controlled and displacement-controlled conditions to account for the viscoelastic behavior.[344,350,351] For example, one recent study uses a range of loading rates to obtain the creep compliance and relaxation modulus of a sample.[352] Alternatively, oscillation of the indenter shaft can be superposed at a relatively high frequency (so-called Dynamic Indentation Testing or Continuous Stiffness Measurement), which allows the stiffness of the material to be characterized as a function of time and indentation depth.[293,353] Even with this advancement in instrumentation, obtaining reliable nanoindentation data from polymeric samples and interpreting such data remains difficult, particularly with very soft samples and samples that adhere to the indenter tip.[293,351,353] One must also be aware of the effects of sample microstructure, especially in regard to structures with dimensions on the order of the indenter tip.[293] Additionally, a related challenge is that the poroe-

lastic time (characteristic relaxation time due to fluid flow through the swollen deformable medium) is reduced with the decrease in length scale from the macro- to nanoscale and can become comparable to the viscoelastic time scales of the sample for polymeric gels, contributing significantly to the observed modulus and hardness.[354–356]

Adhesion between the sample and the tip can also complicate the analysis of nanoindentation data, but forms the basis of adhesion testing such as the Johnson–Kendall–Roberts (JKR) method,[357] which has been widely utilized for measuring the adhesive properties of an elastomer with various surfaces. It is particularly powerful for determining the modulus and adhesion energy of low-modulus solids. This method is qualitatively similar to the fracture experiments discussed below. Two surfaces (both elastomers or an elastomer with another substrate) are brought together and the force needed to pull them apart is measured.[358–362] Similar methods are available for characterization of the friction and lubrication between elastomeric surfaces under shear.[363]

5.2 Fracture

A number of molecular structural and dynamic details are correlated with the fracture energy of polymer networks. The fracture, or tearing, energy Γ is a measure of the intrinsic resistance to crack propagation in a material. This energy is equal to the strain energy release rate, G, that drives crack propagation. Despite its designation as a release "rate," G characterizes the potential energy U_σ that is lost per area A, on one face of the crack:[364]

$$G = -\frac{\partial U_\sigma}{\partial A} = -\frac{\partial \left(U_{\text{el}} - U_{\text{w}}\right)}{\partial A} = \Gamma \qquad (5.14)$$

where U_{w} is the external work input and U_{el} is the stored elastic energy. Griffith first proposed that crack propagation could be related to the newly created surface energy per unit area.[365] While this simple theory successfully explained the fracture of some materials,[365] it significantly underestimated the threshold for crack propagation in rubbery polymer networks.[366] Rivlin and Thomas corrected for this deficiency, proposing that the free energy per unit area for crack propagation should be the characteristic energy of tearing instead of the surface energy.[367] Evidenced by experiments, the fracture energy Γ has a critical value Γ_0, below which the crack cannot propagate. Lake and Thomas incorporated molecular level details of polymer networks in the absence of structural heterogeneities, entanglements, or other dissipative processes.[368] The Lake–Thomas theory predicts that the critical fracture energy Γ_0 is related to the number of bridging strands per unit cross-sectional area β and the energy $\hat{U}_{\text{break}}$ of a single bridging-strand breaking event,

$$\Gamma_0 = \beta \hat{U}_{\text{break}} \approx \nu_{\text{eff}} R_0 n U \qquad (5.15)$$

where R_0 is the effective end-to-end displacement of an average elastically active network sub-chain in its undeformed state, ν_{eff} is the number density of elastically active sub-chains, n is the number of repeat units in the average elastically active bridging strand, and U is the energy stored in each repeat unit at the time of rupture.[368]

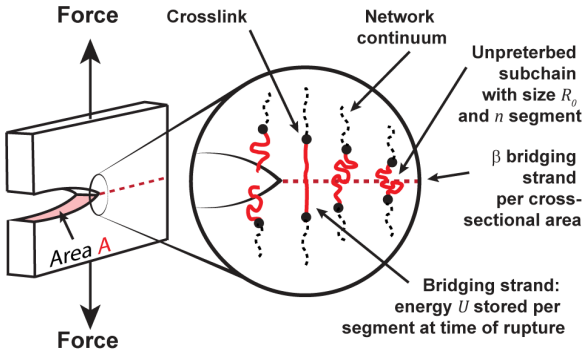

Figure 23: Schematic illustration of crack propagation at the crack tip, creating new surface of area A (red shaded area). Inset: Molecular illustration of cross-links (black dots), bridging strands (thick red lines), and network continuum connecting the bridging strands (black dashed lines) at crack propagation plane (red dashed line). Figure adapted with permission from Ref. 92. Copyright © 2019 American Chemical Society.

The Lake–Thomas theory has been used successfully to interpret experimental measures of

Γ_0,[369–371] but it is based on a set of limiting assumptions and the equations only capture a very simple ideal situation. Interest in tear-resistant networks has sparked a current interest in further modifications for quantitative and predictive use in real polymer networks. For example, the energy U has historically been widely treated as the bond dissociation energy, but recent principles of covalent mechanochemistry have been applied to show that this approximation leads to a significant overestimate of U.[92] In addition, the original Lake–Thomas theory assumes that all of the energy relevant to $\hat{U}_{\text{break}}$ is stored in the strands that bridge the propagating crack face; sub-chains that are connected to the bridging strands are not included.[368] Considering the tension is transmitted through cross-links in polymer networks, when a bridging strand is under high tension and is about to break, other sub-chains that are connected to it should also be under tension (albeit less than that of the bridging strand). The elastic energy stored in these strands is also released once the bridging strand is broken and future theories need to account for those contributions to $\hat{U}_{\text{break}}$.

Fracture measurements using a multitude of geometries and conditions have been developed, although rubbery polymers are usually analyzed in pre-notched thin films.[367,369,372] In the trousers test[367] (Figure 24a), the sample is cut into a trousers-like shape with cut length c larger than half the height h_0 of the undeformed state. One leg of the cut sample is clamped stationary, while the other leg is pulled away at a constant velocity v. The applied tearing force f during propagation is recorded, yielding the fracture energy:[367,372]

$$\Gamma = \frac{2\lambda f}{t_0} - W(\lambda)\cdot h_0 \approx \frac{2f}{t_0} \qquad (5.16)$$

where $W(\lambda)$ is the stored elastic energy per unit volume of material when the shaded arms in Figure 24a are at stretch λ, and t_0 is the thickness of the sample in its undeformed state. The observed fracture energy $\Gamma(v)$ depends on the pulling velocity v; slower extension results in lower value of $\Gamma(v)$. The rate dependence can be extrapolated to give a threshold value Γ_0—the critical fracture energy, which is the minimum energy per unit area required for crack propagation to occur, and which corresponds to the critical energy release rate G_c.[367,372]

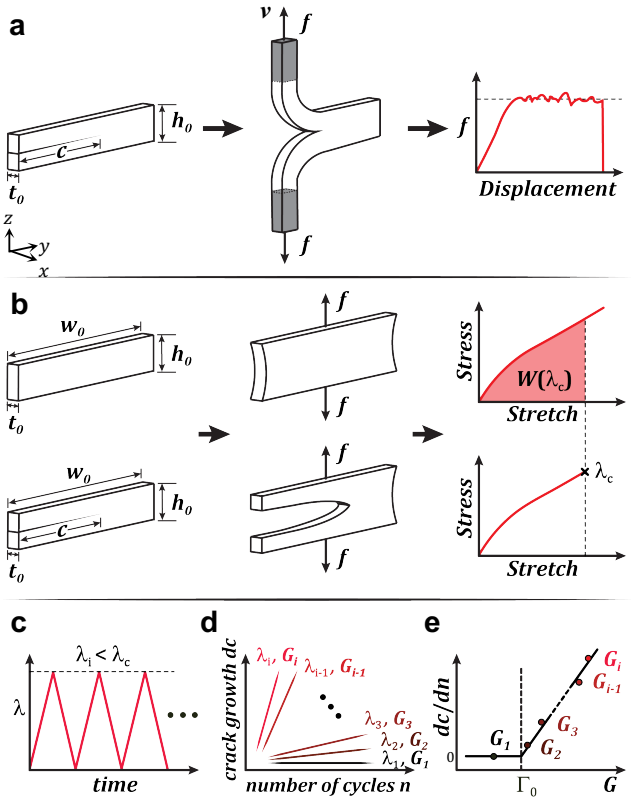

Figure 24: Schematic illustrations of (a) trousers test, (b) pure shear test, (c) cyclic load with stretch amplitude λ_i for specimens i at a constant frequency, (d) crack growth as a function of cycles for all specimens, and (e) crack growth per cycle as a function of energy release rate.

In the pure shear test[367] (Figure 24b), the sample is elongated in one direction ($\lambda_x \equiv \lambda > 1$), shortened in a perpendicular direction ($\lambda_y = 1/\lambda < 1$), and clamped in its third direction. This test requires two samples of identical dimensions with small thickness t_0 and width w_0 sufficiently ($> 2\times$) larger than height h_0. One specimen is un-notched and is pulled to obtain the stress–stretch curve and the stored elastic energy per unit volume $W(\lambda)$ at stretch λ; the other specimen is pre-notched and is pulled to measure the critical stretch λ_c at which the

crack starts to propagate. The fracture energy is[367]

$$\Gamma = W(\lambda_c) \cdot h_0 \tag{5.17}$$

where $W(\lambda_c)$ is the elastic energy per volume at critical strain λ_c (crack starts to propagate). The pure shear geometry is advantageous in steady-state fracture measurements for providing an energy release rate G that is independent of the cut length c when c is sufficiently ($> 2\times$) larger than its half-height $h_0/2$. Fatigue fracture measurements are also benefited from the pure shear geometry,[366,369] where a series of pre-notched specimens ($i = 1, 2, 3...$) are cyclically loaded to different stretch amplitudes $\lambda_i < \lambda_c$ (Figure 24c). For each specimen i, the corresponding $W(\lambda_i)$ and energy release rates $G_i = W(\lambda_i) \cdot h_0$ are calculated and the crack growth dc and total number of cycles n are recorded to obtain the crack growth per cycle $(dc/dn)_i$ (Figure 24d). The crack does not propagate (i.e., the crack growth rate is zero) at small G but begins to propagate above the critical fracture energy Γ_0 (Figure 24e).

5.3 Particle Velocimetry

The flow of polymeric or polymer-containing fluids is central to behaviors that range from industrial to biomedical. Particle image velocimetry (PIV) and particle tracking velocimetry (PTV) are optical techniques for imaging such flow fields of simple and complex fluids.[373–375] In these techniques, tracer particles are introduced into the sample; by following and analyzing the motion of a representative sample of particles, the flow fields can be visualized. The size, density, refractive index, and (existence or non-existence) of fluorescence of the particles must be carefully chosen to follow, but not alter, the flow and to allow sufficient imaging quality. Particles are illuminated by a thin laser sheet, and images are captured and processed.

PIV uses an Eulerian method, determining displacement and velocity by cross-correlation analysis of small subsections between each image frame.[374,376,377] PTV uses a Lagrangian method, tracking the trajectories of independent particles.[374,376,377] Regardless of the image processing method, strain and vorticity can be locally determined from the flow fields. More recently these techniques have been advanced to visualize micron-scale (μ-PIV)[376,378–380] and three-dimensional (3D PIV/PTV)[381,382] flow fields.

These techniques are suitable for inhomogeneous polymer flows,[375,383–388] and therefore useful for polymer processing applications, where polymer flows play important roles. PIV and PTV experiments have enabled investigation of the non-linear rheological behavior of entangled polymers[375,389,390] and transient networks,[391] highlighting strain localization and deformation confined to a shear zone with thickness on the order of the mesh size of the gel. For example, particle velocimetry has been used for analysis of inhomogeneous flows of associative networks, such as peptide- or protein-based hydrogels for drug delivery: the quiescent hydrogel containing therapeutic agents is initially solid-like, flows due to shear-thinning upon injection into the body, and then solidifies again inside the target site. PIV/PTV visualized the flow profile under such a large deformation, indicating a fractured layer of the hydrogel around the interface with the shearing wall (Figure 25).[387,388]

Particle velocimetry can also be used in conjunction with rheometry to verify assumptions of the deformation, such as the "no-slip" boundary condition of the complex fluid against the shearing wall. By viewing the motion of particles at or near the boundary, the existence of slip at the wall (or within a fluid layer on the order of the tracer particle's diameter) can be inferred.[301,392] Finally, information on microscopic structures and molecules inside a flow can be obtained with the aid of optical techniques (e.g., birefringence, X-ray and neutron scattering) in conjunction with PIV and PTV.[375,393,394]

5.4 Mechano-Optics

5.4.1 Stress–Optic Effect: Polarimetry

The stress–optic effect, generally, is the optical activity occurring in response to stress or flow

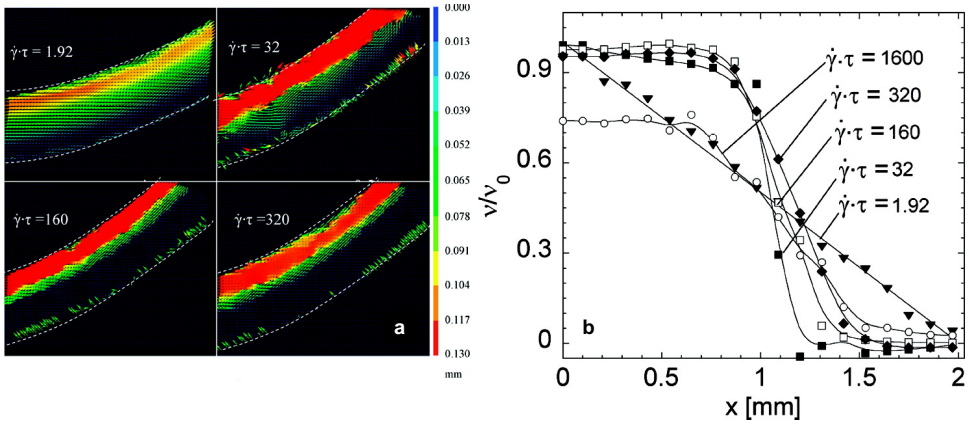

Figure 25: (a) Snapshots of the velocity vector field at steady state for several applied shear rates for a protein hydrogel. The color scale indicates the displacement in mm of tracked particles between two frames with a time interval: 100 s for $\dot{\gamma}\tau = 1.92$, 7 s for $\dot{\gamma}\tau = 32$, 1.4 s for $\dot{\gamma}\tau = 1600$, and 0.6 s for $\dot{\gamma}\tau = 320$. (b) Calculated velocity profiles with $v(x)$ normalized by the velocity of the wall v_0. Figure reproduced with permission from Ref. 388. Copyright © 2003 American Chemical Society.

and can be measured with polarimetry to extract clues regarding the molecular origins of unique stress–strain behavior in a gel or network under strain. Specifically, polarimetry is the measurement of the polarization of transverse waves that have been reflected, slowed down (refracted), or diffracted by the material. Measurable optical activity includes birefringence, the property of having a refractive index dependent on the polarization and propagation direction of light, and dichroism, a loss of transmitted light intensity which depends on the incident polarization state.[393] A sample's optical activity can be caused by both birefringence and dichroism, as well as a variety of other phenomena. Optical techniques are nondestructive, specific, and rapid; they can be used to image the sample like in polarized optical microscopy (Section 4.2.2) or easily be combined with other characterization techniques, as covered in the following section on rheo-optics (Section 5.4.2).[158] While many systems of interest have intrinsic optical signatures, others may require clever molecular design to probe a particular length scale or process.

In polymeric gels, the gelation process is typically not due to a single, easily isolated phenomenon. In many cases, it is necessary to attempt to separate multiple effects which often take place in competition over many length scales in order to extract the physical origins of gelation, shear, or flow behavior. For example, in the case of physical gelation of gelatin, both the formation and lengthening of triple helices contribute to gelation, albeit at different time scales dependent on temperature. The contribution of each in a "fast" and "slow" gelation regime was determined by measuring the specific optical rotation during the gelation process (Figure 26).[395]

5.4.2 Rheo-optics and Rheofluorescence

Rheo-optics combines traditional rheology with optical methods to track the changes in optical properties of a material under stress, correlating rheological behavior to microstructure. These techniques are enabled by micromechanical properties with distinct optical signals resulting from material deformation.[393] Many different experimental techniques fall into the category of rheo-optics, depending on which rheological property (viscosity, modulus, characteristic relaxation time) is of interest, the kinds of optical changes which can be observed (including refraction, absorption, fluorescence, scattering, diffraction, birefringence),[158] and the relevant length scale of interest.

Due to the heterogeneous, hierarchical nature of many gels and networks, rheological data alone is often insufficient to fully understand the material. For example, rheology may

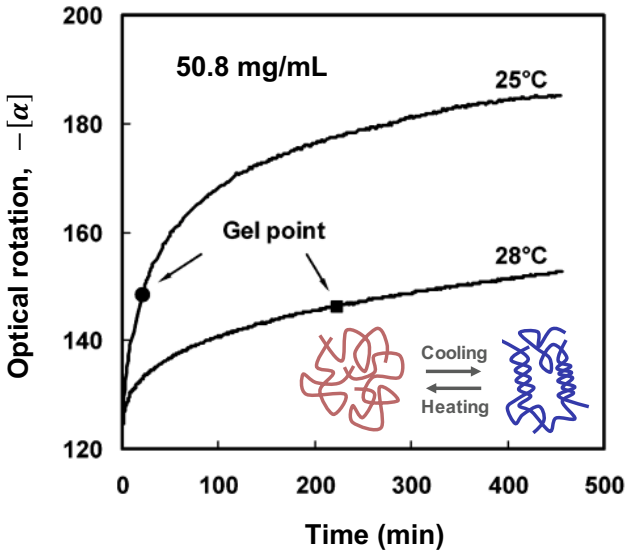

Figure 26: Specific optical rotation $-[\alpha]$ of a 50.8 mg mL^{-1} gelatin solution quenched to 25 °C and 28 °C, indicating "fast" and "slow" helical cross-link formation. Figure adapted with permission from Ref. 395. Copyright © 2003 American Chemical Society.

show when a system reaches the gel point, but an additional optical technique is often needed to quantify the corresponding reaction conversion; or, in an associative system, rheology may demonstrate shear thinning behavior but with no clear indication of the mechanism. Combining rheological and optical techniques, often with a home-built or modified apparatus, can offer critical insight into the physical behavior of both physical and chemical gels, leading to improvements in material engineering capabilities.[393,395–399] One example from a recent study on shear-thinning behavior in an associative metal-coordinated gel utilized rheo-fluorescence with a system in which un-associated bonds fluoresced, allowing for a direct measurement of physical bond dissociation behavior under nonlinear shear stress.[397]

5.4.3 Stress Distribution Imaging

Recent advances in mechanochemistry has seen the development of myriad "mechanophores;" molecules that respond to a stress or strain stimulus through an easily decipherable chemical change.[90,400,401] Mechanochromophores have been incorporated into a variety of polymer gels, with colorimetric (changes in visible/UV light absorbance or chemiluminescence) response tracking with the breaking of bonds and the release of chain tension in response to bulk material deformation, swelling, or high-intensity ultrasound.[401–409] Monitoring the activation of mechanophores during material deformation thus allows direct visualization of the chain tension distribution within a sample with micron-level spatial resolution.[410–412] One recent study examined the bond breaking patterns during swelling of PMMA using a mechanoluminescent molecule with a transient signal; unlike the signal of fluorescent mechanophores which accumulate additively over time, these short burst-like flashes allowed for visualization of singular bond breaking events.[403] Mechanochromic mechanophores are a visually pleasing method for the optical quantification and mapping of stress distribution in a material under stress, tension, or compression. As such, they are often incorporated into materials for use in rheo-optical set-ups and continue to be applied for novel uses and visualization techniques.

While stress imaging can give clues about fundamental mechanisms of stress relaxation or dissipation, it is also employed in practice to detect imminent failure by quantifying gradual bond breakage before the material macroscopically fails, which is of obvious utility in many critical load-bearing applications. On a macroscopic measurement level, stress distribution imaging may involve large, fabricated, model networks where individual "bonds" can be observed with the naked eye,[413] or a paint splatter method, where the position of paint spots or other visual markers on the surface of a material are tracked as the material deforms, imaging the strain in the material. The latter of these two methods is particularly useful in industrial coating and extrusion processes. In all of these applications, an advantage of the mechanophore approach is that it reports on the mechanical state of individual molecules within the bulk material, allowing molecular behavior (or the distribution of molecular behaviors) and its dependence on the chemical structure of the

polymer network to be assessed quantitatively.

5.5 Microrheology

Microrheology is the study of the viscoelastic properties of small volumes of materials probed through thermal or forced excitations of colloidal particles.[414,415] The technique is divided into passive microrheology, in which the probe experiences Brownian motion caused by thermal fluctuations, typically in equilibrium; and active microrheology, in which probe motion is generated by an external force and may be extended to the non-linear viscoelastic regime. The central assumption of microrheology is that the motion of the particles is determined by the mechanical properties of the surrounding medium. Mean-square displacement data of the probe are analyzed over time to extract frequency-dependent viscosity or elastic moduli by using the generalized Stokes–Einstein relation (GSER):[416]

$$\tilde{G}(s) = \frac{k_{\mathrm{B}}T}{\pi a \left\langle \Delta\tilde{r}^2(s) \right\rangle} \tag{5.18}$$

where $\tilde{G}(s)$ is the Laplace transformed relaxation modulus, $\Delta\tilde{r}^2(s)$ is the Laplace transformed mean-square displacement, s is the Laplace frequency, $k_{\mathrm{B}}T$ is the thermal energy, and a is the hydrodynamic radius of the spherical probe. The GSER above can be extended by making an analytic continuation ($s = i\omega$) and taking a Fourier transformation to obtain the complex modulus $G^*(\omega)$:[417]

$$G^*(\omega) = \frac{k_{\mathrm{B}}T}{\pi a i\omega \mathcal{F}\{\langle \Delta r^2(\tau) \rangle\}} \tag{5.19}$$

where $\mathcal{F}\{\langle \Delta r^2(\tau) \rangle\}$ is the Fourier transformed MSD as a function of the Fourier time τ. The time-domain response of the material can also be calculated using a Laplace transformation by invoking the continuum viscoelastic identity in Laplace space $s\tilde{J}(s)\tilde{G}(s)$ to extract the compliance $J(t)$:[418]

$$J(t) = \frac{\pi a}{k_{\mathrm{B}}T} \left\langle \Delta r^2(t) \right\rangle \tag{5.20}$$

which is directly proportional to the mean-square displacement. The compliance $J(t)$, as well as storage (G') and loss (G'') moduli calculated from $G^*(\omega)$, can be compared directly against macrorheology (Section 5.1.4) In some instances, the viscoelastic properties measured from microrheology agree well with those obtained from macroscopic rheological measurements, but in many situations, microrheology does not appear to fully capture the macroscopic viscoelastic properties due to length-scale dependent dynamics in heterogeneous and non-ergodic samples.[419–421] Further, both the probe and soft material must meet the underlying assumptions of both components of the GSER; importantly, the probe particles should not interact with, bind to, or repel the sample, as this would affect long-time, large length-scale displacement.[422,423]

One approach to mitigate artifacts and increase agreement between microrheology and macrorheology has been the introduction of two-point microrheology. This method studies the cross-correlation of two tracer particles in the same sample. Instead of measuring the MSD of individual particles, the relative displacement between two particles is measured,[424]

$$\tilde{G}(s) = \frac{k_{\mathrm{B}}T}{2\pi R \left\langle \Delta\tilde{r}_1(s)\Delta\tilde{r}_2(s) \right\rangle} \tag{5.21}$$

which depends on the distance between the tracers R, assuming $R \gg a$.

Microrheology is often an ideal technique for studying polymeric networks due to its exceptional sensitivity and ability to characterize weak, incipient gels over a wide frequency range, track rapid kinetics of the sol to gel transition, and probe small quantities of material that would make macroscopic rheology challenging or impossible.[425,426] It has been shown that microrheology measurements on entangled and cross-linked networks can agree with macroscopic rheology, making it a valid alternative when material is limited.[420] Microrheology is particularly useful for measuring the gel point and critical exponents of physically or chemically cross-linked gels, as well as prob-

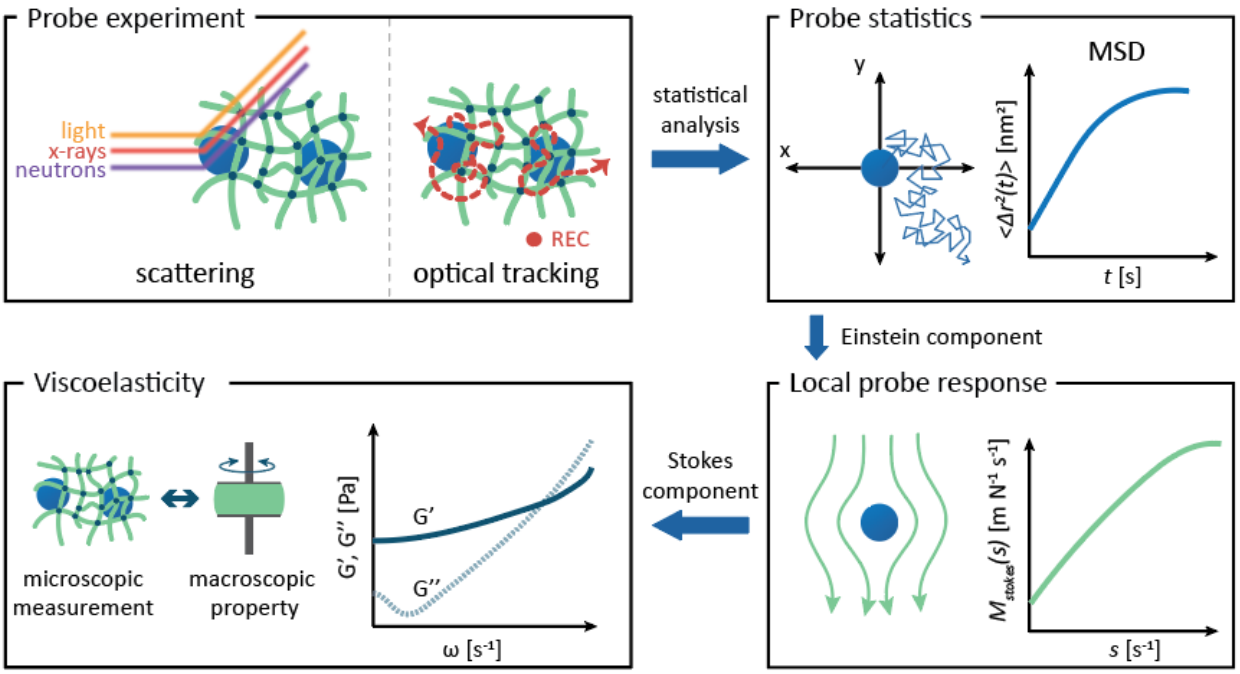

Figure 27: The main underlying principle of passive microrheology is the generalized Stokes–Einstein relation, in which the Einstein component, using the fluctuation–dissipation theorem, bridges the thermal, stochastic fluctuations of a probe particle to its frequency-dependent complex mobility $M_{\text{Stokes}}(s)$, which the Stokes component further connects to the rheological properties of the material in which it resides.[414]

ing position-dependent properties in specific regions of heterogeneous materials, such as phase separated or incipient gels.[425,427–432]

Microrheology measurements can be conducted using any experimental method which monitors fluctuations of particles as a function of time, including real-space methods, most commonly particle tracking microscopy (using high-speed optical or fluorescence microscopes) and its many variations, as well as Fourier-space methods like differential dynamic microscopy[433] or scattering techniques to be discussed below, such as dynamic light spectroscopy (DLS, Section 5.5.1), diffusing-wave spectroscopy (DWS, Section 5.5.2), and more recently X-ray photocorrelation spectroscopy (XPCS, Section 5.5.3).[414] The typical analysis pathway for passive microrheology is shown in Figure 27. While microrheology is advantageous for sensitive measurements on small volumes of valuable samples, care must be taken to ensure samples are clean and dust-free, as any additional micron-sized impurities may convolute the results.

5.5.1 Dynamic Light Scattering

Dynamic light scattering (DLS) excels at characterizing colloidal and nanoparticle systems; in soft matter it has been used to determine the size and diffusion coefficient of microgel particles and of interacting building blocks for supramolecular polymer networks.[434–437] DLS utilizes fluctuations in the intensity of scattered, monochromatic light to probe dynamic properties of matter at length scales ranging from 100 nm − 1 mm and time scales of 10^{-6} − 10 s.[438] Like many of scattering spectroscopy techniques in this section, DLS measures the intensity correlation function of scattered light, normalized as:

$$g_2(q,t) = \frac{\langle I(0)I(t)\rangle}{\langle I(t)\rangle^2} = 1+\beta \exp\left[-\frac{q^2\langle \Delta r^2(t)\rangle}{6}\right] \tag{5.22}$$

where $I(0)$ and $I(t)$ are intensities at time 0 and a delayed time t at a given scattering vector q, corresponding to the MSD $\langle \Delta r^2(t)\rangle$ at time t.[434] The intensity correlation function

captures dynamic fluctuations experienced by the scatterer due to Brownian motion. By analyzing the time-resolved scattering intensity, the mean-square displacement of the scatterers can be calculated and related to the viscoelastic properties of the sample by the GSER (eqs. 5.18, 5.19, and 5.20).[438]

DLS requires a material with strong scattering signal and analysis of DLS assumes only a single scattering event, so scatters are typically dilute in a homogeneous matrix (either polymer in solvent as in Section 2.2.6 or a microrheology experiment with tracer particles in dense networks). The scattering intensity fluctuates due to local fluctuations in concentration caused by the thermal motion (diffusion) of the polymer chains in and out of a given volume $\sim 1/q^3$. In the case of polymer networks, fluctuations may be suppressed due to entanglements or the formation of cross-links in a gel restricting motion on the size of the colloidal tracer particle (Figure 28). Particles with larger radii relative to the network mesh size undergo slower fluctuations, resulting in a longer decay time in the auto-correlation curve.

The technique has also been used to probe the sol–gel transition in a variety of systems[439–444] with a power-law behavior of the intensity correlation function

$$g_2(q,t) - 1 \propto t^{-\mu} \tag{5.23}$$

with a single self-similar exponent $0.2 \leq \mu \leq 0.9$ at the gel point (similar to the stress relaxation exponent u observed at the gel point in macrorheology, Section 5.1.4), implying a self-similar or fractal structure of the clusters of the incipient gel. However, due to the non-ergodic nature of solutions undergoing gelation, the time and ensemble-averaged intensity correlation functions begin to deviate at the onset of gelation as a result of significant inhomogeneities from pre-gel clusters. Because of the challenges in accurately interpreting sol–gel DLS data such as multiple scattering, detailed quantification of dynamic behavior near the gel point is typically done with a related light scattering technique, diffusing-wave spectroscopy.

5.5.2 Diffusing-Wave Spectroscopy

Diffusing-wave spectroscopy (DWS) is a light scattering method which accounts for strong multiple scattering events. As in DLS experiments, an incoming beam travels through a sample cell, but scatters off of many particles before detection; unlike DLS, the time scale does not depend on the angle of detection but rather on the sample cell geometry and path length distribution.[445,446] The scattered light intensity is monitored over time, and the auto-correlation function is used to extract quantitative information such as the mean-square displacement of tracer particles and the complex elastic modulus of the material. DWS is a common alternative to optical tracking for microrheology measurements (Section 5.5), and is preferable in some cases due to its higher sensitivity (superb statistics from many probes and multiple scattering compared to a single probe particle) and broader range of accessible length scales (down to $\lambda/1000$).[445] While DWS is often easier to implement experimentally than DLS, the user must ensure that all light is multiply scattered, which is often done by adding probe particles. Selection of the probes is important: proper size ($0.5 - 2$ µm), material, and concentration are necessary to minimize interactions of the particles with the system or have noticeable effects on the rheological properties being measured.[447] Static light scattering (Sections 2.2.6 and 4.3) can be used to verify that the tracer particles are the dominant source of scattering, are isotropically dispersed in the sample, and that their mean-square displacement scales inversely with their radius.

DWS was originally developed as an analysis method to expand DLS into the limit of multiple scattering events. Initial studies done on colloidal glasses[446] were extended to probe viscoelastic behavior[416] and creep compliance[448] over a wide frequency range, providing characterization in good agreement with macroscopic mechanical measurements. In addition to elasticity measurements, DWS has been employed to measure the gel point in many polymeric systems; this is advantageous due the high sensitivity of the probe particles and the small sample

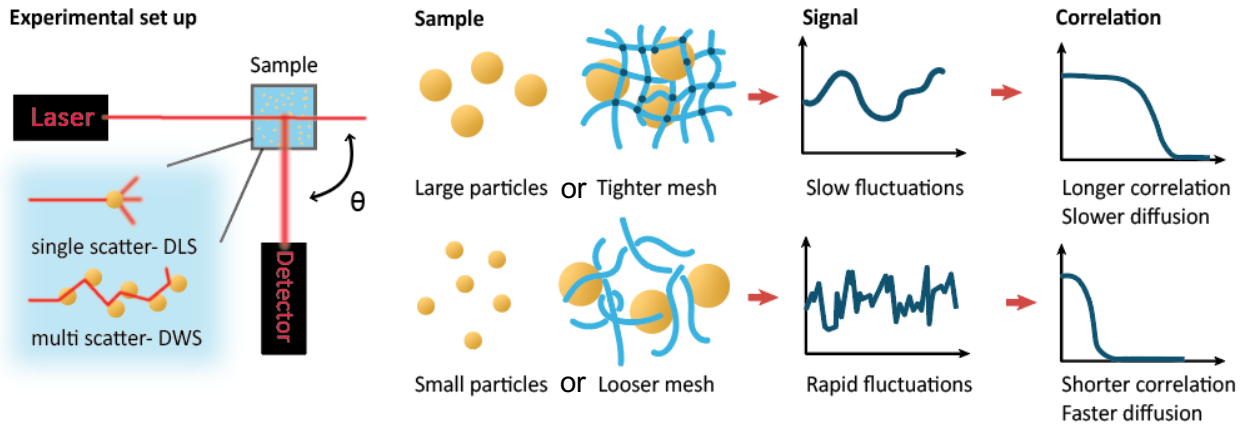

Figure 28: In light scattering spectroscopies, including DLS and DWS, the intensity of scattered light is detected at a specified angle θ, typically 90°. The intensity auto-correlation over time is dependent on dynamic fluctuations and can be analyzed to yield hydrodynamic radii and MSD values in the case of DLS, and further analyzed to quantify viscoelastic moduli or creep compliance in DWS.

volumes required.[449,450] DWS can also be paired with a complementary spectroscopic technique such as UV-Vis or FTIR to couple gel point and conversion measurements.[450]

5.5.3 X-Ray Photoelectron Correlation

X-ray photon correlation spectroscopy (XPCS) utilizes a coherent synchrotron X-ray beam to measure the intensity correlation function, probing slow dynamics in condensed matter systems on 1 Å − 1 µm length and $10^{-6} - 100$ s time scales.[451] The speckle pattern formed when X-rays interact with randomly distributed scatterers (typically in soft matter systems due to added probe particles, but can also be high X-ray contrast components of the material) exhibits intensity variations which are directly related to order parameter fluctuations in real space. Analysis of the intensity correlation function yields information on nanoscale dynamics such as diffusion or relaxation processes. Advantages of the technique include no complication from multiple scattering, an opportunity to test opaque samples, and an experimental window not available with visible light or neutron scattering techniques. The sample must have adequate X-ray contrast, which in soft matter systems often requires the addition of particles. Some samples, particularly soft matter or biological systems, may be badly damaged when exposed to the beam for long periods of time, limiting the longest accessible time scale.

XPCS is a relatively new technique which has been used extensively in colloids and block copolymers, while applications to polymer networks have recently emerged.[451–453] With the addition of tracers such as silica or gold nanoparticles, XPCS measurements have provided novel microscopic characterization of gelation and entangled dynamics.[454–456] The technique has also recently been recognized as a potential form of microrheology, using MSD data derived from the auto-correlation function to yield viscoelastic measurements. This is a promising avenue for future work, especially in systems which are not ideal candidates for traditional DWS or optical particle tracking methods, which preclude opaque samples.[457,458]

5.6 Nanorheology

Like its microscopic relative, nanorheology probes viscoelastic properties of a material through analyzing the motion of a nanoscale probe embedded in, or pressed onto, a material. Specifically, this technique looks at the rheological response of materials in confined geometries and involves adhesion, friction and lubri-

cation between particles and surfaces.[459] Two major experimental techniques are surface force apparatus (SFA) and atomic force microscopy (AFM), which measure the normal and lateral forces between two curved surfaces (SFA) or between a tip and a flat surface (AFM) with a high force sensitivity. AFM provides improved force sensitivity while SFA measures absolute separation distance and surface deformation, which then lead to rheological properties and structure-property relationships of confined, complex soft materials.[459]

The sub-nanometer length scales accessible with nanorheology (< 0.1 nm resolution with SFA) make this technique suitable for probing the mesh size, relaxation times on monomer or Kuhn length scales, and viscoelastic properties in polymer gels and networks.[460] Recent work has included improved analysis of AFM data and application to probing biomaterials;[461,462] model studies on entangled and supramolecular networks using magnetic particle nanorheology;[460,463] as well as accompanying molecular simulations probing local viscoelasticity of an entangled melt and scaling theory of storage and loss moduli as a function of length scale.[464,465]

Active particle methods, (i) optical tweezer nanorheology, which employs lasers to optically trap dielectric particles and measures the mean-square displacement, as well as (ii) magnetic particle nanorheology, which employs oscillating magnetic fields to drive magnetic nanoparticle motion and measures the AC susceptibility, also enable quantification of rheological properties on the nanometer scale.[85,466] Optical tweezers can be used to exert forces in excess of 100 pN in the range of $1 - 100$ nm with sub-nanometer accuracy and sub-millisecond time resolution. However, the lasers used for optical trapping lack selectivity and exclusivity, while also resulting in local heating, which can affect the sample viscosity. Magnetic tweezers are more straightforward to implement and can impose forces in excess of 1 nN across a wider length scale but are not nearly as versatile in nanorheology experiments.[85]

5.7 Nuclear Magnetic Resonance

Emerging nuclear magnetic resonance (NMR) spectroscopies, due to the broad range of accessible time scales ($10^{-12} - 10^{3}$ s), are ideally suited for characterization of polymer dynamics in addition to the characterization of structure as discussed in Sections 2.1.1, 2.2.1, and 4.5.

5.7.1 NMR Relaxometry and ^{1}H Field-Cycling NMR

NMR relaxometry measures how an excited magnetic state returns to its equilibrium distribution and can be used to study exchange dynamics on the milliseconds to hundreds of seconds time scale. The longitudinal or spin–lattice relaxation time T_1 is related to inter-segment and intra-segment molecular motions modulating the magnetic dipole–dipole interaction of ^{1}H–^{1}H spin pairs (or other NMR-active nuclei of interest). The value of T_1 can be easily determined by fitting the signal buildup curve saturation recovery experiment with a variable relaxation delay to an exponential. The transverse or spin–spin relaxation time T_2 can be measured in an analogous manner, by quantifying the decay of the magnetization perpendicular to the magnetic field.

^{1}H field-cycling NMR relaxometry (FC-NMR) measures the dependence of the proton spin-lattice relaxation rate, $R_1 = 1/T_1$, on the Larmor frequency, ν or $\omega = 2\pi\nu$. This is also referred to as the nuclear magnetic relaxation dispersion (NMRD), which reflect the spectrum of reorientational and translational dynamics of polymer segments.[467,468] Time–temperature superposition (TTS, applicable for polymers at temperatures exceeding their glass transition temperature, $T \gg T_g$) enables transformation of R_1 measurements to a susceptibility representation:

$$\chi_{\mathrm{NMR}}''(\omega) = \omega R_1(\omega) \tag{5.24}$$

and the construction of master curves. Such master curves enable deconvolution of contributions from reorientational and translational motions to relaxations at different frequencies. Recently, FC-NMR has been applied in this man-

ner to investigate the glassy behavior and restrictions of cross-links on the polymer dynamics of a series of industrially relevant rubbers across three decades of frequency ($0.01 - 100$ MHz).[469–471]

5.7.2 Pulsed-Field-Gradient NMR

Pulsed-field-gradient NMR (PFG-NMR) provides a powerful technique to probe the self-diffusion of NMR-active nuclei on the micrometer length and millisecond time scales. PFG-NMR is based on the dependence of the Larmor frequency on the amplitude of the applied magnetic field. Magnetic-field-gradient pulses of stimulated echoes are added, which process the magnetic spins according to their Larmor frequency. If the molecules do not change their positions during the time of diffusion measurements, the signal retains its maximum intensity; otherwise, the signal loses part of its intensity and the resulting signal attenuation gives a measure of the movement of the molecules. The attenuation of the echo ψ measures the diffusion coefficient D according to

$$\psi = \exp\left(-q^2 D t\right) = \exp\left[-\gamma^2 g^2 \delta^2 D \left(\Delta - \frac{\delta}{3}\right)\right] \tag{5.25}$$

where γ is the gyromagnetic ratio, g is the gradient strength, δ is the gradient pulse length, Δ is the interval between gradient pulses, $t = \Delta - \delta/3$ is the diffusion time, and $q = \gamma g \delta$ is analogous to a scattering vector.[472]

PFG-NMR is experimentally very similar to neutron spin echo (NSE, Section 5.8) spectroscopy. Both measure dynamical information through the procession of spins in an applied magnetic field. The time and length scales of measurement and correspondingly of the information measured, however, are well-separated. NSE is capable of measuring polymer dynamics at the 1 Å $-$ 1 µm length and $1 - 1000$ ns time scales, while PFG-NMR excels at measuring dynamics on the $1 - 100$ µm length and $1 - 100$ ms time scales. The principal application of PFG-NMR to soft materials is in the measurement of self-diffusion of polymers, solvents, or ions, according to the nuclei of interest. The long-range self-diffusion of high-molecular-weight PDMS chains in a melt have been measured by PFG-NMR and the calculated monomeric friction coefficient was found to be in agreement with data from viscosity and quasielastic neutron scattering measurements.[473] Diffusion measurements of water through hydrogels or ions through solid polymer electrolytes are also common.[474–477] One interesting application for polymer networks is in measuring the diffusion of junctions or strands in reversible networks,[478] such as the motion of metal ions in metallo-cross-linked polymeric ionic liquids.[479]

5.7.3 Diffusion-Ordered NMR Spectroscopy

Closely related, diffusion-ordered NMR spectroscopy (DOSY) techniques are commonly used for facile measurements of small-molecule or polymer diffusion coefficients in solution.[480–482] In dilute solution, the molecular weight of polymer strands can be obtained by correlation with the measured diffusion coefficient (Section 2.2.1).[480–483] Further, as discussed previously in Section 4.7, the diffusion of molecular probes within polymer gels can provide information related to network structure on various length scales.[239,241,484] DOSY has also proven valuable for characterization of pre-gel components prior to, and during network formation, for example, in the analysis of gel point for optimization of network formation conditions.[485,486] The diffusion of the polymer strands and junctions themselves in reversible networks or the diffusion of probe particles (commonly polystyrene latex particles of different sizes) in covalent networks can be measured using this technique. The latter is closely related to nanorheology (Section 5.6), with a focus on the terminal diffusion.

5.7.4 Rheo-NMR

Recent advances in instrumentation have enabled the simultaneous characterization of polymeric materials with NMR and rheometry (Section 5.1.4, termed rheo-NMR. Concurrent steady or dynamic rheological measurements

and time-domain NMR spectroscopy can provide information about the relationship between polymer mobility, orientation or crystallization on sample deformation or mechanical properties. For example, shear induced changes in entanglement dynamics, shear history effects on crystallization, and polymer-inorganic filler interactions and their effect on crystallization have all been characterized through rheo-NMR techniques.[487–489] Rheo-NMR has many potential applications in the study of reversible gels to understand the coupling between macroscopic mechanical deformation and molecular cross-linking and dynamics. For example, rheo-NMR has shown that shear reduces the intermolecular linkages between κ-carrageenan, a seaweed extract that undergoes thermoreversible gelation in solution and is used as a polysaccharide thickener in the food industry.[490]

5.8 Neutron Spin-Echo

Neutron spin-echo spectroscopy (NSE) is an inelastic time-of-fight scattering technique used to directly probe material dynamics at 1 Å − 1 µm length and 1 − 1000 ns time scales.[491] The technique measures the Fourier transform of the dynamic structure factor $S(q, \omega)$, termed the intermediate scattering function, $I(q, \tau)$, which is a function of the momentum transfer vector, q, and Fourier time, τ.[492] The intermediate scattering function is the spatial Fourier transform of the van Hove function $G(r, t)$, which is the real-space dynamical correlation function characterizing the spatial and temporal density distributions in the fluid. The basic principle of NSE is that if a neutron with a polarized spin rotates anticlockwise and clockwise by the same amount it should return to its original orientation provided the speed of the neutron is constant. If the velocity changes due to inelastic scattering off of a molecule, the spin will not return to the same orientation and the difference in energy will be measurable. Similar to the Hahn echo used in NMR, NSE relies on the de-phasing and re-phasing of neutron spins over time using a spin-echo—the refocusing of spin magnetization with a pulse of electromagnetic radiation. A typical experimental set up is show schematically in Figure 29. Advantages of NSE include the ability to directly measure in the time domain without the need of Fourier transforms, which avoids some of the deconvolution necessary in other scattering techniques and allows for a more direct interpretation of the data. As in SANS (Section 4.3), strategic deuterium labelling can provide information on the microscopic fluctuations of particular substructures of interest, such as the junctions in a polymer network. Disadvantages of the technique include the long counting times and large sample volumes necessary to obtain adequate signal.

As the dynamical complement to SANS (Section 4.3), NSE is ideally suited to provide detailed information on the motion of macromolecular objects on length scales several orders of magnitude smaller than those accessible with FRS (Section 5.9 below).[493] NSE studies have established microscopic evidence for entanglement tube effects and contour length fluctuations in reptation theory[494–496] and measured the extent of junction fluctuations in cross-linked polymer networks.[497–499] More recent studies have examined dynamics in novel network types, including polyelectrolyte double networks[500] and networks with slide-ring cross-links.[501] Future studies could further delve into networks with dynamic cross-links or systems under shear, such as a recent contribution probing nanoscale dynamics in flowing liquids.[502]

5.9 Forced-Rayleigh Scattering

Forced-Rayleigh Scattering (FRS) is ideally suited for measuring slow dynamical processes such as the self-diffusion of polymer chains. Molecule displacements are quantified over micron-level length scales, enabling diffusivity measurements ranging $(10^{-17} - 10^{-5})$ $\mathrm{cm^2\,s^{-1}}$.[503] FRS is a holographic grating technique in which the user first generates a grating with two intersecting laser beams and then subsequently measures the diffracted light intensity as the gradient diffuses, as shown schematically in Figure 30. The resulting decay curve is used to determine the diffusivity of a molecule of in-

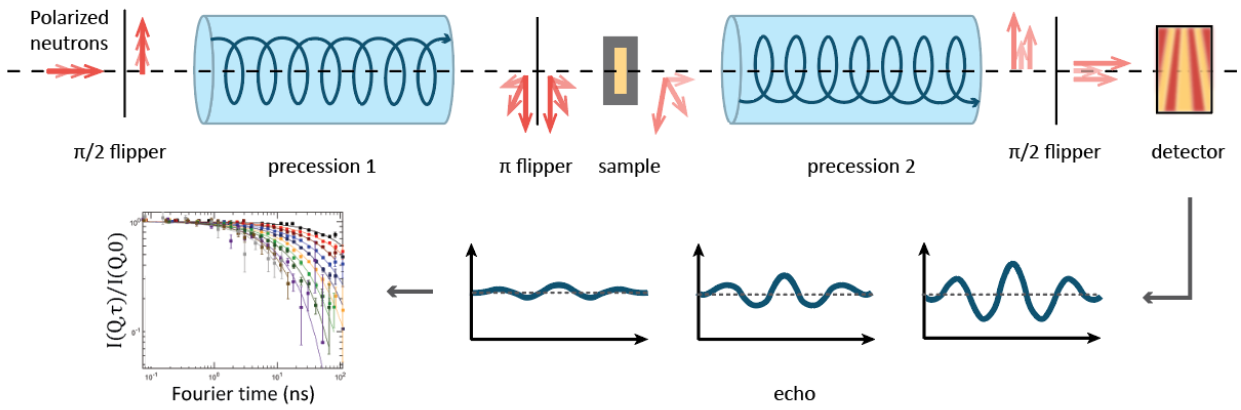

Figure 29: Neutron Spin-Echo Spectroscopy. In a typical NSE experiment, initially polarized neutrons are flipped 90° into the x–y plane to proceed through a Larmor precession. Following an 180° flip the neutrons interact with the sample and complete a second Larmor precession. If inelastic scattering occurs, this second precession will fail to completely realign the neutrons, resulting in a detectable scattering pattern. A final spin flip aligns the neutrons towards the detector for analysis. Echo signals over time are translated directly to an intermediate scattering function. Data from Ref. 493.

terest (the tracer) through another material of arbitrary complexity (the matrix). Calculated variables such as the relaxation time constant and diffusion coefficient are extracted by fitting an exponential function to the intensity decay curve.[503–510] The matrix can be almost any material, including polymer solutions, melts, and associative or covalent networks. However, the tracer must be labelled with a photosensitive dye; tracers are usually dilute within the matrix (tracer diffusion) or selectively labeled matrix components (self-diffusion).[509,510]

FRS studies on associative polymer networks have probed diffusivity behavior over four decades of mean-square-distance, resulting in the discovery of a region of anomalous super-diffusion below a specific length scale, attributable to a diffusing species in dynamic equilibrium between a fast-diffusing molecular state and a slow-diffusing associated state.[493,509–513] Despite the requirement of a photochromic dye, FRS is a versatile technique uniquely capable of probing slow diffusion processes over a range of length scales in a variety of isotropic and oriented soft materials.

5.10 Dielectric Spectroscopy

Dielectric spectroscopy is a sensitive technique for probing molecular relaxations and has been used extensively to develop structure–property relationships in polymers.[514–516] A principal advantage is the ability to measure the molecular motions over a wide temperature window and a broad dynamic range ($10^{-2} - 10^{9}$ Hz), covering many decades in time scales with a single bench-top technique. The technique works by measuring the electrostatic fluctuation of molecular dipoles and charges, as the complex permittivity:

$$\varepsilon^*(\omega) = \varepsilon'(\omega) - i\varepsilon''(\omega) \qquad (5.26)$$

as a function of angular frequency ω of the applied electric field.[514,517] With a knowledge of the molecular structure, the fluctuation of dipole moments can be related to different relaxation processes of functional groups, segments, and even entire polymer chains. This spectrum of relaxations can be further interpreted as a probe for the structure and dynamics of different components of the material.

Since these molecular motions are affected by cross-linking in polymer networks, dielectric spectroscopy can be a sensitive tool to as-

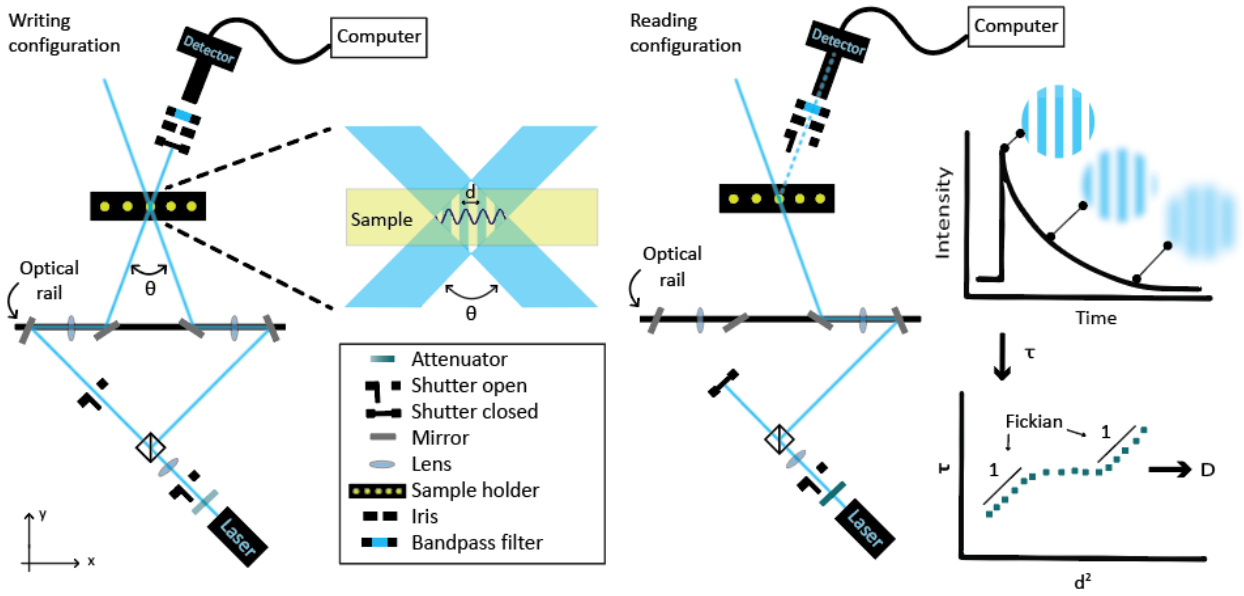

Figure 30: Forced Rayleigh Scattering. The writing configuration, shown on the left, uses the interference pattern of two intense, mutually coherent laser beams to generate a sinusoidal optical grating of selectively excited dye molecules. The reading configuration, on the right, monitors the diffracted intensity of the reading beam as the dye isomers diffuse. The resulting decay curves are processed to yield diffusivity measurements.

sess mobility as a function of network topology and formation (Figure 31).[518–522] Cross-linking slows down the segmental dynamics, leading to a shift in the position of the maximum in the dielectric spectrum corresponding to segmental motion to lower frequencies. Low-frequency motion corresponding to the large-scale motion of the polymer backbone is also completely suppressed with cross-linking. As such, studies have used dielectric spectroscopy to follow the evolution of segmental dynamics during vulcanization, healing of damage, and the addition of nanoparticle fillers in natural rubbers.[523–528]

Dielectric spectroscopy is also termed electrochemical impedance spectroscopy or AC impedance spectroscopy when measuring ionic or electronic conductivity. In this way, the DC conductivity (σ_{DC}) can be determined from the frequency-independent plateau in the spectral dependence of the real conductivity

$$\sigma' = \omega \varepsilon_0 \varepsilon'' \tag{5.27}$$

where ε_0 is the permittivity of vacuum.[529,530] Typically, the conductivity is determined from the real component of the conductivity at the

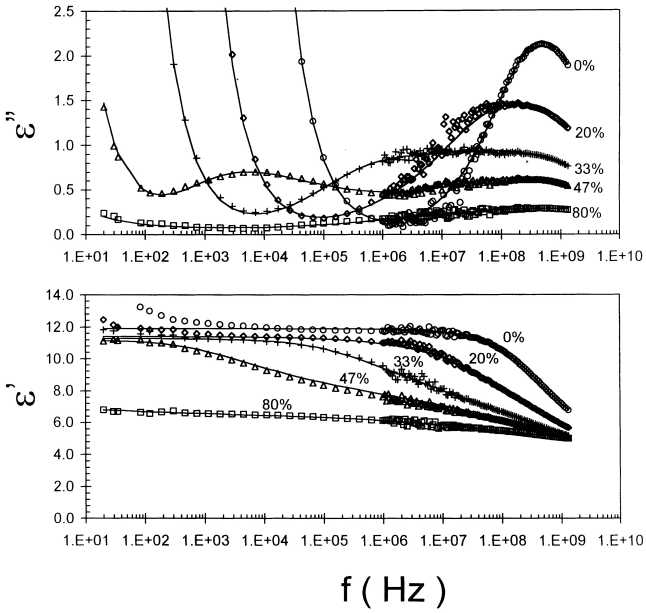

Figure 31: Dielectric storage and loss in the frequency f domain at different extents of curing (%), showing sensitivity to monitoring the gelation process. Figure reproduced with permission from Ref. 519. Copyright © 1999 American Chemical Society.

maximum in $\tan(\delta) = \varepsilon''/\varepsilon'$. An interesting application of impedance spectroscopy to polymer

networks is in metallo-cross-linked networks formed from polymeric ionic liquids, where in conjunction with rheology (Section 5.1.4), the microscopic effects of ionic junctions and counterions mobility on the conductivity and mechanics can be unraveled.[479,531–534]

6 Prediction: Computer Simulation

Computer simulations have proved invaluable for the study of molecular systems, with the main advantage to link macroscopic and microscopic phenomena, as well as to test predictions and assumptions of theoretical models. Molecular simulations of polymers can be crudely divided into two main methods: Molecular Dynamics (MD) and Monte Carlo (MC) simulations. In classical MD simulations, trajectories of the system are generated by numerically propagating particle coordinates in time using carefully parameterized molecular models (or "force-fields"). These trajectories can then in principle be analyzed to extract data on the various properties of the system—structural, dynamical, thermodynamical, mechanical, etc. In MC simulations, the particle coordinates are randomly transformed between microstates in a way that captures the thermodynamic ensemble, sacrificing the real time evolution in favor of efficient sampling of phase space. Both methods have many implementations and extensions that have been developed to increase computational efficiency.[535,536]

Computer simulation techniques have been extensively used to study polymer solutions, melts, brushes, and networks.[536] Regardless of the method employed, the molecular model is a key ingredient in the execution and interpretation of computer simulation and is a limiting factor in the physical quantities that can be sampled. In classical simulations, all-atom (AA) simulations are the most detailed models, and as such they provide details on the atomic and molecular levels. For example, AA simulations can be used to study interactions between components,[537,538] structure,[539] dynamics and mechanical properties[540] of polymer networks. Coarse graining (CG) of the molecular model enables increased computational efficiency, which allows longer time and length scales to be explored, at the expense of limited chemical detail. Both CG and AA simulations of polymer systems that include solvent (as solutions and gels) can represent the solvent either *explicitly*, by incorporating solvent molecules into the system, or *implicitly*, by modifying the effective polymer's intra- and inter-molecular interactions. The bead–spring model by Kremer and Grest[541,542] is a powerful CG method for polymers, in which each Kuhn monomer in the chain is represented by a single bead. The beads are connected by finitely extensible springs, and inter-bead interactions are modeled with a Lennard–Jones potential that can be tuned to represent different solvent qualities at the implicit-solvent level. It can also be used for explicit-solvent simulations, which allows realistic consideration of solvent entropy and interaction with the polymer. This particular CG model has been used extensively to study polymer systems and to examine various physical theoretical predictions at and above the scale of a monomer or Kuhn length.[543] Though much more computational demanding than CG, AA models with explicit solvent can be necessary to answer questions related to molecular interactions, hydration, and structure and dynamics at the atomic or monomeric scales.

A key advantage of computer simulation techniques in the context of polymer science is their ability to conclusively determine the effect of a limited set of parameters on the physical behavior, while constraining all others. One can design specific network architecture, network strand distribution, chain stiffness and many more characteristics. With a reductionist model used in computer simulation, one can even test an "idealized" network devoid of defects to exclude their effect,[544,545] or to emulate the gelation process in order to render more realistic networks that include defects (Figure 8).[546] To create these realistic networks in silico one can follow synthetic routes similar to those employed experimentally, namely: (i) random cross-linking an equilibrated melt[547] or semidi-

lute solution[548,549] of the precursor chains up to some degree of reaction, p, mimicking vulcanization,[546] (ii) end-linking of such a melt or solution by extending the MD trajectory and allowing un-reacted chain ends to bond if they are within some cutoff distance and the chain end has not yet saturated its bonding ability,[550] and (iii) emulation of free-radical polymerization of reactive monomers.[551]

The model networks can be studied in the unperturbed state for structural and dynamical quantities,[550,552] or be subjected to different processes and environments such as extension and compression, shear,[553] fracture,[554] electric field,[555] or changes in solvent quality.[556] The mechanical properties of polymer networks (Section 5.1), including stress–strain curves,[274,557,558] stress relaxation,[559,560] damage evolution,[561] etc. can then be extracted from the trajectories. These quantities help evaluating the microscopic contributions to macroscopic quantities; see Figure 19 as an example of the collapse of simulation data on a universal curve for network elasticity.[112]

One of the major limitations of computer simulations is that limited computational resources determine the length and time scales that can be studied. This limitation becomes more severe as the model resolution increases, i.e., from CG to AA. For networks, this problem is even worse as a chemically cross-linked polymer network is inherently a quenched system with many inhomogeneities, implying computer simulation results might differ between realizations. Therefore, one must average over several "replicas" of the system, to get meaningful reproducible results over the entire ensemble, especially if fracture is involved.[310,554] The same limitations on system size set bounds to the accessible physical quantities, as finite-size effects might become non-negligible.[562] To minimize artifacts, it is useful to simulate several system sizes, L, and extrapolate the considered property as a function of L^{-1} to infinite system size. It is also helpful to compare the computer simulation results with experimental measurements if available. It is common that such comparisons lead to further calibration of the molecular model, allowing for refinement of the model parameters. At the same time, for certain purposes, computer simulations can utilize non-physical mechanisms to allow sampling of longer time scales. For example, to vulcanize high-molecular-weight precursor chains to form highly entangled networks, as mentioned above, one needs to properly equilibrate melts. To avoid the long equilibration time of highly entangled melts, MC algorithms have been developed to allow large conformational changes by allowing chains to swap bonds,[547,563] or to progressively equilibrate the melt at different length scales.[564]

The raw data produced by an MD run is a trajectory in the $6n$-dimensional position–momentum phase-space of the system, n being the number of particles in the system. Since the scope of the applicability of computer simulation to networks is vast, it is constructive to first consider several representative examples. As mentioned earlier, the high-resolution data available in computer simulations can serve as a link between theoretical models and experiments. In an illuminating example for the virtues of computer simulation, Everaers et al. have studied deformation of well-defined polymer networks with constant network-strand length; by (unrealistically) switching the ability of network strands to cross one another, i.e., making them "phantom", they were able to elucidate the effect of entanglements on various network properties including their contribution to the elastic modulus.[545] Gel swelling (Section 4.1) can also be systematically followed, for example, by varying solvent quality in an isobaric-isothermic ensemble. Designing these simulations to match changes of experimental conditions, such as changes to solvent condition (e.g., temperature, salt concentration, pH, etc.) or addition of solvent, enable a thorough exploration of the gel behavior.[556,565,566] Alternatively, gel swelling by extra solvent can be followed in the canonical ensemble by gradually changing volume.[567,568]

Moreover, the ability to gauge the system at the monomer level allows for the study of the gelation process itself and comparing it to percolation and mean-field theories (Section 3). Of specific interest is the ability to directly mea-

sure network strand distributions, $P(M_x)$,[546] while in experiments it is usually only possible to determine the average $\overline{M}_x$ or make predictions regarding the distribution based on the sol fraction. Furthermore, the computer simulations can be used to determine the gel point and its suppression,[569] systematically identify and quantify network "defects" (dangling ends and primary loops such as those in Figure 8),[213,570] and determine network topology including all higher-order loops (Structure 4).

More specifically, the coordinates generated by computer simulations can be analyzed for various distribution functions such as distributions of bond and chain tensions, internal distances, angular orientations, etc. The structure of networks can be analyzed in much more detail by considering the time- and ensemble-averaged distributions of networks strands' end-to-end distances and orientations. Additional information is gathered through spatial or dynamical correlation functions of different network properties such as velocities, particle positions, orientations, and other degrees of freedom. All these quantities can be compared against theoretical predictions and dynamical ($S(q,\omega)$) or intermediate structure factor ($S(q,t)$) data from techniques such as NSE (Section 5.8) and thereby serve as a crucial link between theory and experiments.

Perhaps the most important for networks is the stress–strain relationship, extracted by deforming the polymer network (stretching, compression, or shear) and measuring the average elastic stress. The instantaneous stress tensor is derived from the virial theorem and calculated through the sum over all beads n,[571]

$$\sigma_{ij} = V^{-1} \sum_{k}^{n} \left(m_k v_{k,i} v_{k,j} + r_{k,i} f_{k,i} \right) \qquad (6.1)$$

where m_k is the mass of bead k, and $v_{k,i}$, $r_{k,i}$, and $f_{k,i}$ denote its velocity, coordinate, and force along the i direction. The stress–strain curves allow one to test elasticity theories, parsing contributions of entanglements (as mentioned above), assessing contributions of finite extensibility, and the contributions from single network strands.[274,310,540,557,572] Importantly, the shear-stress relaxation modulus[559,560] ($G(t)$, Section 5.1.2) characterizing the linear viscoelastic response of the network can be derived from the stress auto-correlation function with the Green—Kubo formula,

$$G_{ij}(t) = \frac{V}{k_B T} \left\langle \sigma_{ij}(t) \sigma_{ij}(0) \right\rangle , \qquad (6.2)$$

where V is the volume, $k_B T$ is the thermal energy, and i, j are Cartesian coordinates with $i \neq j$.[573,574] Additional transforms of the stress-relaxation modulus to frequency (ω) space can then provide rheological information on the storage $G'(\omega)$ and loss moduli $G''(\omega)$, reflecting the extent of energy storage and dissipation in the network. These quantities can be compared against predictions from theoretical models for the network's dynamics as well as with rheological measurements (Section 5.1.4).

The network structure can be directly measured by examining structural distributions and spatial correlations functions. For instance, the structure of networks can be characterized directly by the size distributions of networks strands or loops. The form factor of individual chains and the structure factor of the network itself can be readily obtained and compared with scattering experiments (Section 4.3). Furthermore, the pair correlation function (also known as the radial distribution function) informs on the *local* spatial correlations of monomers and is defined as[575]

$$g(r) = \rho^{-2} \left\langle \sum_{i} \sum_{j \neq i} \delta(\mathbf{r}_i) \delta(\mathbf{r}_j - \mathbf{r}) \right\rangle \qquad (6.3)$$

where ρ is the bulk density, i, j are monomer indices, and the brackets $\langle \cdots \rangle$ denote ensemble average.[552,575] Another important example for a correlation function accessible through computer simulations is the mean-square displacement of a particle

$$\mathrm{MSD} = \left\langle [\mathbf{r}(t) - \mathbf{r}(0)]^2 \right\rangle , \qquad (6.4)$$

which can, for example, inform on the anomalous diffusion of probe particles in a network (Sections 5.5, 5.6).[576,577] The probe diffusion can then shed light on the coupling between

polymer relaxation modes and the particle dynamics as well as on the network structure itself, i.e., mesh-size distribution and swelling. For example, the diffusion of a probe particle moderately larger than the network mesh size is sub-diffusive at short time scales at which the coupling with polymer dynamics hinders the particle motion, whereas at longer time scales the particle behave diffusively, through a hopping mechanism.[578] The time dependence of the MSD can then be used to extract nanorheological information on the network.[464] The diffusion coefficient of probe particles can then be calculated from the MSD[15] at these long time scales.

It is also worthwhile to mention the recent development of alternative methodologies to the molecular simulations discussed thus far in studying self-assembly, thermodynamic behavior, and dynamics of polymer networks. In particular, molecularly informed field theories, with their associated analytical approximations and numerical simulations, are a powerful tool in polymer physics, with applications to many categories of polymer systems, including solutions and melts of polymers of arbitrary architecture and molecular features.[579,580] Field theories, traditionally, however, have had difficulties in application to networks due to the need to explicitly enumerate all the possible structures.[581–585] Recently, a reformulation of the field theory in a coherent-states (CS) framework was developed to implicitly account for the full ensemble of supramolecular polymer reaction products and is expected to supplement existing methods for reversible and inhomogeneous polymer networks,[586,587] pending advancement in the numerical methods.[588] Such techniques can possibly be applied to networks with quenched disorder,[589] as well, by application of replica methods as in MD to obtain an ensemble average of the disorder. Finally, it should be noted that a plethora of mesoscopic and macroscopic methods exist to describe the continuum mechanics of gels and elastomers, albeit without the explicit connection to the molecular properties of the polymer strands and junctions; the reader is directed elsewhere in the literature.[590–604]

7 Perspective

The interdisciplinary nature of polymer network chemistry involves an interdisciplinary mix of characterization techniques that probe structure and dynamics at the level of individual strands, junctions, topology, and statistical mixtures. In general, each technique offers one piece of a much larger characterization puzzle, and combinations of techniques (both experimental and theoretical/computational) are often necessary in order to adequately assess the molecular structural details that are germane to a given structure–property relationship. This complexity presents a barrier to polymer network chemistry, because both the purpose and the technical details of many of the characterization techniques are unfamiliar to most chemists. In our view, this unfamiliarity obscures a tremendous opportunity. The intrinsic molecular characteristics of polymer networks can be resolved with increasing precision, and the contributions of specific molecular structure and behavior to the properties of polymer networks can be increasingly assessed. In the long run, these connections will allow chemists, through creative (macro)molecular design and synthetic control, to program properties and function into individual polymer molecules, including precise conformational behavior, unusual extensional profiles, and covalent chemical responses.

The characterization challenge presents something of a linchpin. One part of the challenge, addressed in this review, is to make the motivation for, and the limits of, available techniques increasingly accessible to the broader chemistry community. Looking ahead and beyond the scope of this review, a second set of challenges involve the further development of characterization tools and methods. Areas of particular interest to us include: (i) extensions of network disassembly methods, including those that follow the gradual evolution of disassembly with time to obtain greater insight into heterogeneities on multiple length scales; (ii) techniques for characterizing the time-dependent behavior of individual probe strands within networks, for example through approaches simi-

lar to super-resolution spectroscopy; (iii) robust data collection schemes that allow primary characterization data from multiple techniques and at multiple stages of network formation (e.g., strands, junction, and ensemble network characterization) to be input directly into machine learning protocols.[605–609] We keenly anticipate development of advanced techniques, improvements in computational power, and informatics will enable molecular optimization of polymer networks.

Acknowledgement This work was funded by Duke University and the Center for the Chemistry of Molecularly Optimized Networks (MONET), a National Science Foundation (NSF) Center for Chemical Innovation (CHE-1832256).

References

(1) Spiess, H. W. 50th Anniversary Perspective: The Importance of NMR Spectroscopy to Macromolecular Science. *Macromolecules* **2017**, *50*, 1761–1777, DOI: 10.1021/acs.macromol.6b02736.

(2) Wolf, A.; Desport, J. S.; Dieden, R.; Frache, G.; Weydart, M.; Poorters, L.; Schmidt, D. F.; Verge, P. Sequence-Controlled α-Methylstyrene/Styrene Copolymers: Syntheses and Sequence Distribution Resolution. *Macromolecules* **2020**, *53*, 8032–8040, DOI: 10.1021/acs.macromol.0c01649.

(3) Koenig, J. L. Raman Scattering of Synthetic Polymers—a Review. *Appl. Spectrosc. Rev.* **1971**, *4*, 233–305, DOI: 10.1080/05704927108082605.

(4) Hollandmoritz, K.; Siesler, H. W. Infrared Spectroscopy of Polymers. *Appl. Spectrosc. Rev.* **1976**, *11*, 1–55, DOI: 10.1080/05704927608081704.

(5) Bokobza, L. Some Applications of Vibrational Spectroscopy for the Analysis of Polymers and Polymer Composites. *Polymers* **2019**, *11*, 1159, DOI: 10.3390/polym11071159.

(6) Barrios, V. A. E.; Mendez, J. R. R.; Aguilar, N. V. P.; Espinosa, G. A.; Rodriguez, J. L. D. In *Infrared Spectroscopy—Materials Science, Engineering and Technology*; Theophile, T., Ed.; 2012; DOI: 10.5772/36044.

(7) Åmand, L.-E.; Tullin, C. J. *The Theory Behind FTIR Analysis*; Report.

(8) Stuart, B. H. Polymer Crystallinity Studied using Raman Spectroscopy. *Vib. Spectrosc.* **1996**, *10*, 79–87, DOI: 10.1016/0924-2031(95)00042-9.

(9) Fontoura, J. M. R.; Santos, A. F.; Silva, F. M.; Lenzi, M. K.; Lima, E. L.; Pinto, J. C. Monitoring and Control of Styrene Solution Polymerization using NIR Spectroscopy. *J. Appl. Polym. Sci.* **2003**, *90*, 1273–1289, DOI: 10.1002/app.12746.

(10) Scherzer, T.; Langguth, H. The Effect of Temperature on the Induction Period in the Photoinitiated Polymerization of Tripropylene Glycol Diacrylate. *Nucl. Instrum. Methods Phys. Res., Sect. B* **2001**, *185*, 276–282, DOI: 10.1016/S0168-583x(01)00778-9.

(11) Frauendorfer, E.; Hergeth, W. D. Industrial Application of Raman Spectroscopy for Control and Optimization of Vinyl Acetate Resin Polymerization. *Anal. Bioanal. Chem.* **2017**, *409*, 631–636, DOI: 10.1007/s00216-016-0001-3.

(12) Dazzi, A.; Prater, C. B.; Hu, Q. C.; Chase, D. B.; Rabolt, J. F.; Marcott, C. AFM-IR: Combining Atomic Force Microscopy and Infrared Spectroscopy for Nanoscale Chemical Characterization. *Appl. Spectrosc.* **2012**, *66*, 1365–1384, DOI: 10.1366/12-06804.

(13) Ward, T. C. Molecular-Weight and Molecular-Weight Distributions in Synthetic-Polymers. *J. Chem. Educ.* **1981**, *58*, 867–879, DOI: 10.1021/ed058p867.

(14) Schick, C. Differential Scanning Calorimetry (DSC) of Semicrystalline Polymers. *Anal. Bioanal. Chem.* **2009**, *395*, 1589–1611, DOI: 10.1007/s00216-009-3169-y.

(15) Rubinstein, M.; Colby, R. H. *Polymer Physics*; Oxford University Press: New York, 2003.

(16) Pach, M.; Zehm, D.; Lange, M.; Dambowsky, I.; Weiss, J.; Laschewsky, A. Universal Polymer Analysis by 1H NMR Using Complementary Trimethylsilyl End Groups. *J. Am. Chem. Soc.* **2010**, *132*, 8757–8765, DOI: 10.1021/ja102096u.

(17) Mirau, P. A.; Heffner, S. A.; Koegler, G.; Bovey, F. A. 2D-NMR and 3D-NMR for Polymer Characterization. *Polym. Int.* **1991**, *26*, 29–34, DOI: 10.1002/pi.4990260106.

(18) Brar, A. S.; Goyal, A. K.; Hooda, S. Two-dimensional NMR studies of Acrylate Copolymers. *Pure Appl. Chem.* **2009**, *81*, 389–415, DOI: 10.1351/Pac-Con-08-06-01.

(19) Bovey, F. A.; Mirau, P. A. The Two-Dimensional Nuclear Magnetic-Resonance Spectroscopy of Macromolecules. *Acc. Chem. Res.* **1988**, *21*, 37–43, DOI: 10.1021/ar00145a006.

(20) Jerschow, A.; Muller, N. Diffusion-Separated Nuclear Magnetic Resonance Spectroscopy of Polymer Mixtures. *Macromolecules* **1998**, *31*, 6573–6578, DOI: 10.1021/ma9801772.

(21) Cheng, H. N.; Neiss, T. G. Solution NMR Spectroscopy of Food Polysaccharides. *Polym. Rev.* **2012**, *52*, 81–114, DOI: 10.1080/15583724.2012.668154.

(22) Hansen, M. R.; Graf, R.; Spiess, H. W. Solid-State NMR in Macromolecular Systems: Insights on How Molecular Entities Move. *Acc. Chem. Res.* **2013**, *46*, 1996–2007, DOI: 10.1021/ar300338b.

(23) Foster, M. P.; McElroy, C. A.; Amero, C. D. Solution NMR of Large Molecules and Assemblies. *Biochemistry* **2007**, *46*, 331–340, DOI: 10.1021/bi0621314.

(24) Martinez-Richa, A.; Silvestri, R. L. In *Spectroscopic Analyses—Developments and Applications*; Sharmin, E., Zafar, F., Eds.; 2017; DOI: 10.5772/intechopen.70116.

(25) Hanton, S. D. Mass Spectrometry of Polymers and Polymer Surfaces. *Chem. Rev.* **2001**, *101*, 527–569, DOI: 10.1021/cr9901081.

(26) Wesdemiotis, C. Multidimensional Mass Spectrometry of Synthetic Polymers and Advanced Materials. *Angew. Chem., Int. Ed.* **2017**, *56*, 1452–1464, DOI: 10.1002/anie.201607003.

(27) Gruendling, T.; Weidner, S.; Falkenhagen, J.; Barner-Kowollik, C. Mass Spectrometry in Polymer Chemistry: a State-of-the-Art Update. *Polym. Chem.* **2010**, *1*, 599–617, DOI: 10.1039/b9py00347a.

(28) Byrd, H. C. M.; McEwen, C. N. The Limitations of MALDI-TOF Mass Spectrometry in the Analysis of Wide Polydisperse Polymers. *Anal. Chem.* **2000**, *72*, 4568–4576, DOI: 10.1021/ac0002745.

(29) Rader, H. J.; Schrepp, W. MALDI-TOF Mass Spectrometry in the Analysis of Synthetic Polymers. *Acta Polym.* **1998**, *49*, 272–293, DOI: 10.1002/(SICI)1521-4044(199806)49:6.

(30) Nielen, M. W. F. MALDI Time-of-Flight Mass Spectrometry of Synthetic Polymers. *Mass Spectrom. Rev.* **1999**, *18*, 309–344, DOI: 10.1002/(SICI)1098-2787(1999)18:5.

(31) Zhu, H. H.; Yalcin, T.; Li, L. Analysis of the Accuracy of Determining Average Molecular Weights of Narrow Polydispersity Polymers by Matrix-Assisted

Laser Desorption Ionization Time-of-Flight Mass Spectrometry. *J. Am. Soc. Mass Spectrom.* **1998**, *9*, 275–281, DOI: 10.1016/S1044-0305(97)00292-4.

(32) Wesdemiotis, C.; Solak, N.; Polce, M. J.; Dabney, D. E.; Chaicharoen, K.; Katzenmeyer, B. C. Fragmentation Pathways of Polymer Ions. *Mass Spectrom. Rev.* **2011**, *30*, 523–559, DOI: 10.1002/mas.20282.

(33) Altuntas, E.; Krieg, A.; Baumgaertel, A.; Crecelius, A. C.; Schubert, U. S. ESI, APCI, and MALDI Tandem Mass Spectrometry of Poly(methylacrylate)s: a Comparison Study for the Structural Characterization of Polymers Synthesized via CRP Techniques and the Software Application to Analyze MS/MS data. *J. Polym. Sci., Part A: Polym. Chem.* **2013**, *51*, 1595–1605, DOI: 10.1002/pola.26529.

(34) Campbell, D.; Pethrick, R. A.; White, J. R. *Polymer Characterization: Physical Techniques*; CRC Press, 2000.

(35) Cleverdon, D. Practice of Osmometry—Its Contribution to the Characterization of a High Polymer. *J. Appl. Chem.* **1951**, *1*, 272–280, DOI: 10.1002/jctb.5010010609.

(36) Young, R.; Lovell, P. *Introduction to Polymers*; CRC Press, 2011.

(37) Wagner, R. H. Osmometry of High-Polymer Solutions Apparatus. *Ind. Eng. Chem. Anal. Ed.* **1944**, *16*, 520–523, DOI: 10.1021/i560132a015.

(38) Cleverdon, D.; Laker, D. The Osmometry of High Polymers .1. Technique of Osmometry. *J. Appl. Chem.* **1951**, *1*, 2–6, DOI: 10.1002/jctb.5010010102.

(39) Lovell, P. A. In *Comprehensive Polymer Science and Supplements*; Allen, G., Bevington, J. C., Eds.; Elsevier, 1989.

(40) Striegel, A. M. Viscometric Detection in Size-Exclusion Chromatography: Principles and Select Applications. *Chromatographia* **2016**, *79*, 945–960, DOI: 10.1007/s10337-016-3078-0.

(41) Kraj, A.; Brouwer, H. J.; Reinhoud, N.; Chervet, J. P. A Novel Electrochemical Method for Efficient Reduction of Disulfide Bonds in Peptides and Proteins Prior to MS Detection. *Anal. Bioanal. Chem.* **2013**, *405*, 9311–9320, DOI: 10.1007/s00216-013-7374-3.

(42) Morris, M. J.; Striegel, A. M. Determining the Solution Conformational Entropy of Oligosaccharides by SEC with On-line Viscometry Detection. *Carbohydr. Polym.* **2014**, *106*, 230–237, DOI: 10.1016/j.carbpol.2014.02.027.

(43) *Modern Methods of Particle Size Analysis*; Wiley, 1984.

(44) Engelke, J.; Brandt, J.; Barner-Kowollik, C.; Lederer, A. Strengths and Limitations of Size-Exclusion Chromatography for Investigating Single Chain Folding—Current Status and Future Perspectives. *Polym. Chem.* **2019**, *10*, 3410–3425, DOI: 10.1039/c9py00336c.

(45) Colby, R. H.; Rubinstein, M.; Gillmor, J. R.; Mourey, T. H. Scaling Properties of Branched Polyesters .2. Static Scaling above the Gel Point. *Macromolecules* **1992**, *25*, 7180–7187, DOI: 10.1021/ma00052a017.

(46) Berek, D. Size-Exclusion Chromatography—A Blessing and a Curse of Science and Technology of Synthetic Polymers. *J. Sep. Sci.* **2010**, *33*, 315–335, DOI: 10.1002/jssc.200900709.

(47) Barth, H. G.; Boyes, B. E.; Jackson, C. Size Exclusion Chromatography. *Anal. Chem.* **1994**, *66*, 595–620, DOI: 10.1021/ac00084a022.

(48) Hiller, W.; Pasch, H.; Macko, T.; Hofmann, M.; Ganz, J.; Spraul, M.; Braumann, U.; Streck, R.; Mason, J.; Van Damme, F. On-Line Coupling of High Temperature GPC and H-1 NMR for the Analysis of Polymers. *J. Magn. Reson.* **2006**, *183*, 290–302, DOI: 10.1016/j.jmr.2006.09.004.

(49) Hiller, W.; Hehn, M.; Hofe, T.; Oleschko, K. Online Size Exclusion Chromatography-NMR for the Determination of Molar Mass Distributions of Copolymers. *Anal. Chem.* **2010**, *82*, 8244–8250, DOI: 10.1021/ac1013095.

(50) Cudaj, M.; Guthausen, G.; Hofe, T.; Wilhelm, M. SEC-MR-NMR: Online Coupling of Size Exclusion Chromatography and Medium Resolution NMR Spectroscopy. *Macromol. Rapid Commun.* **2011**, *32*, 665–670, DOI: 10.1002/marc.201000760.

(51) Jovic, K.; Nitsche, T.; Lang, C.; Blinco, J. P.; De Bruycker, K.; Barner-Kowollik, C. Hyphenation of Size-Exclusion Chromatography to Mass Spectrometry for Precision Polymer Analysis—a Tutorial Review. *Polym. Chem.* **2019**, *10*, 3241–3256, DOI: 10.1039/c9py00370c.

(52) Rosenbloom, S. I.; Fors, B. P. Shifting Boundaries: Controlling Molecular Weight Distribution Shape for Mechanically Enhanced Thermoplastic Elastomers. *Macromolecules* **2020**, *53*, 7479–7486, DOI: 10.1021/acs.macromol.0c00954.

(53) Walsh, D. J.; Wade, M. A.; Rogers, S. A.; Guironnet, D. Challenges of Size-Exclusion Chromatography for the Analysis of Bottlebrush Polymers. *Macromolecules* **2020**, *53*, 8610–8620, DOI: 10.1021/acs.macromol.0c01357.

(54) Liu, Y. L.; Wang, Z. Q.; Zhang, X. Characterization of Supramolecular Polymers. *Chem. Soc. Rev.* **2012**, *41*, 5922–5932, DOI: 10.1039/c2cs35084j.

(55) Inglis, A. J.; Nebhani, L.; Altintas, O.; Schmidt, F. G.; Barner-Kowollik, C. Rapid Bonding/Debonding on Demand: Reversibly Cross-Linked Functional Polymers via Diels-Alder Chemistry. *Macromolecules* **2010**, *43*, 5515–5520, DOI: 10.1021/ma100945b.

(56) Brandt, J.; Guimard, N. K.; Barner-Kowollik, C.; Schmidt, F. G.; Lederer, A. Temperature-Dependent Size-Exclusion Chromatography for the in situ Investigation of Dynamic Bonding/Debonding Reactions. *Anal. Bioanal. Chem.* **2013**, *405*, 8981–8993, DOI: 10.1007/s00216-013-7203-8.

(57) Brandt, J.; Lenz, J.; Pahnke, K.; Schmidt, F. G.; Barner-Kowollik, C.; Lederer, A. Investigation of Thermoreversible Polymer Networks by Temperature-Dependent Size-Exclusion Chromatography. *Polym. Chem.* **2017**, *8*, 6598–6605, DOI: 10.1039/c7py01262d.

(58) Oberlerchner, J. T.; Rosenau, T.; Potthast, A. Overview of Methods for the Direct Molar Mass Determination of Cellulose. *Molecules* **2015**, *20*, 10313–10341, DOI: 10.3390/molecules200610313.

(59) Podzimek, S. Multi-Angle Light Scattering: An Efficient Tool Revealing Molecular Structure of Synthetic Polymers. *Macromol. Symp.* **2019**, *384*, DOI: 10.1002/masy.201800174.

(60) Chartoff, R. P.; Sircar, A. K. *Encyclopedia of Polymer Science and Technology*; John Wiley & Sons, Ltd., 2004.

(61) Maccallum, J. R. Thermogravimetric Analysis of Polymers for Assessing Thermal-Degradation. *Thermochim. Acta* **1985**, *96*, 275–281, DOI: 10.1016/0040-6031(85)80068-X.

(62) Mackanic, D. G.; Michaels, W.; Lee, M.; Feng, D. W.; Lopez, J.; Qin, J.; Cui, Y.; Bao, Z. N. Crosslinked Poly(tetrahydrofuran) as a Loosely Coordinating Polymer Electrolyte. *Adv. Energy Mater.* **2018**, *8*, 1800703, DOI: 10.1002/aenm.201800703.

(63) Leibfarth, F. A.; Kang, M.; Ham, M.; Kim, J.; Campos, L. M.; Gupta, N.; Moon, B.; Hawker, C. J. A Facile Route to Ketene-Functionalized Polymers for General Materials Applications. *Nat. Chem.* **2010**, *2*, 207–212, DOI: 10.1038/Nchem.538.

(64) Skoog, D. A.; Holler, F. J.; Nieman, T. A. *Principles of Instrumental Analysis*; Saunders College Pub., 1998.

(65) Hohne, G. W. H.; Hemminger, W. F.; Flammersheim, H.-J. *Differential Scanning Calorimetry*; Springer, 2003.

(66) Anseth, K. S.; Kline, L. M.; Walker, T. A.; Anderson, K. J.; Bowman, C. N. Reaction-Kinetics and Volume Relaxation during Polymerizations of Multiethylene Glycol Dimethacrylates. *Macromolecules* **1995**, *28*, 2491–2499, DOI: 10.1021/ma00111a050.

(67) Wang, Y. X.; Wang, C. G.; Wu, J. W.; Jing, M. High-Temperature DSC Study of Polyacrylonitrile Precursors During their Conversion to Carbon Fibers. *J. Appl. Polym. Sci.* **2007**, *106*, 1787–1792, DOI: 10.1002/app.26862.

(68) Rief, M.; Gautel, M.; Oesterhelt, F.; Fernandez, J. M.; Gaub, H. E. Reversible Unfolding of Individual Titin Immunoglobulin Domains by AFM. *Science* **1997**, *276*, 1109–1112, DOI: 10.1126/science.276.5315.1109.

(69) Rief, M.; Clausen-Schaumann, H.; Gaub, H. E. Sequence-Dependent Mechanics of Single DNA molecules. *Nat. Struct. Biol.* **1999**, *6*, 346–349, DOI: 10.1038/7582.

(70) Liphardt, J.; Onoa, B.; Smith, S. B.; Tinoco, I.; Bustamante, C. Reversible Unfolding of Single RNA molecules by Mechanical Force. *Science* **2001**, *292*, 733–737, DOI: 10.1126/science.1058498.

(71) Rief, M.; Oesterhelt, F.; Heymann, B.; Gaub, H. E. Single Molecule Force Spectroscopy on Polysaccharides by Atomic Force Microscopy. *Science* **1997**, *275*, 1295–1297, DOI: 10.1126/science.275.5304.1295.

(72) Marszalek, P. E.; Oberhauser, A. F.; Pang, Y. P.; Fernandez, J. M. Polysaccharide Elasticity Governed by Chair–Boat Transitions of the Glucopyranose Ring. *Nature* **1998**, *396*, 661–664, DOI: 10.1038/25322.

(73) Li, H. B.; Linke, W. A.; Oberhauser, A. F.; Carrion-Vazquez, M.; Kerkviliet, J. G.; Lu, H.; Marszalek, P. E.; Fernandez, J. M. Reverse Engineering of the Giant Muscle Protein Titin. *Nature* **2002**, *418*, 998–1002, DOI: 10.1038/nature00938.

(74) Klukovich, H. M.; Kouznetsova, T. B.; Kean, Z. S.; Lenhardt, J. M.; Craig, S. L. A Backbone Lever-Arm Effect Enhances Polymer Mechanochemistry. *Nat. Chem.* **2013**, *5*, 110–114, DOI: 10.1038/Nchem.1540.

(75) Gossweiler, G. R.; Kouznetsova, T. B.; Craig, S. L. Force-Rate Characterization of Two Spiropyran-Based Molecular Force Probes. *J. Am. Chem. Soc.* **2015**, *137*, 6148–6151, DOI: 10.1021/jacs.5b02492.

(76) Churnside, A. B.; Sullan, R. M. A.; Nguyen, D. M.; Case, S. O.; Bull, M. S.; King, G. M.; Perkins, T. T. Routine and Timely Sub-picoNewton Force Stability and Precision for Biological Applications of Atomic Force Microscopy. *Nano Lett.* **2012**, *12*, 3557–3561, DOI: 10.1021/nl301166w.

(77) Verdorfer, T.; Bernardi, R. C.; Meinhold, A.; Ott, W.; Luthey-Schulten, Z.; Nash, M. A.; Gaub, H. E. Combining in Vitro and in Silico Single-Molecule Force Spectroscopy to Characterize and Tune Cellulosomal Scaffoldin Mechanics. *J. Am. Chem. Soc.* **2017**, *139*, 17841–17852, DOI: 10.1021/jacs.7b07574.

(78) Milles, L. F.; Unterauer, E. M.; Nicolaus, T.; Gaub, H. E. Calcium Stabilizes the Strongest Protein Fold. *Nat. Commun.* **2018**, *9*, 4764, DOI: 10.1038/s41467-018-07145-6.

(79) Ortiz, C.; Hadziioannou, G. Entropic Elasticity of Single Polymer Chains of Poly(methacrylic Acid) Measured by Atomic Force Microscopy. *Macromolecules* **1999**, *32*, 780–787, DOI: 10.1021/ma981245n.

(80) Zhang, W. K.; Zou, S.; Wang, C.; Zhang, X. Single Polymer Chain Elongation of Poly(N-isopropylacrylamide) and Poly(acrylamide) by Atomic Force Microscopy. *J. Phys. Chem. B* **2000**, *104*, 10258–10264, DOI: 10.1021/jp000459f.

(81) Marszalek, P. E.; Li, H. B.; Fernandez, J. M. Fingerprinting Polysaccharides with Single-Molecule Atomic Force Microscopy. *Nat. Biotechnol.* **2001**, *19*, 258–262, DOI: 10.1038/85712.

(82) Brown, C. L.; Craig, S. L. Molecular Engineering of Mechanophore Activity for Stress-Responsive Polymeric Materials. *Chem. Sci.* **2015**, *6*, 2158–2165, DOI: 10.1039/c4sc01945h.

(83) Wang, J. P.; Kouznetsova, T. B.; Niu, Z. B.; Ong, M. T.; Klukovich, H.; Rheingold, A. L.; Martinez, T. J.; Craig, S. L. Inducing and Quantifying Forbidden Reactivity with Single-Molecule Polymer Mechanochemistry. *Nat. Chem.* **2015**, *7*, 323–327, DOI: 10.1038/Nchem.2185.

(84) Zhang, W.; Zhang, X. Single-Molecule Mechanochemistry of Macromolecules. *Prog. Polym. Sci.* **2003**, *28*, 1271–1295, DOI: 10.1016/S0079-6700(03)00046-7.

(85) Neuman, K. C.; Nagy, A. Single-Molecule Force Spectroscopy: Optical Tweezers, Magnetic Tweezers and Atomic Force Microscopy. *Nat. Methods* **2008**, *5*, 491–505, DOI: 10.1038/Nmeth.1218.

(86) Svoboda, K.; Schmidt, C. F.; Schnapp, B. J.; Block, S. M. Direct Observation of Kinesin Stepping by Optical Trapping Interferometry. *Nature* **1993**, *365*, 721–727, DOI: 10.1038/365721a0.

(87) Herbert, K. M.; La Porta, A.; Wong, B. J.; Mooney, R. A.; Neuman, K. C.; Landick, R.; Block, S. M. Sequence-Resolved Detecton of Pausing by Single RNA Polymerase Molecules. *Cell* **2006**, *125*, 1083–1094, DOI: 10.1016/j.cell.2006.04.032.

(88) Charvin, G.; Strick, T. R.; Bensimon, D.; Croquette, V. Tracking Topoisomerase Activity at the Single-Molecule Level. *Annu. Rev. Biophys. Biomol. Struct.* **2005**, *34*, 201–219, DOI: 10.1146/annurev.biophys.34.040204.144433.

(89) Strick, T. R.; Croquette, V.; Bensimon, D. Single-Molecule Analysis of DNA Uncoiling by a Type II Topoisomerase. *Nature* **2000**, *404*, 901–904, DOI: 10.1038/35009144.

(90) Willis-Fox, N.; Rognin, E.; Aljohani, T. A.; Daly, R. Polymer Mechanochemistry: Manufacturing Is Now a Force to Be Reckoned With. *Chem* **2018**, *4*, 2499–2537, DOI: 10.1016/j.chempr.2018.08.001.

(91) Binder, W. H. The "Labile" Chemical Bond: A Perspective on Mechanochemistry in Polymers. *Polymer* **2020**, *202*, 122639, DOI: 10.1016/j.polymer.2020.122639.

(92) Wang, S.; Panyukov, S.; Rubinstein, M.; Craig, S. L. Quantitative Adjustment

to the Molecular Energy Parameter in the Lake–Thomas Theory of Polymer Fracture Energy. *Macromolecules* **2019**, *52*, 2772–2777, DOI: 10.1021/acs.macromol.8b02341.

(93) Wiita, A. P.; Perez-Jimenez, R.; Walther, K. A.; Grater, F.; Berne, B. J.; Holmgren, A.; Sanchez-Ruiz, J. M.; Fernandez, J. M. Probing the Chemistry of Thioredoxin Catalysis with Force. *Nature* **2007**, *450*, 124–127, DOI: 10.1038/nature06231.

(94) Ainavarapu, S. R. K.; Wiita, A. P.; Dougan, L.; Uggerud, E.; Fernandez, J. M. Single-Molecule Force Spectroscopy Measurements of Bond Elongation During a Bimolecular Reaction. *J. Am. Chem. Soc.* **2008**, *130*, 6479–6487, DOI: 10.1021/ja800180u.

(95) Kouznetsova, T. B.; Wang, J. P.; Craig, S. L. Combined Constant-Force and Constant-Velocity Single-Molecule Force Spectroscopy of the Conrotatory Ring Opening Reaction of Benzocyclobutene. *ChemPhysChem* **2017**, *18*, 1486–1489, DOI: 10.1002/cphc.201600463.

(96) Patton, E. V.; Wesson, J. A.; Rubinstein, M.; Wilson, J. C.; Oppenheimer, L. E. Scaling Properties of Branched Polyesters. *Macromolecules* **1989**, *22*, 1946–1959, DOI: 10.1021/ma00194a072.

(97) Stauffer, D.; Coniglio, A.; Adam, M. Gelation and Critical Phenomena. *Adv. Polym. Sci.* **1982**, *44*, 103–158.

(98) Stauffer, D. *Introduction to Percolation Theory*; Taylor & Francis: Philadelphia, 1985; p 124.

(99) Wang, R.; Sing, M. K.; Avery, R. K.; Souza, B. S.; Kim, M.; Olsen, B. D. Classical Challenges in the Physical Chemistry of Polymer Networks and the Design of New Materials. *Acc. Chem. Res.* **2016**, *49*, 2786–2795, DOI: 10.1021/acs.accounts.6b00454.

(100) Gu, Y. W.; Zhao, J. L.; Johnson, J. A. A (Macro)Molecular-Level Understanding of Polymer Network Topology. *Trends Chem.* **2019**, *1*, 318–334, DOI: 10.1016/j.trechm.2019.02.017.

(101) Gu, Y. W.; Zhao, J. L.; Johnson, J. A. Polymer Networks: From Plastics and Gels to Porous Frameworks. *Angew. Chem., Int. Ed.* **2020**, 5022–5049, DOI: 10.1002/anie.201902900.

(102) Flory, P. J.; Rehner, J. Statistical Mechanics of Cross-Linked Polymer Networks II Swelling. *J. Chem. Phys.* **1943**, *11*, 521–526, DOI: 10.1063/1.1723792.

(103) Flory, P. J.; Rehner, J. Statistical Mechanics of Cross-Linked Polymer Networks I Rubber-like Elasticity. *J. Chem. Phys.* **1943**, *11*, 512–520, DOI: 10.1063/1.1723791.

(104) Flory, P. J. *Principles of Polymer Chemistry*; Cornell University Press: Ithaca, NY, 1953.

(105) Flory, P. J. Thermodynamics of High Polymer Solutions. *J. Chem. Phys.* **1942**, *10*, 51–61, DOI: 10.1063/1.1723621.

(106) Huggins, M. L. Theory of Solutions of High Polymers. *J. Am. Chem. Soc.* **1942**, *64*, 1712–1719, DOI: 10.1021/ja01259a068.

(107) Erman, B.; Flory, P. J. Relationships between Stress, Strain, and Molecular Constitution of Polymer Networks — Comparison of Theory with Experiments. *Macromolecules* **1982**, *15*, 806–811, DOI: 10.1021/ma00231a023.

(108) Kloczkowski, A.; Mark, J. E.; Erman, B. A Diffused-Constraint Theory for the Elasticity of Amorphous Polymer Networks .1. Fundamentals and Stress–Strain Isotherms in Elongation. *Macromolecules* **1995**, *28*, 5089–5096, DOI: 10.1021/ma00118a043.

(109) Edwards, S. F. Statistical Mechanics of Polymerized Material. *Proc. Phys. Soc., London* **1967**, *92*, 9–16, DOI: 10.1088/0370-1328/92/1/303.

(110) Edwards, S. F.; Vilgis, T. The Effect of Entanglements in Rubber Elasticity. *Polymer* **1986**, *27*, 483–492, DOI: 10.1016/0032-3861(86)90231-4.

(111) Gaylord, R. J.; Douglas, J. F. The Localization Model of Rubber Elasticity .2. *Polym. Bull.* **1990**, *23*, 529–533, DOI: 10.1007/Bf00419973.

(112) Rubinstein, M.; Panyukov, S. Elasticity of Polymer Networks. *Macromolecules* **2002**, *35*, 6670–6686, DOI: 10.1021/ma0203849.

(113) Zhong, M. J.; Wang, R.; Kawamoto, K.; Olsen, B. D.; Johnson, J. A. Quantifying the Impact of Molecular Defects on Polymer Network Elasticity. *Science* **2016**, *353*, 1264–1268, DOI: 10.1126/science.aag0184.

(114) de Gennes, P. G. *Scaling Concepts in Polymer Physics*; Cornell University Press: Ithaca, NY, 1979.

(115) Li, J. Y.; Hu, Y. H.; Vlassak, J. J.; Suo, Z. G. Experimental Determination of Equations of State for Ideal Elastomeric Gels. *Soft Matter* **2012**, *8*, 8121–8128, DOI: 10.1039/c2sm25437a.

(116) Hisatake, K.; Tanaka, S.; Aizawa, Y. Evaporation Rate of Water in a Vessel. *J. Appl. Phys.* **1993**, *73*, 7395–7401, DOI: 10.1063/1.354031.

(117) Dogu, Y.; Okay, O. Swelling–Deswelling Kinetics of Poly(N-isopropylacrylamide) Hydrogels formed in PEG Solutions. *J. Appl. Polym. Sci.* **2006**, *99*, 37–44, DOI: 10.1002/app.22140.

(118) Yamaue, T.; Doi, M. The Stress Diffusion Coupling in the Swelling Dynamics of Cylindrical Gels. *J. Chem. Phys.* **2005**, *122*, 084703, DOI: 10.1063/1.1849153.

(119) Yamamoto, T.; Masubuchi, Y.; Doi, M. S. Large Network Swelling and Solvent Redistribution Are Necessary for Polymer Gels to Show Negative Normal Stress. *ACS Macro Lett.* **2017**, *6*, 512–514, DOI: 10.1021/acsmacrolett.7b00153.

(120) Yoon, J. W.; Cai, S. Q.; Suo, Z. G.; Hayward, R. C. Poroelastic Swelling Kinetics of Thin Hydrogel Layers: Comparison of Theory and Experiment. *Soft Matter* **2010**, *6*, 6004–6012, DOI: 10.1039/c0sm00434k.

(121) van der Sman, R. G. M. Biopolymer Gel Swelling Analysed with Scaling Laws and Flory–Rehner Theory. *Food Hydrocolloids* **2015**, *48*, 94–101, DOI: 10.1016/j.foodhyd.2015.01.025.

(122) Button, B.; Goodell, H. P.; Atieh, E.; Chen, Y. C.; Williams, R.; Shenoy, S.; Lackey, E.; Shenkute, N. T.; Cai, L. H.; Dennis, R. G.; Boucher, R. C.; Rubinstein, M. Roles of mucus adhesion and cohesion in cough clearance. *Proc. Natl. Acad. Sci. U. S. A.* **2018**, *115*, 12501–12506, DOI: 10.1073/pnas.1811787115.

(123) Button, B.; Cai, L. H.; Ehre, C.; Kesimer, M.; Hill, D. B.; Sheehan, J. K.; Boucher, R. C.; Rubinstein, M. A Periciliary Brush Promotes the Lung Health by Separating the Mucus Layer from Airway Epithelia. *Science* **2012**, *337*, 937–941, DOI: 10.1126/science.1223012.

(124) Oh, K. S.; Oh, J. S.; Choi, H. S.; Bae, Y. C. Effect of Cross-Linking Density on Swelling Behavior of NIPA Gel Particles. *Macromolecules* **1998**, *31*, 7328–7335, DOI: 10.1021/ma971554y.

(125) Illeperuma, W. R. K.; Sun, J. Y.; Suo, Z. G.; Vlassak, J. J. Force and Stroke of a Hydrogel Actuator. *Soft Matter* **2013**, *9*, 8504–8511, DOI: 10.1039/c3sm51617b.

(126) Pescosolido, L.; Feruglio, L.; Farra, R.; Fiorentino, S.; Colombo, I.; Coviello, T.; Matricardi, P.; Hennink, W. E.; Vermonden, T.; Grassi, M. Mesh-Size Distribution Determination of Interpenetrating Polymer Network Hydrogels. *Soft Matter* **2012**, *8*, 7708–7715, DOI: 10.1039/c2sm25677k.

(127) Hagel, V.; Haraszti, T.; Boehm, H. Diffusion and Interaction in PEG-DA hydrogels. *Biointerphases* **2013**, *8*, DOI: 10.1186/1559-4106-8-36.

(128) Canal, T.; Peppas, N. A. Correlation between Mesh Size and Equilibrium Degree of Swelling of Polymeric Networks. *J. Biomed. Mater. Res.* **1989**, *23*, 1183–1193, DOI: 10.1002/jbm.820231007.

(129) Tsuji, Y.; Li, X.; Shibayama, M. Evaluation of Mesh Size in Model Polymer Networks Consisting of Tetra-Arm and Linear Poly(ethylene glycol)s. *Gels* **2018**, *4*, DOI: 10.3390/gels4020050.

(130) Tosaka, M.; Tsuji, M.; Kohjiya, S. High-Resolution Transmission Electron Microscopy of Polymer Crystals. *Mater. Sci. Res. Int.* **1998**, *4*, 79–85.

(131) Sherman, E. S.; Adams, W. W.; Thomas, E. L. Dark-Field Imaging of Semi-Crystalline Polymers by Scanning-Transmission Electron-Microscopy. *J. Mater. Sci.* **1981**, *16*, 1–9, DOI: 10.1007/Bf00552052.

(132) O'Hara, K.; Takacs, C. J.; Liu, S. J.; Cruciani, F.; Beaujuge, P.; Hawker, C. J.; Chabinyc, M. L. Effect of Alkyl Side Chains on Intercrystallite Ordering in Semiconducting Polymers. *Macromolecules* **2019**, *52*, 2853–2862, DOI: 10.1021/acs.macromol.8b02760.

(133) Taylor, G. R.; Darin, S. R. Birefringence and Crystallization in Elastomers. *J. Appl. Phys.* **1955**, *26*, 1075–1079, DOI: 10.1063/1.1722153.

(134) Di Credico, B.; Cobani, E.; Callone, E.; Conzatti, L.; Cristofori, D.; D'Arienzo, M.; Dire, S.; Giannini, L.; Hanel, T.; Scotti, R.; Stagnaro, P.; Tadiello, L.; Morazzoni, F. Size-Controlled Self-Assembly of Anisotropic Sepiolite Fibers in Rubber Nanocomposites. *Appl. Clay Sci.* **2018**, *152*, 51–64, DOI: 10.1016/j.clay.2017.10.032.

(135) Park, S.; He, S. Y.; Wang, J. N.; Stein, A.; Macosko, C. W. Graphene–Polyethylene Nanocomposites: Effect of Graphene Functionalization. *Polymer* **2016**, *104*, 1–9, DOI: 10.1016/j.polymer.2016.09.058.

(136) Voorhaar, L.; Diaz, M. M.; Leroux, F.; Rogers, S.; Abakumov, A. M.; Van Tendeloo, G.; Van Assche, G.; Van Mele, B.; Hoogenboom, R. Supramolecular Thermoplastics and Thermoplastic Elastomer Materials with Self-Healing Ability Based on Oligomeric Charged Triblock Copolymers. *NPG Asia Mater.* **2017**, *9*, DOI: 10.1038/am.2017.63.

(137) Botterhuis, N. E.; van Beek, D. J. M.; van Gemert, G. M. L.; Bosman, A. W.; Sijbesma, R. P. Self-Assembly and Morphology of Polydimethylsiloxane Supramolecular Thermoplastic Elastomers. *J. Polym. Sci., Part A: Polym. Chem.* **2008**, *46*, 3877–3885, DOI: 10.1002/pola.22680.

(138) Qin, C. L.; Jin, Z.; Bai, X. D.; Jiang, H. J.; Ca, W. M. Compatibility of Polyurethane/(Vinyl Ester Resin)(Ethyl Acrylate) Interpenetrating Polymer Network. *Polym. J.* **2007**, *39*, 1365–1372, DOI: 10.1295/polymj.PJ2006186.

(139) Shi, W. C.; Hamilton, A. L.; Delaney, K. T.; Fredrickson, G. H.; Kramer, E. J.; Ntaras, C.; Avgeropoulos, A.; Lynd, N. A.; Demassieux, Q.; Creton, C. Aperiodic "Bricks and Mortar" Mesophase: a New Equilibrium State of Soft Matter and Application as

a Stiff Thermoplastic Elastomer. *Macromolecules* **2015**, *48*, 5378–5384, DOI: 10.1021/acs.macromol.5b01210.

(140) Feng, X. Y.; Burke, C. J.; Zhuo, M. J.; Guo, H.; Yang, K. Q.; Reddy, A.; Prasad, I.; Ho, R. M.; Avgeropoulos, A.; Grason, G. M.; Thomas, E. L. Seeing Mesoatomic Distortions in Soft-Matter Crystals of a Double-Gyroid Block Copolymer. *Nature* **2019**, *575*, 175–179, DOI: 10.1038/s41586-019-1706-1.

(141) Khandpur, A. K.; Macosko, C. W.; Bates, F. S. Transmission Electron-Microscopy of Saturated-Hydrocarbon Block-Copolymers. *J. Polym. Sci., Part B: Polym. Phys.* **1995**, *33*, 247–252, DOI: 10.1002/polb.1995.090330209.

(142) Oostergetel, G. T.; Esselink, F. J.; Hadzioannou, G. Cryoelectron Microscopy of Block-Copolymers in an Organic-Solvent. *Langmuir* **1995**, *11*, 3721–3724, DOI: 10.1021/la00010a022.

(143) Hernandez-Cerdan, P.; Mansel, B. W.; Leis, A.; Lundin, L.; Williams, M. A. K. Structural Analysis of Polysaccharide Networks by Transmission Electron Microscopy: Comparison with Small-Angle X-ray Scattering. *Biomacromolecules* **2018**, *19*, 989–995, DOI: 10.1021/acs.biomac.7b01773.

(144) Danielsen, S. P. O.; Sanoja, G. E.; McCuskey, S. R.; Hammouda, B.; Bazan, G. C.; Fredrickson, G. H.; Segalman, R. A. Mixed Conductive Soft Solids by Electrostatically Driven Network Formation of a Conjugated Polyelectrolyte. *Chem. Mater.* **2018**, *30*, 1417–1426, DOI: 10.1021/acs.chemmater.7b05303.

(145) Marmorat, C.; Arinstein, A.; Koifman, N.; Talmon, Y.; Zussman, E.; Rafailovich, M. Cryo-Imaging of Hydrogels Supermolecular Structure. *Sci. Rep.* **2016**, *6*, 25495, DOI: 10.1038/srep25495.

(146) Zasadzinski, J. A. N.; Chu, A.; Prudhomme, R. K. Transmission Electron-Microscopy of Gel Network Morphology — Relating Network Microstructure to Mechanical-Properties. *Macromolecules* **1986**, *19*, 2960–2964, DOI: 10.1021/ma00166a014.

(147) Michler, G. H. *Electron Microscopy of Polymers*; Springer Laboratory Manuals in Polymer Science; Springer: Berlin, 2008; p 473.

(148) Ercius, P.; Alaidi, O.; Rames, M. J.; Ren, G. Electron Tomography: A Three-Dimensional Analytic Tool for Hard and Soft Materials Research. *Adv. Mater.* **2015**, *27*, 5638–5663, DOI: 10.1002/adma.201501015.

(149) Trent, J. S.; Scheinbeim, J. I.; Couchman, P. R. Ruthenium Tetraoxide Staining of Polymers for Electron-Microscopy. *Macromolecules* **1983**, *16*, 589–598, DOI: 10.1021/ma00238a021.

(150) Severs, N. J. Freeze-Fracture Electron Microscopy. *Nat. Protoc.* **2007**, *2*, 547–76, DOI: 10.1038/nprot.2007.55.

(151) Filippidi, E.; Cristiani, T. R.; Eisenbach, C. D.; Waite, J. H.; Israelachvili, J. N.; Ahn, B. K.; Valentine, M. T. Toughening Elastomers using Mussel-Inspired Iron–Catechol Complexes. *Science* **2017**, *358*, 502–505, DOI: 10.1126/science.aao0350.

(152) Möckl, L.; Moerner, W. E. Super-Resolution Microscopy with Single Molecules in Biology and Beyond—Essentials, Current Trends, and Future Challenges. *J. Am. Chem. Soc.* **2020**, *142*, 17828–17844, DOI: 10.1021/jacs.0c08178.

(153) Qiang, Z.; Wang, M. Z. 100th Anniversary of Macromolecular Science Viewpoint: Enabling Advances in Fluorescence Microscopy Techniques. *ACS Macro Lett.* **2020**, *9*, 1342–1356, DOI: 10.1021/acsmacrolett.0c00506.

(154) Tagaya, A. In *Encyclopedia of Polymeric Nanomaterials*; Kobayashi, S., Mullen, K., Eds.; Springer: Berlin, 2015; DOI: 10.1007/978-3-642-29648-2_116.

(155) Hao, X. B.; Zeng, Y. C. A Review on the Studies of Air Flow Field and Fiber Formation Process during Melt Blowing. *Ind. Eng. Chem. Res.* **2019**, *58*, 11624–11637, DOI: 10.1021/acs.iecr.9b01694.

(156) Wang, H.; Newstein, M. C.; Chang, M. Y.; Balsara, N. P.; Garetz, B. A. Birefringence and Depolarized Light Scattering of an Ordered Block Copolymer Melt under Shear Flow. *Macromolecules* **2000**, *33*, 3719–3730, DOI: 10.1021/ma991982z.

(157) Tosaka, M.; Kohjiya, S.; Ikeda, Y.; Toki, S.; Hsiao, B. S. Molecular Orientation and Stress Relaxation during Strain-Induced Crystallization of Vulcanized Natural Rubber. *Polym. J.* **2010**, *42*, 474–481, DOI: 10.1038/pj.2010.22.

(158) Stein, R. S. Rheo-Optical Studies of Rubbers. *Rubber Chem. Technol.* **1976**, *49*, 458–535, DOI: 10.5254/1.3534975.

(159) Es-Haghi, S. S.; Offenbach, I.; Debnath, D.; Weiss, R. A.; Cakmak, M. Mechano-Optical Behavior of Loosely Crosslinked Double-Network Hydrogels: Modeling and Real-Time Birefringence Measurement During Uniaxial Extension. *Polymer* **2017**, *115*, 239–245, DOI: 10.1016/j.polymer.2017.03.047.

(160) Balsara, N. P.; Perahia, D.; Safinya, C. R.; Tirrell, M.; Lodge, T. P. Birefringence Detection of the Order-to-Disorder Transition in Block Copolymer Liquids. *Macromolecules* **1992**, *25*, 3896–3901, DOI: 10.1021/ma00041a011.

(161) Balsara, N. P.; Garetz, B. A.; Dai, H. J. Relationship between Birefringence and the Structure of Ordered Block Copolymer Materials. *Macromolecules* **1992**, *25*, 6072–6074, DOI: 10.1021/ma00048a036.

(162) Renard, D.; Axelos, M. A. V.; Boué, F.; Lefebvre, J. "Ordered" Structure in Solutions and Gels of a Globular Protein as Studied by Small Angle Neutron Scattering. *Biopolymers* **1996**, *39*, 149–159, DOI: 10.1002/(SICI)1097-0282(199608)39.

(163) Vallera, A. M.; Cruz, M. M.; Ring, S.; Boué, F. The Structure of Amylose Gels. *J. Phys.: Condens. Matter* **1994**, *6*, 311–320, DOI: 10.1088/0953-8984/6/2/003.

(164) Mendes, E.; Girard, B.; Picot, C.; Buzier, M.; Boué, F.; Bastide, J. Small-Angle Neutron-Scattering Study of End-Linked Gels. *Macromolecules* **1993**, *26*, 6873–6877, DOI: 10.1021/ma00077a025.

(165) Mendes, E.; Lutz, P.; Bastide, J.; Boué, F. Soft Order in High-Functionality Star Polymer-Solutions and Gels — a Small-Angle Neutron-Scattering Study. *Macromolecules* **1995**, *28*, 174–179, DOI: 10.1021/ma00105a023.

(166) Matsunaga, T.; Sakai, T.; Akagi, Y.; Chung, U. I.; Shibayama, M. SANS and SLS Studies on Tetra-Arm PEG Gels in As-Prepared and Swollen States. *Macromolecules* **2009**, *42*, 6245–6252, DOI: 10.1021/ma901013q.

(167) Tian, J.; Seery, T. A. P.; Ho, D. L.; Weiss, R. A. Physically Cross-Linked Alkylacrylamide Hydrogels: A SANS Analysis of the Microstructure. *Macromolecules* **2004**, *37*, 10001–10008, DOI: 10.1021/ma049474z.

(168) Tominaga, T.; Tirumala, V. R.; Lin, E. K.; Gong, J. P.; Furukawa, H.; Osada, Y.; Wu, W. L. The Molecular Origin of Enhanced Toughness in Double-Network Hydrogels: A

Neutron Scattering Study. *Polymer* **2007**, *48*, 7449–7454, DOI: 10.1016/j.polymer.2007.10.016.

(169) Ohira, M.; Tsuji, Y.; Watanabe, N.; Morishima, K.; Gilbert, E. P.; Li, X.; Shibayama, M. Quantitative Structure Analysis of a Near-Ideal Polymer Network with Deuterium Label by Small-Angle Neutron Scattering. *Macromolecules* **2020**, *53*, 4047–4054, DOI: 10.1021/acs.macromol.9b02695.

(170) de Gennes, P. G.; Pincus, P.; Velasco, R. M.; Brochard, F. Remarks on Polyelectrolyte Conformation. *J. Phys.* **1976**, *37*, 1461–1473, DOI: 10.1051/jphys:0197600370120146100.

(171) Nierlich, M.; Williams, C. E.; Boué, F.; Cotton, J. P.; Daoud, M.; Farnoux, B.; Jannink, G.; Picot, C.; Moan, M.; Wolff, C.; Rinaudo, M.; de Gennes, P. G. Small-Angle Neutron Scattering by Semi-Dilute Solutions of Polyelectrolytes. *J. Phys.* **1979**, *40*, 701–704, DOI: 10.1051/jphys:01979004007070100.

(172) Ise, N.; Okubo, T. Ordered Distribution of Electrically Charged Solutes in Dilute-Solutions. *Acc. Chem. Res.* **1980**, *13*, 303–309, DOI: 10.1021/ar50153a002.

(173) Ise, N.; Okubo, T.; Yamamoto, K.; Matsuoka, H.; Kawai, H.; Hashimoto, T.; Fujimura, M. Ordered Structure in Dilute-Solutions of Poly-L-Lysine as Studied by Small-Angle X-Ray-Scattering. *J. Chem. Phys.* **1983**, *78*, 541–545, DOI: 10.1063/1.444480.

(174) Ise, N.; Okubo, T.; Kunugi, S.; Matsuoka, H.; Yamamoto, K.; Ishii, Y. Ordered Structure in Dilute-Solutions of Sodium Polystyrenesulfonates as Studied by Small-Angle X-Ray-Scattering. *J. Chem. Phys.* **1984**, *81*, 3294–3306, DOI: 10.1063/1.448009.

(175) Drifford, M.; Dalbiez, J. P. Light-Scattering by Dilute-Solutions of Salt-Free Polyelectrolytes. *J. Phys. Chem.* **1984**, *88*, 5368–5375, DOI: 10.1021/j150666a052.

(176) Nierlich, M.; Boué, F.; Lapp, A.; Oberthur, R. Characteristic Lengths and the Structure of Salt Free Polyelectrolyte Solutions—a Small-Angle Neutron-Scattering Study. *Colloid and Polymer Science* **1985**, *263*, 955–964, DOI: 10.1007/Bf01410988.

(177) Borsali, R.; Nguyen, H.; Pecora, R. Small-Angle Neutron Scattering and Dynamic Light Scattering from a Polyelectrolyte Solution: DNA. *Macromolecules* **1998**, *31*, 1548–1555, DOI: 10.1021/ma970919b.

(178) Prabhu, V. M.; Muthukumar, M.; Wignall, G. D.; Melnichenko, Y. B. Polyelectrolyte Chain Dimensions and Concentration Fluctuations near Phase Boundaries. *J. Chem. Phys.* **2003**, *119*, 4085–4098, DOI: 10.1063/1.1592496.

(179) Panyukov, S.; Rabin, Y. Statistical Physics of Polymer Gels. *Phys. Rep.* **1996**, *269*, 1–131, DOI: 10.1016/0370-1573(95)00068-2.

(180) Nishi, K.; Asai, H.; Fujii, K.; Han, Y. S.; Kim, T. H.; Sakai, T.; Shibayama, M. Small-Angle Neutron Scattering Study on Defect-Controlled Polymer Networks. *Macromolecules* **2014**, *47*, 1801–1809, DOI: 10.1021/ma402590n.

(181) Mariani, G.; Colard-Itte, J. R.; Moulin, E.; Giuseppone, N.; Buhler, E. Structural Properties of Contractile Gels Based on Light-Driven Molecular Motors: a Small-Angle Neutron and X-ray Study. *Soft Matter* **2020**, *16*, 4008–4023, DOI: 10.1039/d0sm00031k.

(182) Cristiani, T. R.; Filippidi, E.; Behrens, R. L.; Valentine, M. T.; Eisenbach, C. D. Tailoring the

Toughness of Elastomers by Incorporating Ionic Cross-Linking. *Macromolecules* **2020**, *53*, 4099–4109, DOI: 10.1021/acs.macromol.0c00500.

(183) Mendes, E.; Oeser, R.; Hayes, C.; Boué, F.; Bastide, J. Small-Angle Neutron Scattering Study of Swollen Elongated Gels: Butterfly Patterns. *Macromolecules* **1996**, *29*, 5574–5584, DOI: 10.1021/ma960043t.

(184) Rouf-George, C.; Munch, J. P.; Schosseler, F.; Pouchelon, A.; Beinert, G.; Boué, F.; Bastide, J. Thermal and Quenched Fluctuations of Polymer Concentration in Poly(dimethylsiloxane) Gels. *Macromolecules* **1997**, *30*, 8344–8359, DOI: 10.1021/ma970916z.

(185) Mendes, E.; Hakiki, A.; Herz, J.; Boué, F.; Bastide, J. Structure of Trifunctional End-Link Polymer Gels Studied by SANS. *Macromolecules* **2004**, *37*, 2643–2649, DOI: 10.1021/ma034411m.

(186) Boué, F.; Bastide, J.; Buzier, M.; Lapp, A.; Herz, J.; Vilgis, T. A. Strain-Induced Large Fluctuations during Stress-Relaxation in Polymer Melts Observed by Small-Angle Neutron-Scattering — Lozenges, Butterflies, and Related Theory. *Colloid Polym. Sci.* **1991**, *269*, 195–216, DOI: 10.1007/Bf00665493.

(187) Ramzi, A.; Zielinski, F.; Bastide, J.; Boué, F. Butterfly Patterns — Small-Angle Neutron-Scattering from Deuterated Mobile Chains in a Randomly Cross-Linked Polystyrene Network. *Macromolecules* **1995**, *28*, 3570–3587, DOI: 10.1021/ma00114a010.

(188) Mischenko, N.; Reynders, K.; Mortensen, K.; Overberg, N.; Reynaers, H. "Butterfly"-like Patterns of Triblock Copolymer Gels as Observed by Small-Angle Neutron Scattering. *J. Polym. Sci., Part B: Polym. Phys.* **1996**, *34*, 2739–2745, DOI: 10.1002/polb.1996.946.

(189) Bastide, J.; Herz, J.; Boué, F. Loss of Affineness in Gels and Melts. *J. Phys.* **1985**, *46*, 1967–1979, DOI: 10.1051/jphys:019850046011019670O.

(190) Ramzi, A.; Mendes, E.; Zielinski, F.; Rouf, C.; Hakiki, A.; Herz, J.; Oeser, R.; Boué, F.; Bastide, J. Strain-Induced Fluctuations in Polymer Networks, Melts and Gels (Butterfly Patterns). *J. Phys. IV* **1993**, *3*, 91–98, DOI: 10.1051/jp4:1993818.

(191) Falcao, A. N.; Pedersen, J. S.; Mortensen, K.; Boué, F. Polydimethylsiloxane Networks at Equilibrium Swelling: Extracted and Nonextracted Networks. *Macromolecules* **1996**, *29*, 809–818, DOI: 10.1021/ma941014q.

(192) RoufGeorge, C.; Munch, J. P.; Beinert, G.; Isel, F.; Pouchelon, A.; Palierne, J. F.; Boué, F.; Bastide, J. About "Defects" in Networks Made by End-Linking. *Polym. Gels Networks* **1996**, *4*, 435–450, DOI: 10.1016/S0966-7822(96)00023-8.

(193) Panyukov, S.; Rabin, Y. Polymer Gels: Frozen Inhomogeneities and Density Fluctuations. *Macromolecules* **1996**, *29*, 7960–7975, DOI: 10.1021/ma960164t.

(194) Rabin, Y.; Panyukov, S. Scattering Profiles of Charged Gels: Frozen Inhomogeneities, Thermal Fluctuations, and Microphase Separation. *Macromolecules* **1997**, *30*, 301–312, DOI: 10.1021/ma960826e.

(195) Shiwa, Y.; Shibayama, M. Anisotropic Scattering Profiles of Charged Gels in a Deformed State. *Phys. Rev. E* **1999**, *59*, 5891–5894, DOI: 10.1103/PhysRevE.59.5891.

(196) Norisuye, T.; Masui, N.; Kida, Y.; Ikuta, D.; Kokufuta, E.; Ito, S.; Panyukov, S.; Shibayama, M. Small-

Angle Neutron Scattering Studies on Structural Inhomogeneities in Polymer Gels: Irradiation Cross-Linked Gels vs. Chemically Cross-Linked Gels. *Polymer* **2002**, *43*, 5289–5297, DOI: 10.1016/S0032-3861(02)00343-9.

(197) Shibayama, M. Spatial Inhomogeneity and Dynamic Fluctuations of Polymer Gels. *Macromol. Chem. Phys.* **1998**, *199*, 1–30, DOI: 10.1002/(SICI)1521-3935(19980101)199.

(198) Mischenko, N.; Reynders, K.; Koch, M. H. J.; Mortensen, K.; Pedersen, J. S.; Fontaine, F.; Graulus, R.; Reynaers, H. Small-Angle X-Ray and Neutron-Scattering from Bulk and Oriented Triblock Copolymer Gels. *Macromolecules* **1995**, *28*, 2054–2062, DOI: 10.1021/ma00110a045.

(199) Mendes, E.; Lindner, P.; Buzier, M.; Boué, F.; Bastide, J. Experimental-Evidence for Inhomogeneous Swelling and Deformation in Statistical Gels. *Phys. Rev. Lett.* **1991**, *66*, 1595–1598, DOI: 10.1103/PhysRevLett.66.1595.

(200) Eberle, A. P. R.; Porcar, L. Flow-SANS and Rheo-SANS applied to Soft Matter. *Curr. Opin. Colloid Interface Sci.* **2012**, *17*, 33–43, DOI: 10.1016/j.cocis.2011.12.001.

(201) Ruocco, N.; Dahbi, L.; Driva, P.; Hadjichristidis, N.; Allgaier, J.; Radulescu, A.; Sharp, M.; Lindner, P.; Straube, E.; Pyckhout-Hintzen, W.; Richter, D. Microscopic Relaxation Processes in Branched-Linear Polymer Blends by Rheo-SANS. *Macromolecules* **2013**, *46*, 9122–9133, DOI: 10.1021/ma4014498.

(202) Takahashi, N.; Kanaya, T.; Nishida, K.; Takahashi, Y.; Arai, M. Rheo-SANS Study on Gelation of Poly(vinyl alcohol). *Phys. B* **2006**, *385*, 810–813, DOI: 10.1016/j.physb.2006.06.096.

(203) Lee, J. C. W.; Porcar, L.; Rogers, S. A. Recovery Rheology via Rheo-SANS: Application to Step-Strains under Out-of-Equilibrium Conditions. *AIChE J.* **2019**, *65*, DOI: 10.1002/aic.16797.

(204) Dechnarong, N.; Kamitani, K.; Cheng, C.-H.; Masuda, S.; Nozaki, S.; Nagano, C.; Amamoto, Y.; Kojio, K.; Takahara, A. In Situ Synchrotron Radiation X-ray Scattering Investigation of a Microphase-Separated Structure of Thermoplastic Elastomers under Uniaxial and Equi-Biaxial Deformation Modes. *Macromolecules* **2020**, *53*, 8901–8909, DOI: 10.1021/acs.macromol.0c00962.

(205) Murphy, R. P.; Riedel, Z. W.; Nakatani, M. A.; Salipante, P. F.; Weston, J. S.; Hudson, S. D.; Weigandt, K. M. Capillary RheoSANS: Measuring the Rheology and Nanostructure of Complex Fluids at High Shear Rates. *Soft Matter* **2020**, *16*, 6285–6293, DOI: 10.1039/d0sm00941e.

(206) Lopez, C. G.; Watanabe, T.; Martel, A.; Porcar, L.; Cabral, J. T. Microfluidic-SANS: Flow Processing of Complex Fluids. *Sci. Rep.* **2015**, *5*, 7727, DOI: 10.1038/srep07727.

(207) Corona, P. T.; Ruocco, N.; Weigandt, K. M.; Leal, L. G.; Helgeson, M. E. Probing Flow-Induced Nanostructure of Complex Fluids in Arbitrary 2D Flows using a Fluidic Four-Roll Mill (FFoRM). *Sci. Rep.* **2018**, *8*, 15559, DOI: 10.1038/s41598-018-33514-8.

(208) Zhou, H. X.; Woo, J.; Cok, A. M.; Wang, M. Z.; Olsen, B. D.; Johnson, J. A. Counting primary loops in polymer gels. *Proc. Natl. Acad. Sci. U. S. A.* **2012**, *109*, 19119–19124, DOI: 10.1073/pnas.1213169109.

(209) Zhou, H. X.; Schon, E. M.; Wang, M. Z.; Glassman, M. J.; Liu, J.; Zhong, M. J.; Diaz, D. D.; Olsen, B. D.; Johnson, J. A.

Crossover Experiments Applied to Network Formation Reactions: Improved Strategies for Counting Elastically Inactive Molecular Defects in PEG Gels and Hyperbranched Polymers. *J. Am. Chem. Soc.* **2014**, *136*, 9464–9470, DOI: 10.1021/ja5042385.

(210) Kawamoto, K.; Zhong, M. J.; Wang, R.; Olsen, B. D.; Johnson, J. A. Loops versus Branch Functionality in Model Click Hydrogels. *Macromolecules* **2015**, *48*, 8980–8988, DOI: 10.1021/acs.macromol.5b02243.

(211) Wang, J. P.; Lin, T. S.; Gu, Y. W.; Wang, R.; Olsen, B. D.; Johnson, J. A. Counting Secondary Loops Is Required for Accurate Prediction of End-Linked Polymer Network Elasticity. *ACS Macro Lett.* **2018**, *7*, 244–249, DOI: 10.1021/acsmacrolett.8b00008.

(212) Wang, J. P.; Wang, R.; Gu, Y. W.; Sourakov, A.; Olsen, B. D.; Johnson, J. A. Counting Loops in Side-Chain Cross-Linked Polymers from Elastic Solids to Single-Chain Nanoparticles. *Chem. Sci.* **2019**, *10*, 5332–5337, DOI: 10.1039/c9sc01297d.

(213) Wang, R.; Lin, T. S.; Johnson, J. A.; Olsen, B. D. Kinetic Monte Carlo Simulation for Quantification of the Gel Point of Polymer Networks. *ACS Macro Lett.* **2017**, *6*, 1414–1419, DOI: 10.1021/acsmacrolett.7b00586.

(214) Lin, T. S.; Wang, R.; Johnson, J. A.; Olsen, B. D. Revisiting the Elasticity Theory for Real Gaussian Phantom Networks. *Macromolecules* **2019**, *52*, 1685–1694, DOI: 10.1021/acs.macromol.8b01676.

(215) Lin, T. S.; Wang, R.; Johnson, J. A.; Olsen, B. D. Topological Structure of Networks Formed from Symmetric Four-Arm Precursors. *Macromolecules* **2018**, *51*, 1224–1231, DOI: 10.1021/acs.macromol.7b01829.

(216) Saalwächter, K. Proton Multiple-Quantum NMR for the Study of Chain Dynamics and Structural Constraints in Polymeric Soft Materials. *Prog. Nucl. Mag. Res. Sp.* **2007**, *51*, 1–35, DOI: 10.1016/j.pnmrs.2007.01.001.

(217) Chasse, W.; Lang, M.; Sommer, J. U.; Saalwächter, K. Cross-Link Density Estimation of PDMS Networks with Precise Consideration of Networks Defects. *Macromolecules* **2012**, *45*, 899–912, DOI: 10.1021/ma202030z.

(218) Lange, F.; Schwenke, K.; Kurakazu, M.; Akagi, Y.; Chung, U. I.; Lang, M.; Sommer, J. U.; Sakai, T.; Saalwächter, K. Connectivity and Structural Defects in Model Hydrogels: A Combined Proton NMR and Monte Carlo Simulation Study. *Macromolecules* **2011**, *44*, 9666–9674, DOI: 10.1021/ma201847v.

(219) Saalwächter, K.; Kleinschmidt, F.; Sommer, J. U. Swelling Heterogeneities in End-Linked Model Networks: A Combined Proton Multiple-Quantum NMR and Computer Simulation Study. *Macromolecules* **2004**, *37*, 8556–8568, DOI: 10.1021/ma048803k.

(220) Callaghan, P. T.; Samulski, E. T. Molecular Weight Dependence of Nuclear Spin Correlations in PDMS Networks. *Macromolecules* **2000**, *33*, 3795–3802, DOI: 10.1021/ma0000125.

(221) Saalwächter, K.; Herrero, B.; Lopez-Manchado, M. A. Chain Order and Cross-Link Density of Elastomers as Investigated by Proton Multiple-Quantum NMR. *Macromolecules* **2005**, *38*, 9650–9660, DOI: 10.1021/ma051238g.

(222) Saleesung, T.; Reichert, D.; Saalwächter, K.; Sirisinha, C. Correlation of Crosslink Densities using Solid State NMR and Conventional Techniques in Peroxide-Crosslinked EPDM rubber. *Polymer* **2015**, *56*, 309–317, DOI: 10.1016/j.polymer.2014.10.057.

(223) Zou, X. T.; Kui, X.; Zhang, R. C.; Zhang, Y.; Wang, X. L.; Wu, Q.; Chen, T. H.; Sun, P. C. Viscoelasticity and Structures in Chemically and Physically Dual-Cross-Linked Hydrogels: Insights from Rheology and Proton Multiple-Quantum NMR Spectroscopy. *Macromolecules* **2017**, *50*, 9340–9352, DOI: 10.1021/acs.macromol.7b01854.

(224) Saalwächter, K.; Chasse, W.; Sommer, J. U. Structure and Swelling of Polymer Networks: Insights from NMR. *Soft Matter* **2013**, *9*, 6587–6593, DOI: 10.1039/c3sm50194a.

(225) Litvinov, V. M. EPDM/PP thermoplastic vulcanizates as studied by proton NMR relaxation: Phase composition, molecular mobility, network structure in the rubbery phase, and network heterogeneity. *Macromolecules* **2006**, *39*, 8727–8741, DOI: 10.1021/ma061911h.

(226) Li, Y.; Sariyer, O. S.; Ramachandran, A.; Panyukov, S.; Rubinstein, M.; Kumacheva, E. Universal Behavior of Hydrogels Confined to Narrow Capillaries. *Sci. Rep.* **2015**, *5*, DOI: 10.1038/srep17017.

(227) Prince, E.; Alizadehgiashi, M.; Campbell, M.; Khuu, N.; Albulescu, A.; De France, K.; Ratkov, D.; Li, Y. F.; Hoare, T.; Kumacheva, E. Patterning of Structurally Anisotropic Composite Hydrogel Sheets. *Biomacromolecules* **2018**, *19*, 1276–1284, DOI: 10.1021/acs.biomac.8b00100.

(228) Batchelor, G. *An Introduction to Fluid Dynamics*; Cambridge University Press: Cambridge, UK, 1967.

(229) Fujiyabu, T.; Li, X.; Shibayama, M.; Chung, U.; Sakai, T. Permeation of Water through Hydrogels with Controlled Network Structure. *Macromolecules* **2017**, *50*, 9411–9416, DOI: 10.1021/acs.macromol.7b01807.

(230) Kapur, V.; Charkoudian, J. C.; Kessler, S. B.; Anderson, J. L. Hydrodynamic Permeability of Hydrogels Stabilized within Porous Membranes. *Ind. Eng. Chem. Res.* **1996**, *35*, 3179–3185, DOI: 10.1021/ie960015z.

(231) Tokita, M.; Tanaka, T. Friction Coefficient of Polymer Networks of Gels. *J. Chem. Phys.* **1991**, *95*, 4613–4619, DOI: 10.1063/1.461729.

(232) Brochard, F.; de Gennes, P. G. Dynamical Scaling for Polymers in Theta-Solvents. *Macromolecules* **1977**, *10*, 1157–1161, DOI: 10.1021/ma60059a048.

(233) Fujiyabu, T.; Yoshikawa, Y.; Kim, J.; Sakumichi, N.; Chung, U.; Sakai, T. Shear Modulus Dependence of the Diffusion Coefficient of a Polymer Network. *Macromolecules* **2019**, *52*, 9613–9619, DOI: 10.1021/acs.macromol.9b01654.

(234) Fujiyabu, T.; Li, X.; Chung, U.; Sakai, T. Diffusion Behavior of Water Molecules in Hydrogels with Controlled Network Structure. *Macromolecules* **2019**, *52*, 1923–1929, DOI: 10.1021/acs.macromol.8b02488.

(235) Fujiki, M.; Ito, M.; Mortensen, K.; Yashima, S.; Tokita, M.; Annaka, M. Friction Coefficient of Well-Defined Hydrogel Networks. *Macromolecules* **2016**, *49*, 634–642, DOI: 10.1021/acs.macromol.5b01997.

(236) Tokita, M.; Miyoshi, T.; Takegoshi, K.; Hikichi, K. Probe Diffusion in Gels. *Phys. Rev. E* **1996**, *53*, 1823–1827, DOI: 10.1103/PhysRevE.53.1823.

(237) Saalwächter, K.; Seiffert, S. Dynamics-Based Assessment of Nanoscopic Polymer-Network Mesh Structures and their Defects. *Soft Matter* **2018**, *14*, 1976–1991, DOI: 10.1039/c7sm02444d.

(238) Axpe, E.; Chan, D.; Offeddu, G. S.; Chang, Y.; Merida, D.; Hernandez, H. L.; Appel, E. A. A Multiscale Model for

Solute Diffusion in Hydrogels. *Macromolecules* **2019**, *52*, 6889–6897, DOI: 10.1021/acs.macromol.9b00753.

(239) Yamane, Y.; Matsui, M.; Kimura, H.; Kuroki, S.; Ando, I. Diffusional Inhomogeneity of Probe Molecules in Chemically Cross-Linked Polymer Gels as Studied by Time-Dependent Diffusion NMR. *Macromolecules* **2003**, *36*, 5655–5660, DOI: 10.1021/ma030163i.

(240) Kamiguchi, K.; Kuroki, S.; Satoh, M.; Ando, I. Diffusional Behaviors of Polystyrenes with Different Molecular Weights in the Same PMMA Gel Network Elucidated by Time-Dependent Diffusion NMR spectroscopy. *Macromolecules* **2008**, *41*, 1318–1322, DOI: 10.1021/ma070488p.

(241) Valentine, M. T.; Kaplan, P. D.; Thota, D.; Crocker, J. C.; Gisler, T.; Prud'homme, R. K.; Beck, M.; Weitz, D. A. Investigating the Microenvironments of Inhomogeneous Soft Materials with Multiple Particle Tracking. *Phys. Rev. E* **2001**, *64*, 061506, DOI: 10.1103/PhysRevE.64.061506.

(242) Lee, C. H.; Crosby, A. J.; Emrick, T.; Hayward, R. C. Characterization of Heterogeneous Polyacrylamide Hydrogels by Tracking of Single Quantum Dots. *Macromolecules* **2014**, *47*, 741–749, DOI: 10.1021/ma402373s.

(243) Bharadwaj, N. A.; Schweizer, K. S.; Ewoldt, R. H. A Strain Stiffening Theory for Transient Polymer Networks under Asymptotically Nonlinear Oscillatory Shear. *J. Rheol.* **2017**, *61*, 643–665, DOI: 10.1122/1.4979368.

(244) Hyun, K.; Wilhelm, M.; Klein, C. O.; Cho, K. S.; Nam, J. G.; Ahn, K. H.; Lee, S. J.; Ewoldt, R. H.; McKinley, G. H. A Review of Nonlinear Oscillatory Shear Tests: Analysis and Application of Large Amplitude Oscillatory Shear (LAOS). *Prog. Polym. Sci.* **2011**, *36*, 1697–1753, DOI: 10.1016/j.progpolymsci.2011.02.002.

(245) Martinetti, L.; Carey-De La Torre, O.; Schweizer, K. S.; Ewoldt, R. H. Inferring the Nonlinear Mechanisms of a Reversible Network. *Macromolecules* **2018**, *51*, 8772–8789, DOI: 10.1021/acs.macromol.8b01295.

(246) Bejenariu, A. G.; Rasmussen, H. K.; Skov, A. L.; Hassager, O.; Frankaer, S. M. Large Amplitude Oscillatory Extension of Soft Polymeric Networks. *Rheo. Acta* **2010**, *49*, 807–814, DOI: 10.1007/s00397-010-0464-7.

(247) Jacob, A. R.; Deshpande, A. P.; Bouteiller, L. Large Amplitude Oscillatory Shear of Supramolecular Materials. *J. Non-Newtonian Fluid Mech.* **2014**, *206*, 40–56, DOI: 10.1016/j.jnnfm.2014.03.001.

(248) Yan, T. Z.; Schroter, K.; Herbst, F.; Binder, W. H.; Thurn-Albrecht, T. What Controls the Structure and the Linear and Nonlinear Rheological Properties of Dense, Dynamic Supramolecular Polymer Networks? *Macromolecules* **2017**, *50*, 2973–2985, DOI: 10.1021/acs.macromol.6b02507.

(249) Amin, D.; Wang, Z. W. Nonlinear Rheology and Dynamics of Supramolecular Polymer Networks Formed by Associative Telechelic Chains under Shear and Extensional Flows. *J. Rheol.* **2020**, *64*, 581–600, DOI: 10.1122/1.5120897.

(250) Suzuki, S.; Uneyama, T.; Inoue, T.; Watanabe, H. Nonlinear Rheology of Telechelic Associative Polymer Networks: Shear Thickening and Thinning Behavior of Hydrophobically Modified Ethoxylated Urethane (HEUR) in Aqueous Solution. *Macromolecules* **2012**, *45*, 888–898, DOI: 10.1021/ma202050x.

(251) Berret, J. F.; Sereo, Y.; Winkelman, B.; Calvet, D.; Collet, A.; Viguier, M. Nonlinear Rheology of Telechelic Polymer

Networks. *J. Rheol.* **2001**, *45*, 477–492, DOI: 10.1122/1.1339245.

(252) Liu, J.; Koenderink, G. H.; Kasza, K. E.; MacKintosh, F. C.; Weitz, D. A. Visualizing the Strain Field in Semiflexible Polymer Networks: Strain Fluctuations and Nonlinear Rheology of F-actin Gels. *Phys. Rev. Lett.* **2007**, *98*, 198304, DOI: 10.1103/PhysRevLett.98.198304.

(253) Callies, X.; Fonteneau, C.; Pensec, S.; Bouteiller, L.; Ducouret, G.; Creton, C. Adhesion and Non-Linear Rheology of Adhesives with Supramolecular Crosslinking Points. *Soft Matter* **2016**, *12*, 7174–7185, DOI: 10.1039/c6sm01154c.

(254) Zhang, Q. H.; Zhu, X. Y.; Li, C. H.; Cai, Y. F.; Jia, X. D.; Bao, Z. N. Disassociation and Reformation Under Strain in Polymer with Dynamic Metal–Ligand Coordination Cross-Linking. *Macromolecules* **2019**, *52*, 660–668, DOI: 10.1021/acs.macromol.8b02414.

(255) Huang, C. W.; Chen, Q.; Weiss, R. A. Nonlinear Rheology of Random Sulfonated Polystyrene Ionomers: The Role of the Sol–Gel Transition. *Macromolecules* **2016**, *49*, 9203–9214, DOI: 10.1021/acs.macromol.6b02057.

(256) Broedersz, C. P.; Kasza, K. E.; Jawerth, L. M.; Munster, S.; Weitz, D. A.; MacKintosh, F. C. Measurement of Nonlinear Rheology of Cross-Linked Biopolymer Gels. *Soft Matter* **2010**, *6*, 4120–4127, DOI: 10.1039/c0sm00285b.

(257) Fan, J. D.; Anastassiou, A.; Macosko, C. W.; Tadmor, E. B. Molecular Dynamics Predictions of Thermomechanical Properties of an Epoxy Thermosetting Polymer. *Polymer* **2020**, *196*, 122477, DOI: 10.1016/j.polymer.2020.122477.

(258) Chen, Y. L.; Kushner, A. M.; Williams, G. A.; Guan, Z. B. Multiphase Design of Autonomic Self-Healing Thermoplastic Elastomers. *Nature Chemistry* **2012**, *4*, 467–472, DOI: 10.1038/Nchem.1314.

(259) Burnworth, M.; Tang, L. M.; Kumpfer, J. R.; Duncan, A. J.; Beyer, F. L.; Fiore, G. L.; Rowan, S. J.; Weder, C. Optically Healable Supramolecular Polymers. *Nature* **2011**, *472*, 334–337, DOI: 10.1038/nature09963.

(260) Koerner, H.; Strong, R. J.; Smith, M. L.; Wang, D. H.; Tan, L. S.; Lee, K. M.; White, T. J.; Vaia, R. A. Polymer Design for High-Temperature Shape Memory: Low-Crosslink-Density Polyimides. *Polymer* **2013**, *54*, 391–402, DOI: 10.1016/j.polymer.2012.11.007.

(261) Larin, D. E.; Lazutin, A. A.; Govorun, E. N.; Vasilevskaya, V. V. Self-Assembly into Strands in Amphiphilic Polymer Brushes. *Langmuir* **2016**, *32*, 7000–7008, DOI: 10.1021/acs.langmuir.6b01208.

(262) Chan, D.; Ding, Y. C.; Dauskardt, R. H.; Appel, E. A. Engineering the Mechanical Properties of Polymer Networks with Precise Doping of Primary Defects. *ACS Appl. Mater. Interfaces* **2017**, *9*, 42217–42224, DOI: 10.1021/acsami.7b14376.

(263) Panyukov, S. Loops in Polymer Networks. *Macromolecules* **2019**, *52*, 4145–4153, DOI: 10.1021/acs.macromol.9b00782.

(264) Nishi, K.; Chijiishi, M.; Katsumoto, Y.; Nakao, T.; Fujii, K.; Chung, U.; Noguchi, H.; Sakai, T.; Shibayama, M. Rubber Elasticity for Incomplete Polymer Networks. *J. Chem. Phys.* **2012**, *137*, DOI: 10.1063/1.4769829.

(265) Lang, M. Elasticity of Phantom Model Networks with Cyclic Defects. *ACS Macro Lett.* **2018**, *7*, 536–539, DOI: 10.1021/acsmacrolett.8b00020.

(266) Panyukov, S. Theory of Flexible Polymer Networks: Elasticity and Heterogeneities. *Polymers* **2020**, *12*, DOI: 10.3390/polym12040767.

(267) Mooney, M. A Theory of Large Elastic Deformation. *J. Appl. Phys.* **1940**, *11*, 582–592, DOI: 10.1063/1.1712836.

(268) Rivlin, R. S. Large Elastic Deformations of Isotropic Materials .IV. Further Developments of the General Theory. *Philos. Trans. R. Soc., A* **1948**, *241*, 379–397, DOI: 10.1098/rsta.1948.0024.

(269) Patel, S. K.; Malone, S.; Cohen, C.; Gillmor, J. R.; Colby, R. H. Elastic Modulus and Equilibrium Swelling of Poly(dimethylsiloxane) Networks. *Macromolecules* **1992**, *25*, 5241–5251, DOI: 10.1021/ma00046a021.

(270) Davidson, J. D.; Goulbourne, N. C. A Non-Affine Network Model for Elastomers Undergoing Finite Deformations. *J. Mech. Phys. Solids* **2013**, *61*, 1784–1797, DOI: 10.1016/j.jmps.2013.03.009.

(271) Fetters, L. J.; Lohse, D. J.; Richter, D.; Witten, T. A.; Zirkel, A. Connection between Polymer Molecular-Weight, Density, Chain Dimensions, and Melt Viscoelastic Properties. *Macromolecules* **1994**, *27*, 4639–4647, DOI: 10.1021/ma00095a001.

(272) Rivlin, R. S.; Saunders, D. W. Large Elastic Deformations of Isotropic Materials .VII. Experiments on the Deformation of Rubber. *Philos. Trans. R. Soc., A* **1951**, *243*, 251–288, DOI: 10.1098/rsta.1951.0004.

(273) Xu, P.; Mark, J. E. Biaxial Extension Studies Using Inflation of Sheets of Unimodal Model Networks. *Rubber Chem. Technol.* **1990**, *63*, 276–284, DOI: 10.5254/1.3538258.

(274) Grest, G. S.; Putz, M.; Everaers, R.; Kremer, K. Stress–Strain Relation of Entangled Polymer Networks. *J. Non-Cryst. Solids* **2000**, *274*, 139–146, DOI: 10.1016/S0022-3093(00)00224-6.

(275) Jeong, S.; Baig, C. Molecular Process of Stress Relaxation for Sheared Polymer Melts. *Polymer* **2020**, *202*, DOI: 10.1016/j.polymer.2020.122683.

(276) Imbernon, L.; Norvez, S.; Leibler, L. Stress Relaxation and Self-Adhesion of Rubbers with Exchangeable Links. *Macromolecules* **2016**, *49*, 2172–2178, DOI: 10.1021/acs.macromol.5b02751.

(277) Hengeller, L.; Huang, Q.; Dorokhin, A.; Alvarez, N. J.; Almdal, K.; Hassager, O. Stress Relaxation of Bidisperse Polystyrene Melts. *Rheol. Acta* **2016**, *55*, 303–314, DOI: 10.1007/s00397-016-0916-9.

(278) Saseendran, S.; Berglund, D.; Varna, J. Stress Relaxation and Strain Recovery Phenomena During Curing and Thermomechanical Loading: Thermorheologically Simple Viscoelastic Analysis. *J. Compos. Mater.* **2019**, *53*, 3841–3859, DOI: 10.1177/0021998319848818.

(279) Krishnakumar, B.; Sanka, R. V. S. P.; Binder, W. H.; Parthasarthy, V.; Rana, S.; Karak, N. Vitrimers: Associative Dynamic Covalent Adaptive Networks in Thermoset Polymers. *Chem. Eng. J.* **2020**, *385*, DOI: 10.1016/j.cej.2019.123820.

(280) Chen, Q.; Tudryn, G. J.; Colby, R. H. Ionomer Dynamics and the Sticky Rouse Model. *J. Rheol.* **2013**, *57*, 1441–1462, DOI: 10.1122/1.4818868.

(281) Capelot, M.; Montarnal, D.; Tournilhac, F.; Leibler, L. Metal-Catalyzed Transesterification for Healing and Assembling of Thermosets. *J. Am. Chem. Soc.* **2012**, *134*, 7664–7667, DOI: 10.1021/ja302894k.

(282) Altuna, F. I.; Hoppe, C. E.; Williams, R. J. J. Epoxy Vitrimers with a Covalently Bonded Tertiary Amine as Catalyst of the Transesterification Reaction. *Eur. Polym. J.* **2019**, *113*, 297–304, DOI: 10.1016/j.eurpolymj.2019.01.045.

(283) Liu, T.; Hao, C.; Zhang, S.; Yang, X. N.; Wang, L. W.; Han, J. R.; Li, Y. Z.; Xin, J. N.; Zhang, J. W. A Self-Healable High Glass Transition Temperature Bioepoxy Material Based on Vitrimer Chemistry. *Macromolecules* **2018**, *51*, 5577–5585, DOI: 10.1021/acs.macromol.8b01010.

(284) Fortman, D. J.; Brutman, J. P.; Hillmyer, M. A.; Dichtel, W. R. Structural Effects on the Reprocessability and Stress Relaxation of Crosslinked Polyhydroxyurethanes. *J. Appl. Polym. Sci.* **2017**, *134*, DOI: 10.1002/app.44984.

(285) Münstedt, H. Rheological Experiments at Constant Stress as Efficient Method to Characterize Polymeric Materials. *J. Rheol.* **2014**, *58*, 565–587, DOI: 10.1122/1.4866049.

(286) Nicholson, L. M.; Whitley, K. S.; Gates, T. S. The Combined Influence of Molecular Weight and Temperature on the Physical Aging and Creep Compliance of a Glassy Thermoplastic Polyimide. *Mech. Time-Depend. Mat.* **2001**, *5*, 199–227, DOI: 10.1023/A:1017911509777.

(287) Wimberger-Friedl, R.; Hut, M. G. T.; Schoo, H. F. M. Chain Stiffness of Copolycarbonates Containing a Spiro Linkage. *Macromolecules* **1996**, *29*, 5453–5458, DOI: 10.1021/ma951227v.

(288) Liu, C. Y.; Li, C. X.; Chen, P.; He, J. S.; Fan, Q. R. Influence of Long-Chain Branching on Linear Viscoelastic Flow Properties and Dielectric Relaxation of Polycarbonates. *Polymer* **2004**, *45*, 2803–2812, DOI: 10.1016/j.polymer.2004.02.030.

(289) Glassman, M. J.; Chan, J.; Olsen, B. D. Reinforcement of Shear Thinning Protein Hydrogels by Responsive Block Copolymer Self-Assembly. *Adv. Funct. Mater.* **2013**, *23*, 1182–1193, DOI: 10.1002/adfm.201202034.

(290) Duffy, J. J.; Rega, C. A.; Jack, R.; Amin, S. An Algebraic Approach for Determining Viscoelastic Moduli from Creep Compliance through Application of the Generalised Stokes-Einstein Relation and Burgers Model. *Appl. Rheol.* **2016**, *26*, DOI: 10.3933/Applrheol-26-15130.

(291) Colby, R. H.; Gillmor, J. R.; Rubinstein, M. Dynamics of Near-Critical Polymer Gels. *Phys. Rev. E* **1993**, *48*, 3712–3716, DOI: 10.1103/PhysRevE.48.3712.

(292) Lusignan, C. P.; Mourey, T. H.; Wilson, J. C.; Colby, R. H. Viscoelasticity of Randomly Branched Polymers in the Critical Percolation Class. *Phys. Rev. E* **1995**, *52*, 6271–6280, DOI: 10.1103/PhysRevE.52.6271.

(293) Bull, S. J. *Scanning Probe Microscopy in Industrial Applications*; John Wiley & Sons, Ltd., 2013; DOI: 10.1002/9781118723111.ch7.

(294) Kavanagh, G. M.; Ross-Murphy, S. B. Rheological Characterisation of Polymer Gels. *Prog. Polym. Sci.* **1998**, *23*, 533–562, DOI: 10.1016/S0079-6700(97)00047-6.

(295) Chen, D. T. N.; Wen, Q.; Janmey, P. A.; Crocker, J. C.; Yodh, A. G. Rheology of Soft Materials. *Annu. Rev. Condens. Matter Phys.* **2010**, *1*, 301–322, DOI: 10.1146/annurev-conmatphys-070909-104120.

(296) Zhang, Z. P.; Rong, M. Z.; Zhang, M. Q. Polymer Engineering Based on Reversible Covalent Chemistry: A Promising Innovative Pathway Towards New Materials and New Functionalities.

Prog. Polym. Sci. **2018**, *80*, 39–93, DOI: 10.1016/j.progpolymsci.2018.03.002.

(297) Jourdain, A.; Asbai, R.; Omaima, A.; Chehimi, M. M.; Drockenmuller, E.; Montarnal, D. Rheological Properties of Covalent Adaptable Networks with 1,2,3-Triazolium Cross-Links: The Missing Link between Vitrimers and Dissociative Networks. *Macromolecules* **2020**, *53*, 1884–1900, DOI: 10.1021/acs.macromol.9b02204.

(298) Abbasi, M.; Faust, L.; Wilhelm, M. Comb and Bottlebrush Polymers with Superior Rheological and Mechanical Properties. *Adv. Mater.* **2019**, *31*, 1806484, DOI: 10.1002/adma.201806484.

(299) Campanella, A.; Dohler, D.; Binder, W. H. Self-Healing in Supramolecular Polymers. *Macromol. Rapid Commun.* **2018**, *39*, 1700739, DOI: 10.1002/marc.201700739.

(300) Saphiannikova, M.; Toshchevikov, V.; Gazuz, I.; Petry, F.; Westermann, S.; Heinrich, G. Multiscale Approach to Dynamic-Mechanical Analysis of Unfilled Rubbers. *Macromolecules* **2014**, *47*, 4813–4823, DOI: 10.1021/ma501159u.

(301) Larson, R. G. *The Structure and Rheology of Complex Fluids*; Topics in Chemical Engineering; Oxford University Press: New York, 1999; p 663.

(302) Macosko, C. W. *Rheology : Principles, Measurements, and Applications*; Advances in Interfacial Engineering Series; VCH: New York, 1994; p 550.

(303) Chen, Q.; Zhang, Z. J.; Colby, R. H. Viscoelasticity of Entangled Random Polystyrene Ionomers. *J. Rheol.* **2016**, *60*, 1031–1040, DOI: 10.1122/1.4955432.

(304) Eckstein, A.; Suhm, J.; Friedrich, C.; Maier, R. D.; Sassmannshausen, J.; Bochmann, M.; Mulhaupt, R. Determination of Plateau Moduli and Entanglement Molecular Weights of Isotactic, Syndiotactic, and Atactic Polypropylenes Synthesized with Metallocene Catalysts. *Macromolecules* **1998**, *31*, 1335–1340, DOI: 10.1021/ma971270d.

(305) Williams, M. L.; Landel, R. F.; Ferry, J. D. Mechanical Properties of Substances of High Molecular Weight .19. The Temperature Dependence of Relaxation Mechanisms in Amorphous Polymers and Other Glass-Forming Liquids. *J. Am. Chem. Soc.* **1955**, *77*, 3701–3707, DOI: 10.1021/ja01619a008.

(306) Colby, R. H.; Fetters, L. J.; Graessley, W. W. Melt Viscosity Molecular-Weight Relationship for Linear Polymers. *Macromolecules* **1987**, *20*, 2226–2237, DOI: 10.1021/ma00175a030.

(307) Rubinstein, M.; Zurek, S.; Mcleish, T. C. B.; Ball, R. C. Relaxation of Entangled Polymers at the Classical Gel Point. *J. Phys.* **1990**, *51*, 757–775, DOI: 10.1051/jphys:01990005108075700.

(308) Das, C.; Read, D. J.; Kelmanson, M. A.; McLeish, T. C. B. Dynamic Scaling in Entangled Mean-Field Gelation Polymers. *Phys. Rev. E* **2006**, *74*, 011404, DOI: 10.1103/PhysRevE.74.011404.

(309) Gasilova, E.; Benyahia, L.; Durand, D.; Nicolai, T. Influence of Entanglements on the Viscoelastic Relaxation of Polyurethane Melts and Gels. *Macromolecules* **2002**, *35*, 141–150, DOI: 10.1021/ma011412a.

(310) Sliozberg, Y. R.; Mrozek, R. A.; Schieber, J. D.; Kroger, M.; Lenhart, J. L.; Andzelm, J. W. Effect of Polymer Solvent on the Mechanical Properties of Entangled Polymer Gels: Coarse-Grained Molecular Simulation. *Polymer* **2013**, *54*, 2555–2564, DOI: 10.1016/j.polymer.2013.03.017.

(311) Langley, N. R.; Polmanteer, K. E. Relation of Elastic-Modulus to Crosslink and Entanglement Concentrations in Rubber Networks. *J. Polym. Sci. B Polym. Phys.* **1974**, *12*, 1023–1034, DOI: 10.1002/pol.1974.180120601.

(312) Vega, D. A.; Sebastian, J. M.; Loo, Y. L.; Register, R. A. Phase Behavior and Viscoelastic Properties of Entangled Block Copolymer Gels. *J. Polym. Sci. B Polym. Phys.* **2001**, *39*, 2183–2197, DOI: 10.1002/polb.1192.

(313) Rubinstein, M.; Colby, R. H. Elastic-Modulus and Equilibrium Swelling of Near-Critical Gels. *Macromolecules* **1994**, *27*, 3184–3190, DOI: 10.1021/ma00090a011.

(314) Kossuth, M. B.; Morse, D. C.; Bates, F. S. Viscoelastic Behavior of Cubic Phases in Block Copolymer Melts. *J. Rheol.* **1999**, *43*, 167–196, DOI: 10.1122/1.550981.

(315) Valentine, C. S.; Walker, L. M. Rheological Characterization of BCC and FCC Structures in Aqueous Diblock Copolymer Liquid Crystals. *Korea Aust. Rheol. J.* **2019**, *31*, 249–254, DOI: 10.1007/s13367-019-0025-2.

(316) Panyukov, S.; Rubinstein, M. Stress-Induced Ordering in Microphase-Separated Multicomponent Networks. *Macromolecules* **1996**, *29*, 8220–8230, DOI: 10.1021/ma960721b.

(317) Sakurai, S.; Aida, S.; Okamoto, S.; Ono, T.; Imaizumi, K.; Nomura, S. Preferential Orientation of Lamellar Microdomains Induced by Uniaxial Stretching of Cross-Linked Polystyrene-*block*-Polybutadiene-*block*-Polystyrene Triblock Copolymer. *Macromolecules* **2001**, *34*, 3672–3678, DOI: 10.1021/ma002123+.

(318) Sakurai, S.; Aida, S.; Okamoto, S.; Sakurai, K.; Nomura, S. Mechanism of Thermally Induced Morphological Reorganization and Lamellar Orientation from the Herringbone Structure in Cross-Linked Polystyrene-*block*-Polybutadiene-*block*-Polystyrene Triblock Copolymers. *Macromolecules* **2003**, *36*, 1930–1939, DOI: 10.1021/ma012259n.

(319) Zeng, D.; Ribbe, A.; Hayward, R. C. Anisotropic and Interconnected Nanoporous Materials from Randomly End-Linked Copolymer Networks. *Macromolecules* **2017**, *50*, 4668–4676, DOI: 10.1021/acs.macromol.7b00007.

(320) Aida, S.; Sakurai, S.; Nomura, S. Strain-Induced Ordering of Microdomain Structures in Polystyrene-*block*-Polybutadiene-*block*-Polystyrene Triblock Copolymers Cross-Linked in the Disordered State. *Polymer* **2002**, *43*, 2881–2887, DOI: 10.1016/S0032-3861(02)00058-7.

(321) Curro, J. G.; Pincus, P. A Theoretical Basis for Viscoelastic Relaxation of Elastomers in the Long-Time Limit. *Macromolecules* **1983**, *16*, 559–562, DOI: 10.1021/ma00238a014.

(322) Cai, L. H.; Kodger, T. E.; Guerra, R. E.; Pegoraro, A. F.; Rubinstein, M.; Weitz, D. A. Soft Poly(dimethylsiloxane) Elastomers from Architecture-Driven Entanglement Free Design. *Adv. Mater.* **2015**, *27*, 5132–5140, DOI: 10.1002/adma.201502771.

(323) Yamazaki, H.; Takeda, M.; Kohno, Y.; Ando, H.; Urayama, K.; Takigawa, T. Dynamic Viscoelasticity of Poly(butyl acrylate) Elastomers Containing Dangling Chains with Controlled Lengths. *Macromolecules* **2011**, *44*, 8829–8834, DOI: 10.1021/ma201941v.

(324) Ross-Murphy, S. B. Structure and Rheology of Gelatin Gels—Recent Progress. *Polymer* **1992**, *33*, 2622–2627, DOI: 10.1016/0032-3861(92)91146-S.

(325) Skrzeszewska, P. J.; de Wolf, F. A.; Stuart, M. A. C.; van der Gucht, J. Kinetics of Network Formation by Telechelic Polypeptides with Trimeric Nodes. *Soft Matter* **2010**, *6*, 416–422, DOI: 10.1039/b911032a.

(326) Winter, H. H.; Chambon, F. Analysis of Linear Viscoelasticity of a Cross-Linking Polymer at the Gel Point. *J. Rheol.* **1986**, *30*, 367–382, DOI: 10.1122/1.549853.

(327) Nijenhuis, K. T.; Winter, H. H. Mechanical Properties at the Gel Point of a Crystallizing Poly(vinyl chloride) Solution. *Macromolecules* **1989**, *22*, 411–414, DOI: 10.1021/ma00191a074.

(328) Chambon, F.; Winter, H. H. Linear Viscoelasticity at the Gel Point of a Cross-Linking PDMS with Imbalanced Stoichiometry. *J. Rheol.* **1987**, *31*, 683–697, DOI: 10.1122/1.549955.

(329) Martin, J. E.; Adolf, D.; Wilcoxon, J. P. Viscoelasticity of Near-Critical Gels. *Phys. Rev. Lett.* **1988**, *61*, 2620–2623, DOI: 10.1103/PhysRevLett.61.2620.

(330) Chen, Q.; Huang, C. W.; Weiss, R. A.; Colby, R. H. Viscoelasticity of Reversible Gelation for Ionomers. *Macromolecules* **2015**, *48*, 1221–1230, DOI: 10.1021/ma502280g.

(331) Semenov, A. N.; Rubinstein, M. Thermoreversible Gelation in Solutions of Associative Polymers. 1. Statics. *Macromolecules* **1998**, *31*, 1373–1385, DOI: 10.1021/ma970616h.

(332) Rubinstein, M.; Semenov, A. N. Thermoreversible Gelation in Solutions of Associating Polymers. 2. Linear Dynamics. *Macromolecules* **1998**, *31*, 1386–1397, DOI: 10.1021/ma970617+.

(333) Huang, C. W.; Wang, C.; Chen, Q.; Colby, R. H.; Weiss, R. A. Reversible Gelation Model Predictions of the Linear Viscoelasticity of Oligomeric Sulfonated Polystyrene Ionomer Blends. *Macromolecules* **2016**, *49*, 3936–3947, DOI: 10.1021/acs.macromol.6b00620.

(334) Leibler, L.; Rubinstein, M.; Colby, R. H. Dynamics of Reversible Networks. *Macromolecules* **1991**, *24*, 4701–4707, DOI: 10.1021/ma00016a034.

(335) Rubinstein, M.; Semenov, A. N. Dynamics of Entangled Solutions of Associating Polymers. *Macromolecules* **2001**, *34*, 1058–1068, DOI: 10.1021/ma0013049.

(336) Semenov, A. N.; Rubinstein, M. Dynamics of Entangled Associating Polymers with Large Aggregates. *Macromolecules* **2002**, *35*, 4821–4837, DOI: 10.1021/ma0117965.

(337) Stukalin, E. B.; Cai, L. H.; Kumar, N. A.; Leibler, L.; Rubinstein, M. Self-Healing of Unentangled Polymer Networks with Reversible Bonds. *Macromolecules* **2013**, *46*, 7525–7541, DOI: 10.1021/ma401111n.

(338) Chen, Q.; Liang, S. W.; Shiau, H. S.; Colby, R. H. Linear Viscoelastic and Dielectric Properties of Phosphonium Siloxane Ionomers. *ACS Macro Lett.* **2013**, *2*, 970–974, DOI: 10.1021/mz400476w.

(339) Yablon, D. G. *Scanning Probe Microscopy in Industrial Applications*; John Wiley & Sons, Ltd., 2013; DOI: 10.1002/9781118723111.ch1.

(340) Fischer-Cripps, A. C. *Nanoindentation*; Springer Science & Business Media, 2011.

(341) Oliver, W. C.; Pharr, G. M. An Improved Technique for Determining Hardness and Elastic-Modulus Using Load and Displacement Sensing Indentation Experiments. *J. Mater. Res.* **1992**, *7*, 1564–1583, DOI: 10.1557/Jmr.1992.1564.

(342) Ferencz, R.; Sanchez, J.; Blumich, B.; Herrmann, W. AFM Nanoindentation to Determine Young's Modulus for Different EPDM elastomers. *Polym. Test.* **2012**, *31*, 425–432, DOI: 10.1016/j.polymertesting.2012.01.003.

(343) Jee, A. Y.; Lee, M. Comparative Analysis on the Nanoindentation of Polymers Using Atomic Force Microscopy. *Polym. Test.* **2010**, *29*, 95–99, DOI: 10.1016/j.polymertesting.2009.09.009.

(344) Tranchida, D.; Piccarolo, S.; Loos, J.; Alexeev, A. Mechanical Characterization of Polymers on a Nanometer Scale through Nanoindentation. A study on Pile-up and Viscoelasticity. *Macromolecules* **2007**, *40*, 1259–1267, DOI: 10.1021/ma062140k.

(345) Bolshakov, A.; Pharr, G. M. Influences of Pile-up on the Measurement of Mechanical Properties by Load and Depth Sensing Indentation Techniques. *J. Mater. Res.* **1998**, *13*, 1049–1058, DOI: 10.1557/Jmr.1998.0146.

(346) Martinez, R.; Xu, L. R. Comparison of the Young's Moduli of Polymers Measured from Nanoindentation and Bending Experiments. *MRS Commun.* **2014**, *4*, 89–93, DOI: 10.1557/mrc.2014.19.

(347) Field, J. S.; Swain, M. V. A Simple Predictive Model for Spherical Indentation. *J. Mater. Res.* **1993**, *8*, 297–306, DOI: 10.1557/Jmr.1993.0297.

(348) Yang, S.; Zhang, Y. W.; Zeng, K. Y. Analysis of Nanoindentation Creep for Polymeric Materials. *J. Appl. Phys.* **2004**, *95*, 3655–3666, DOI: 10.1063/1.1651341.

(349) Jin, T.; Niu, X. Y.; Xiao, G. S.; Wang, Z. H.; Zhou, Z. W.; Yuan, G. Z.; Shu, X. F. Effects of Experimental Variables on PMMA Nanoindentation Measurements. *Polym. Test.* **2015**, *41*, 1–6, DOI: 10.1016/j.polymertesting.2014.09.015.

(350) Oyen, M. L.; Cook, R. F. Load–Displacement Behavior during Sharp Indentation of Viscous–Elastic–Plastic Materials. *J. Mater. Res.* **2003**, *18*, 139–150, DOI: 10.1557/Jmr.2003.0020.

(351) Ebenstein, D. M.; Wahl, K. J. A Comparison of JKR-based Methods to Analyze Quasi-Static and Dynamic Indentation Force Curves. *J. Colloid Interface Sci.* **2006**, *298*, 652–662, DOI: 10.1016/j.jcis.2005.12.062.

(352) Wang, Y. M.; Shang, L.; Zhang, P. P.; Yan, X. Q.; Zhang, K.; Dou, S. L.; Zhao, J. P.; Li, Y. Measurement of Viscoelastic Properties for Polymers by Nanoindentation. *Polym. Test.* **2020**, *83*, 106353, DOI: 10.1016/j.polymertesting.2020.106353.

(353) Cohen, S. R.; Kalfon-Cohen, E. Dynamic Nanoindentation by Instrumented Nanoindentation and Force Microscopy: a Comparative Review. *Beilstein J. Nanotechnol.* **2013**, *4*, 815–833, DOI: 10.3762/bjnano.4.93.

(354) Mijailoyic, A. S.; Qing, B.; Fortunato, D.; Van Vliet, K. J. Characterizing Viscoelastic Mechanical Properties of Highly Compliant Polymers and Biological Tissues using Impact Indentation. *Acta Biomater.* **2018**, *71*, 388–397, DOI: 10.1016/j.actbio.2018.02.017.

(355) Kalcioglu, Z. I.; Mahmoodian, R.; Hu, Y. H.; Suo, Z. G.; Van Vliet, K. J. From Macro- to Microscale Poroelastic Characterization of Polymeric Hydrogels via Indentation. *Soft Matter* **2012**, *8*, 3393–3398, DOI: 10.1039/c2sm06825g.

(356) Xu, Q.; Wilen, L. A.; Jensen, K. E.; Style, R. W.; Dufresne, E. R. Viscoelastic and Poroelastic Relaxations of Soft Solid Surfaces. *Phys. Rev. Lett.* **2020**, *125*, 238002, DOI: 10.1103/PhysRevLett.125.238002.

(357) Johnson, K. L.; Kendall, K.; Roberts, A. D. Surface Energy and Contact of Elastic Solids. *Proc. R. Soc. London, Ser. A* **1971**, *324*, 301–313, DOI: 10.1098/rspa.1971.0141.

(358) Brown, H. R. The Adhesion between Polymers. *Annu. Rev. Mater. Sci.* **1991**, *21*, 463–489, DOI: 10.1146/annurev.ms.21.080191.002335.

(359) Brown, H. R. Effects of Chain Pull-Out on Adhesion of Elastomers. *Macromolecules* **1993**, *26*, 1666–1670, DOI: 10.1021/ma00059a027.

(360) Brown, H. R.; Hui, C. Y.; Raphael, E. Interplay between Intermolecular Interactions and Chain Pullout in the Adhesion of Elastomers. *Macromolecules* **1994**, *27*, 608–609, DOI: 10.1021/ma00080a041.

(361) Brown, H. R. Adhesion of Polymers. *MRS Bull.* **1996**, *21*, 24–27, DOI: 10.1557/S0883769400035107.

(362) Shull, K. R.; Ahn, D.; Mowery, C. L. Finite-Size Corrections to the JKR Technique for Measuring Adhesion: Soft Spherical Caps Adhering to Flat, Rigid Surfaces. *Langmuir* **1997**, *13*, 1799–1804, DOI: 10.1021/la960845h.

(363) Brown, H. R. Chain Pullout and Mobility Effects in Friction and Lubrication. *Science* **1994**, *263*, 1411–1413, DOI: 10.1126/science.263.5152.1411.

(364) Zehnder, A. T. *Fracture Mechanics*; 2012; Vol. 62; pp 33–54, DOI: 10.1007/978-94-007-2595-9_3.

(365) Griffith, A. A. The Phenomena of Rupture and Flow in Solids. *Philos. Trans. R. Soc., A* **1921**, *221*, 163–168.

(366) Lake, G. J.; Lindley, P. B. Mechanical Fatigue Limit for Rubber. *J. Appl. Polym. Sci.* **1965**, *9*, 1233–1251, DOI: 10.1002/app.1965.070090405.

(367) Rivlin, R. S.; Thomas, A. G. Rupture of Rubber .1. Characteristic Energy for Tearing. *J. Polym. Sci.* **1953**, *10*, 291–318, DOI: 10.1002/pol.1953.120100303.

(368) Lake, G. J.; Thomas, A. G. Strength of Highly Elastic Materials. *Proc. R. Soc. London, Ser. A* **1967**, *300*, 108–119, DOI: 10.1098/rspa.1967.0160.

(369) Tang, J. D.; Li, J. Y.; Vlassak, J. J.; Suo, Z. G. Fatigue Fracture of Hydrogels. *Extreme Mech. Lett.* **2017**, *10*, 24–31, DOI: 10.1016/j.eml.2016.09.010.

(370) Akagi, Y.; Sakurai, H.; Gong, J. P.; Chung, U.; Sakai, T. Fracture Energy of Polymer Gels with Controlled Network Structures. *J. Chem. Phys.* **2013**, *139*, 144905, DOI: 10.1063/1.4823834.

(371) Cui, J.; Lackey, M. A.; Tew, G. N.; Crosby, A. J. Mechanical Properties of End-Linked PEG/PDMS Hydrogels. *Macromolecules* **2012**, *45*, 6104–6110, DOI: 10.1021/ma300593g.

(372) Akagi, Y.; Gong, J. P.; Chung, U.; Sakai, T. Transition between Phantom and Affine Network Model Observed in Polymer Gels with Controlled Network Structure. *Macromolecules* **2013**, *46*, 1035–1040, DOI: 10.1021/ma302270a.

(373) Adrian, R. J. Twenty Years of Particle Image Velocimetry. *Exp. Fluids* **2005**, *39*, 159–169, DOI: 10.1007/s00348-005-0991-7.

(374) Adrian, R. J. Particle-Imaging Techniques for Experimental Fluid-Mechanics. *Annu. Rev. Fluid Mech.* **1991**, *23*, 261–304, DOI: 10.1146/annurev.fluid.23.1.261.

(375) Wang, S. Q.; Ravindranath, S.; Boukany, P. E. Homogeneous Shear, Wall Slip, and Shear Banding of Entangled Polymeric Liquids in Simple-Shear Rheometry: A Roadmap of Nonlinear

Rheology. *Macromolecules* **2011**, *44*, 183–190, DOI: 10.1021/ma101223q.

(376) Sinton, D. Microscale Flow Visualization. *Microfluid. Nanofluidics* **2004**, *1*, 2–21, DOI: 10.1007/s10404-004-0009-4.

(377) Uemura, T.; Ueda, Y.; Iguchi, M. *Flow Visualization in Materials Processing: Practical Techniques and Selected Applications*; Mathematics for Industry; Springer, 2018; DOI: 10.1007/978-4-431-56567-3.

(378) Williams, S. J.; Park, C.; Wereley, S. T. Advances and Applications on Microfluidic Velocimetry Techniques. *Microfluid. Nanofluidics* **2010**, *8*, 709–726, DOI: 10.1007/s10404-010-0588-1.

(379) Yoda, M. Super-Resolution Imaging in Fluid Mechanics Using New Illumination Approaches. *Annu. Rev. Fluid Mech.* **2020**, *52*, 369–393, DOI: 10.1146/annurev-fluid-010719-060059.

(380) Wereley, S. T.; Meinhart, C. D. Recent Advances in Micro-Particle Image Velocimetry. *Annu. Rev. Fluid Mech.* **2010**, *42*, 557–576, DOI: 10.1146/annurev-fluid-121108-145427.

(381) Discetti, S.; Coletti, F. Volumetric Velocimetry for Fluid Flows. *Meas. Sci. Technol.* **2018**, *29*, 042001, DOI: 10.1088/1361-6501/aaa571.

(382) Katz, J.; Sheng, J. Applications of Holography in Fluid Mechanics and Particle Dynamics. *Annu. Rev. Fluid Mech.* **2010**, *42*, 531–555, DOI: 10.1146/annurev-fluid-121108-145508.

(383) Rothstein, J. P.; McKinley, G. H. The Axisymmetric Contraction-Expansion: the Role of Extensional Rheology on Vortex Growth Dynamics and the Enhanced Pressure Drop. *J. Non-Newtonian Fluid Mech.* **2001**, *98*, 33–63, DOI: 10.1016/S0377-0257(01)00094-5.

(384) Marin-Santibanez, B. M.; Perez-Gonzalez, J.; Gomez-Herrera, G.; Rodriguez-Gonzalez, F. Capillary Extrusion of Polypropylene/High-Density Polyethylene Immiscible blends as Studied by Rheo-particle Image Velocimetry. *Polym. Test.* **2020**, *84*, 106390, DOI: 10.1016/j.polymertesting.2020.106390.

(385) Gier, S.; Wagner, C. Visualization of the Flow Profile Inside a Thinning Filament During Capillary Breakup of a Polymer Solution via Particle Image Velocimetry and Particle Tracking Velocimetry. *Phys. Fluids* **2012**, *24*, 053102, DOI: 10.1063/1.4718675.

(386) Rothstein, J. P.; McKinley, G. H. Extensional Flow of a Polystyrene Boger fluid Through a 4:1:4 Axisymmetric Contraction/Expansion. *J. Non-Newtonian Fluid Mech.* **1999**, *86*, 61–88, DOI: 10.1016/S0377-0257(98)00202-X.

(387) Sathaye, S.; Mbi, A.; Sonmez, C.; Chen, Y. C.; Blair, D. L.; Schneider, J. P.; Pochan, D. J. Rheology of Peptide- and Protein-based Physical Hydrogels: Are Everyday Measurements Just Scratching the Surface? *Wiley Interdiscip. Rev.: Nanomed. Nanobiotechnol.* **2015**, *7*, 34–68, DOI: 10.1002/wnan.1299.

(388) Skrzeszewska, P. J.; Sprakel, J.; de Wolf, F. A.; Fokkink, R.; Stuart, M. A. C.; van der Gucht, J. Fracture and Self-Healing in a Well-Defined Self-Assembled Polymer Network. *Macromolecules* **2010**, *43*, 3542–3548, DOI: 10.1021/ma1000173.

(389) Zhu, X. Y.; Wang, S. Q. Mechanisms for Different Failure Modes in Startup Uniaxial Extension: Tensile (Rupture-like) Failure and Necking. *J. Rheol.* **2013**, *57*, 223–248, DOI: 10.1122/1.4764081.

(390) Li, X. G.; Wang, S. Q. Strain Localization During Squeeze of an Entangled Polymer Melt under Constant

Force. *J. Rheol.* **2018**, *62*, 491–499, DOI: 10.1122/1.5001526.

(391) Erk, K. A.; Martin, J. D.; Hu, Y. T.; Shull, K. R. Extreme Strain Localization and Sliding Friction in Physically Associating Polymer Gels. *Langmuir* **2012**, *28*, 4472–4478, DOI: 10.1021/la204592r.

(392) Migler, K. B.; Hervet, H.; Leger, L. Slip Transition of a Polymer Melt under Shear-Stress. *Phys. Rev. Lett.* **1993**, *70*, 287–290, DOI: 10.1103/PhysRevLett.70.287.

(393) Wagner, N. J. Rheo-optics. *Curr. Opin. Colloid Interface Sci.* **1998**, *3*, 391–400, DOI: 10.1016/S1359-0294(98)80055-1.

(394) Manneville, S. Recent Experimental Probes of Shear Banding. *Rheol. Acta* **2008**, *47*, 301–318, DOI: 10.1007/s00397-007-0246-z.

(395) Guo, L.; Colby, R. H.; Lusignan, C. P.; Howe, A. M. Physical Gelation of Gelatin Studied with Rheo-Optics. *Macromolecules* **2003**, *36*, 10009–10020, DOI: 10.1021/ma034266c.

(396) Pathak, J. A.; Hudson, S. D. Rheo-Optics of Equilibrium Polymer Solutions: Worm-like Micelles in Elongational Flow in a Microfluidic Cross-Slot. *Macromolecules* **2006**, *39*, 8782–8792, DOI: 10.1021/ma061355r.

(397) Rasid, I. M.; Ramirez, J.; Olsen, B. D.; Holten-Andersen, N. Understanding the Molecular Origin of Shear Thinning in Associative Polymers through Quantification of Bond Dissociation under Shear. *Phys. Rev. Mater.* **2020**, *4*, 055602, DOI: 10.1103/PhysRevMaterials.4.055602.

(398) Ilavsky, M.; Prins, W. Rheo-Optics of Poly(2-Hydroxyethyl Methacrylate) Gels .1. Effect of Nature and Amount of Diluent. *Macromolecules* **1970**, *3*, 415–425, DOI: 10.1021/ma60016a009.

(399) Ilavsky, M.; Prins, W. Rheo-Optics of Poly(2-Hydroxyethyl Methacrylate) Gels .2. Effect of Cross-Linking Density and Stage of Dilution during Network Formation. *Macromolecules* **1970**, *3*, 425–433, DOI: 10.1021/ma60016a010.

(400) Potisek, S. L.; Davis, D. A.; Sottos, N. R.; White, S. R.; Moore, J. S. Mechanophore-Linked Addition Polymers. *J. Am. Chem. Soc.* **2007**, *129*, 13808–13809, DOI: 10.1021/ja076189x.

(401) Davis, D. A.; Hamilton, A.; Yang, J. L.; Cremar, L. D.; Van Gough, D.; Potisek, S. L.; Ong, M. T.; Braun, P. V.; Martinez, T. J.; White, S. R.; Moore, J. S.; Sottos, N. R. Force-Induced Activation of Covalent Bonds in Mechanoresponsive Polymeric Materials. *Nature* **2009**, *459*, 68–72, DOI: 10.1038/nature07970.

(402) Black, A. L.; Lenhardt, J. M.; Craig, S. L. From Molecular Mechanochemistry to Stress-Responsive Materials. *J. Mater. Chem.* **2011**, *21*, 1655–1663, DOI: 10.1039/c0jm02636k.

(403) Clough, J. M.; van der Gucht, J.; Sijbesma, R. P. Mechanoluminescent Imaging of Osmotic Stress-Induced Damage in a Glassy Polymer Network. *Macromolecules* **2017**, *50*, 2043–2053, DOI: 10.1021/acs.macromol.6b02540.

(404) Kim, G.; Lau, V. M.; Halmes, A. J.; Oelze, M. L.; Moore, J. S.; Li, K. C. High-Intensity Focused Ultrasound-Induced Mechanochemical Transduction in Synthetic Elastomers. *Proc. Natl. Acad. Sci. U. S. A.* **2019**, *116*, 10214–10222, DOI: 10.1073/pnas.1901047116.

(405) Imato, K.; Irie, A.; Kosuge, T.; Ohishi, T.; Nishihara, M.; Takahara, A.; Otsuka, H. Mechanophores with a Reversible Radical System and Freezing-Induced Mechanochemistry in Polymer Solutions and Gels. *Angew. Chem.,*

Int. Ed. **2015**, *54*, 6168–6172, DOI: 10.1002/anie.201412413.

(406) Lee, C. K.; Diesendruck, C. E.; Lu, E. J.; Pickett, A. N.; May, P. A.; Moore, J. S.; Braun, P. V. Solvent Swelling Activation of a Mechanophore in a Polymer Network. *Macromolecules* **2014**, *47*, 2690–2694, DOI: 10.1021/ma500195h.

(407) Lee, C. K.; Davis, D. A.; White, S. R.; Moore, J. S.; Sottos, N. R.; Braun, P. V. Force-Induced Redistribution of a Chemical Equilibrium. *J. Am. Chem. Soc.* **2010**, *132*, 16107–16111, DOI: 10.1021/ja106332g.

(408) Jiang, S. C.; Zhang, L. X.; Xie, T. W.; Lin, Y. J.; Zhang, H.; Xu, Y. Z.; Weng, W. G.; Dai, L. Z. Mechanoresponsive PS-PnBA-PS Triblock Copolymers via Covalently Embedding Mechanophore. *ACS Macro Lett.* **2013**, *2*, 705–709, DOI: 10.1021/mz400198n.

(409) Fang, X. L.; Zhang, H.; Chen, Y. J.; Lin, Y. J.; Xu, Y. Z.; Weng, W. G. Biomimetic Modular Polymer with Tough and Stress Sensing Properties. *Macromolecules* **2013**, *46*, 6566–6574, DOI: 10.1021/ma4014862.

(410) Cao, B.; Boechler, N.; Boydston, A. J. Additive Manufacturing with a Flex Activated Mechanophore for Nondestructive Assessment of Mchanochemical Reactivity in Complex Object Geometries. *Polymer* **2018**, *152*, 4–8, DOI: 10.1016/j.polymer.2018.05.038.

(411) Gossweiler, G. R.; Hewage, G. B.; Soriano, G.; Wang, Q. M.; Welshofer, G. W.; Zhao, X. H.; Craig, S. L. Mechanochemical Activation of Covalent Bonds in Polymers with Full and Repeatable Macroscopic Shape Recovery. *ACS Macro Lett.* **2014**, *3*, 216–219, DOI: 10.1021/mz500031q.

(412) Kingsbury, C. M.; May, P. A.; Davis, D. A.; White, S. R.; Moore, J. S.; Sottos, N. R. Shear Activation of Mechanophore-Crosslinked Polymers. *J. Mater. Chem.* **2011**, *21*, 8381–8388, DOI: 10.1039/c0jm04015k.

(413) Yamaguchi, T.; Onoue, Y.; Sawae, Y. Topology and Toughening of Sparse Elastic Networks. *Phys. Rev. Lett.* **2020**, *124*, 068002, DOI: 10.1103/PhysRevLett.124.068002.

(414) Squires, T. M.; Mason, T. G. Fluid Mechanics of Microrheology. *Annu. Rev. Fluid Mech.* **2010**, *42*, 413–438, DOI: 10.1146/annurev-fluid-121108-145608.

(415) Furst, E. M.; Squires, T. M. *Microrheology*; Oxford University Press, 2017; p 480.

(416) Mason, T. G.; Weitz, D. A. Optical Measurements of Frequency-Dependent Linear Viscoelastic Moduli of Complex Fluids. *Phys. Rev. Lett.* **1995**, *74*, 1250–1253, DOI: 10.1103/PhysRevLett.74.1250.

(417) Mason, T. G. Estimating the Viscoelastic Moduli of Complex Fluids using the Generalized Stokes–Einstein Equation. *Rheo. Acta* **2000**, *39*, 371–378, DOI: 10.1007/s003970000094.

(418) Li, Q.; Peng, X. G.; Chen, D. J.; McKenna, G. B. The Laplace Approach in Microrheology. *Soft Matter* **2020**, *16*, 3378–3383, DOI: 10.1039/c9sm02242b.

(419) Cardinaux, F.; Cipelletti, L.; Scheffold, F.; Schurtenberger, P. Microrheology of Giant-Micelle Solutions. *Europhys. Lett.* **2002**, *57*, 738–744, DOI: 10.1209/epl/i2002-00525-0.

(420) Dasgupta, B. R.; Weitz, D. A. Microrheology of Cross-Linked Polyacrylamide Networks. *Phys. Rev. E* **2005**, *71*, 021504, DOI: 10.1103/PhysRevE.71.021504.

(421) Narita, T.; Indei, T. Microrheological Study of Physical Gelation in

Living Polymeric Networks. *Macromolecules* **2016**, *49*, 4634–4646, DOI: 10.1021/acs.macromol.6b00745.

(422) Mukhopadhyay, A.; Granick, S. Micro- and Nanorheology. *Curr. Opin. Colloid Interface Sci.* **2001**, *6*, 423–429, DOI: 10.1016/S1359-0294(01)00119-4.

(423) Park, J.; Bailey, E. J.; Composto, R. J.; Winey, K. I. Single-Particle Tracking of Nonsticky and Sticky Nanoparticles in Polymer Melts. *Macromolecules* **2020**, *53*, 3933–3939, DOI: 10.1021/acs.macromol.0c00457.

(424) Crocker, J. C.; Valentine, M. T.; Weeks, E. R.; Gisler, T.; Kaplan, P. D.; Yodh, A. G.; Weitz, D. A. Two-Point Microrheology of Inhomogeneous Soft Materials. *Phys. Rev. Lett.* **2000**, *85*, 888–891, DOI: 10.1103/PhysRevLett.85.888.

(425) Larsen, T. H.; Furst, E. M. Microrheology of the Liquid–Solid Transition during Gelation. *Phys. Rev. Lett.* **2008**, *100*, 146001, DOI: 10.1103/PhysRevLett.100.146001.

(426) Rizzi, L. G. Microrheological Approach for the Viscoelastic Response of Gels. *J. Rheol.* **2020**, *64*, 969–979, DOI: 10.1122/8.0000034.

(427) Oppong, F. K.; Rubatat, L.; Frisken, B. J.; Bailey, A. E.; de Bruyn, J. R. Microrheology and Structure of a Yield–Stress Polymer Gel. *Phys. Rev. E* **2006**, *73*, 041405, DOI: 10.1103/PhysRevE.73.041405.

(428) Schultz, K. M.; Furst, E. M. Microrheology of Biomaterial Hydrogelators. *Soft Matter* **2012**, *8*, 6198–6205, DOI: 10.1039/c2sm25187f.

(429) Yang, N.; Hutter, J. L.; de Bruyn, J. R. Microrheology, Microstructure, and Aging of Physically Cross-Linked Poly(vinyl alcohol)/Poly(ethylene glycol) Blends. *J. Rheol.* **2012**, *56*, 797–822, DOI: 10.1122/1.4708603.

(430) Adibnia, V.; Hill, R. J. Universal Aspects of Hydrogel Gelation Kinetics, Percolation, and Viscoelasticity from PA-Hydrogel Rheology. *J. Rheol.* **2016**, *60*, 541–548, DOI: 10.1122/1.4948428.

(431) Cheng, L. C.; Hsiao, L. C.; Doyle, P. S. Multiple Particle Tracking Study of Thermally-Gelling Nanoemulsions. *Soft Matter* **2017**, *13*, 6606–6619, DOI: 10.1039/c7sm01191a.

(432) Burla, F.; Sentjabrskaja, T.; Pletikapic, G.; Van Beugen, J.; Koenderink, G. H. Particle Diffusion in Extracellular Hydrogels. *Soft Matter* **2020**, *16*, 1366–1376, DOI: 10.1039/c9sm01837a.

(433) Bayles, A. V.; Squires, T. M.; Helgeson, M. E. Probe Microrheology without Particle Tracking by Differential Dynamic Microscopy. *Rheo. Acta* **2017**, *56*, 863–869, DOI: 10.1007/s00397-017-1047-7.

(434) Stetefeld, J.; McKenna, S.; Patel, T. Dynamic Light Scattering: A Practical Guide and Applications in Biomedical Sciences. *Biophys. Rev.* **2016**, *8*, 409–427, DOI: 10.1007/s12551-016-0218-6.

(435) Kratz, K.; Hellweg, T.; Eimer, W. Structural Changes in PNIPAm Microgel Particles as Seen by SANS, DLS, and EM Techniques. *Polymer* **2001**, *42*, 6631–6639, DOI: 10.1016/S0032-3861(01)00099-4.

(436) Xia, X. H.; Hu, Z. B. Synthesis and Light Scattering Study of Microgels with Interpenetrating Polymer Networks. *Langmuir* **2004**, *20*, 2094–2098, DOI: 10.1021/la0354483.

(437) Hetzer, M.; Schmidt, B. V. K. J.; Barner-Kowollik, C.; Ritter, H. Supramolecular Polymer Networks of Building Blocks Prepared via RAFT Polymerization.

Polym. Chem. **2014**, *5*, 2142–2152, DOI: 10.1039/c3py01624b.

(438) Chu, B. In *Soft Matter Characterization*; Borsali, R., Pecora, R., Eds.; Springer, 2008; pp 336–365.

(439) Fang, L. Q.; Brown, W.; Konak, C. Dynamic Light-Scattering Study of the Sol–Gel Transition. *Macromolecules* **1991**, *24*, 6839–6842, DOI: 10.1021/ma00026a006.

(440) Lang, P.; Burchard, W. Dynamic Light-Scattering at the Gel Point. *Macromolecules* **1991**, *24*, 814–815, DOI: 10.1021/ma00003a028.

(441) Takeda, M.; Norisuye, T.; Shibayama, M. Critical Dynamics of Cross-Linked Polymer Chains Near the Gelation Threshold. *Macromolecules* **2000**, *33*, 2909–2915, DOI: 10.1021/ma9921044.

(442) Shibayama, M.; Okamoto, M. Dynamic Light Scattering Study on Gelatin Aqueous Solutions and Gels. *J. Chem. Phys.* **2001**, *115*, 4285–4291, DOI: 10.1063/1.1391257.

(443) Innocenzi, P. *The Sol-to-Gel Transition*; 2019; pp 67–84, DOI: 10.1007/978-3-030-20030-5_6.

(444) Barretta, P.; Bordi, F.; Rinaldi, C.; Paradossi, G. A Dynamic Light Scattering Study of Hydrogels Based on Telechelic Poly(vinyl alcohol). *J. Phys. Chem. B* **2000**, *104*, 11019–11026, DOI: 10.1021/jp001863h.

(445) Maret, G. Diffusing-Wave Spectroscopy. *Curr. Opin. Colloid Interface Sci.* **1997**, *2*, 251–257, DOI: 10.1016/S1359-0294(97)80032-5.

(446) Pine, D. J.; Weitz, D. A.; Chaikin, P. M.; Herbolzheimer, E. Diffusing-Wave Spectroscopy. *Phys. Rev. Lett.* **1988**, *60*, 1134–1137, DOI: 10.1103/PhysRevLett.60.1134.

(447) Palmer, A.; Mason, T. G.; Xu, J. Y.; Kuo, S. C.; Wirtz, D. Diffusing-Wave Spectroscopy Microrheology of Actin Filament Networks. *Biophys. J.* **1999**, *76*, 1063–1071, DOI: 10.1016/S0006-3495(99)77271-1.

(448) Xu, J. Y.; Viasnoff, V.; Wirtz, D. Compliance of Actin Filament Networks Measured by Particle-Tracking Microrheology and Diffusing-Wave Spectroscopy. *Rheol. Acta* **1998**, *37*, 387–398, DOI: 10.1007/s003970050125.

(449) Dasgupta, B. R.; Tee, S. Y.; Crocker, J. C.; Frisken, B. J.; Weitz, D. A. Microrheology of Poly(ethylene oxide) using Diffusing-Wave Spectroscopy and Single Scattering. *Phys. Rev. E* **2002**, *65*, 051505, DOI: 10.1103/PhysRevE.65.051505.

(450) Liu, W.; Gong, X. J.; Zhu, Y. W.; Wang, J. Q.; Ngai, T.; Wu, C. Probing Sol–Gel Matrices and Dynamics of Star PEG Hydrogels Near Overlap Concentration. *Macromolecules* **2019**, *52*, 8956–8966, DOI: 10.1021/acs.macromol.9b01489.

(451) Shpyrko, O. G. X-Ray Photon Correlation Spectroscopy. *J. Synchrotron Radiat.* **2014**, *21*, 1057–1064, DOI: 10.1107/S1600577514018232.

(452) Leheny, R. L. XPCS: Nanoscale Motion and Rheology. *Curr. Opin. Colloid Interface Sci.* **2012**, *17*, 3–12, DOI: 10.1016/j.cocis.2011.11.002.

(453) Nogales, A.; Fluerasu, A. X-Ray Photon Correlation Spectroscopy for the Study of Polymer Dynamics. *Eur. Polym. J.* **2016**, *81*, 494–504, DOI: 10.1016/j.eurpolymj.2016.03.032.

(454) Ruta, B.; Czakkel, O.; Chushkin, Y.; Pignon, F.; Nervo, R.; Zontone, F.; Rinaudo, M. Silica Nanoparticles as Tracers of the Gelation Dynamics of a Natural Biopolymer Physical Gel. *Soft*

Matter **2014**, *10*, 4547–4554, DOI: 10.1039/c4sm00704b.

(455) Czakkel, O.; Madsen, A. Evolution of dynamics and structure during formation of a cross-linked polymer gel. *EPL* **2011**, *95*, 28001, DOI: 10.1209/0295-5075/95/28001.

(456) Guo, H. Y.; Bourret, G.; Lennox, R. B.; Sutton, M.; Harden, J. L.; Leheny, R. L. Entanglement-Controlled Subdiffusion of Nanoparticles within Concentrated Polymer Solutions. *Phys. Rev. Lett.* **2012**, *109*, 055901, DOI: 10.1103/PhysRevLett.109.055901.

(457) Grein-Iankovski, A.; Riegel-Vidotti, I. C.; Simas-Tosin, F. F.; Narayanan, S.; Leheny, R. L.; Sandy, A. R. Exploring the Relationship between Nanoscale Dynamics and Macroscopic Rheology in Natural Polymer Gums. *Soft Matter* **2016**, *12*, 9321–9329, DOI: 10.1039/c6sm01492e.

(458) Papagiannopoulos, A.; Waigh, T. A.; Fluerasu, A.; Fernyhough, C.; Madsen, A. Microrheology of Polymeric Solutions Using X-Ray Photon Correlation Spectroscopy. *J. Phys.: Condens. Matter* **2005**, *17*, L279–L285, DOI: 10.1088/0953-8984/17/25/L06.

(459) Huang, J.; Yan, B.; Faghihnejad, A.; Xu, H. L.; Zeng, H. B. Understanding Nanorheology and Surface Forces of Confined Thin Films. *Korea-Aust. Rheol. J.* **2014**, *26*, 3–14, DOI: 10.1007/s13367-014-0002-8.

(460) Hess, M.; Roeben, E.; Habicht, A.; Seiffert, S.; Schmidt, A. M. Local Dynamics in Supramolecular Polymer Networks Probed by Magnetic Particle Nanorheology. *Soft Matter* **2019**, *15*, 842–850, DOI: 10.1039/c8sm01802b.

(461) Li, T. D.; Chiu, H. C.; Ortiz-Young, D.; Riedo, E. Nanorheology by Atomic Force Microscopy. *Rev. Sci. Instrum.* **2014**, *85*, 123707, DOI: 10.1063/1.4903353.

(462) Garcia, P. D.; Guerrero, C. R.; Garcia, R. Nanorheology of Living Cells Measured by AFM-Based Force–Distance Curves. *Nanoscale* **2020**, *12*, 9133–9143, DOI: 10.1039/c9nr10316c.

(463) Hess, M.; Roeben, E.; Rochels, P.; Zylla, M.; Webers, S.; Wende, H.; Schmidt, A. M. Size Effects on Rotational Particle Diffusion in Complex Fluids as Probed by Magnetic Particle Nanorheology. *Phys. Chem. Chem. Phys.* **2019**, *21*, 26525–26539, DOI: 10.1039/c9cp04083h.

(464) Ge, T.; Grest, G. S.; Rubinstein, M. Nanorheology of Entangled Polymer Melts. *Phys. Rev. Lett.* **2018**, *120*, 057801, DOI: 10.1103/PhysRevLett.120.057801.

(465) Rabin, Y.; Grosberg, A. Y. Nanorheology of Polymer Solutions: A Scaling Theory. *Macromolecules* **2019**, *52*, 6927–6934, DOI: 10.1021/acs.macromol.9b01272.

(466) Roeben, E.; Roeder, L.; Teusch, S.; Effertz, M.; Deiters, U. K.; Schmidt, A. M. Magnetic Particle Nanorheology. *Colloid Polym. Sci.* **2014**, *292*, 2013–2023, DOI: 10.1007/s00396-014-3289-6.

(467) Weber, H. W.; Kimmich, R. Anomalous Segment Diffusion in Polymers and NMR Relaxation Spectroscopy. *Macromolecules* **1993**, *26*, 2597–2606, DOI: 10.1021/ma00062a031.

(468) Kimmich, R.; Gille, K.; Fatkullin, N.; Seitter, R.; Hafner, S.; Muller, M. Field-Cycling Nuclear Magnetic Resonance Relaxometry of Thermoreversible Polybutadiene Networks. *J. Chem. Phys.* **1997**, *107*, 5973–5978, DOI: 10.1063/1.474322.

(469) Martini, F.; Carignani, E.; Nardelli, F.; Rossi, E.; Borsacchi, S.; Cettolin, M.; Susanna, A.; Geppi, M.; Caluci, L. Glassy and Polymer Dynamics of Elastomers

by ^{1}H Field-Cycling NMR Relaxometry: Effects of Cross-Linking. *Macromolecules* **2020**, *53*, 10028–10039, DOI: 10.1021/acs.macromol.0c01439.

(470) Kariyo, S.; Stapf, S. Influence of Cross-Link Density and Deformation on the NMR Relaxation Dispersion of Natural Rubber. *Macromolecules* **2002**, *35*, 9253–9255, DOI: 10.1021/ma025632f.

(471) Kariyo, S.; Stapf, S. NMR Relaxation Dispersion of Vulcanized Natural Rubber. *Solid State Nucl. Magn. Reson.* **2004**, *25*, 64–71, DOI: 10.1016/j.ssnmr.2003.03.011.

(472) Fleischer, G.; Fujara, F. In *NMR—Basic Principles and Progress*; Kosfeld, R., Blümich, B., Eds.; Springer: Berlin, 1993; Vol. 1.

(473) Appel, M.; Fleischer, G. Investigation of the Chain-Length Dependence of Self-Diffusion of Poly(Dimethylsiloxane) and Poly(Ethylene Oxide) in the Melt with Pulsed-Field Gradient NMR. *Macromolecules* **1993**, *26*, 5520–5525, DOI: 10.1021/ma00072a033.

(474) Gorecki, W.; Jeannin, M.; Belorizky, E.; Roux, C.; Armand, M. Physical-Properties of Solid Polymer Electrolyte Peo(Litfsi) Complexes. *J. Phys.: Condens. Matter* **1995**, *7*, 6823–6832, DOI: 10.1088/0953-8984/7/34/007.

(475) Timachova, K.; Watanabe, H.; Balsara, N. P. Effect of Molecular Weight and Salt Concentration on Ion Transport and the Transference Number in Polymer Electrolytes. *Macromolecules* **2015**, *48*, 7882–7888, DOI: 10.1021/acs.macromol.5b01724.

(476) Arumugam, S.; Shi, J.; Tunstall, D. P.; Vincent, C. A. Cation and Anion Diffusion-Coefficients in a Solid Polymer Electrolyte Measured by Pulsed-Field-Gradient Nuclear-Magnetic-Resonance. *J. Phys.: Condens. Matter* **1993**, *5*, 153–160, DOI: 10.1088/0953-8984/5/2/003.

(477) Xiao, W. C.; Yang, Q.; Zhu, S. L. Comparing Ion Transport in Ionic Liquids and Polymerized Ionic Liquids. *Sci. Rep.* **2020**, *10*, DOI: 10.1038/s41598-020-64689-8.

(478) Bernin, D.; Goudappel, G. J.; van Ruijven, M.; Altskar, A.; Strom, A.; Rudemo, M.; Hermansson, A. M.; Nyden, M. Microstructure of Polymer Hydrogels studied by Pulsed-Field-Gradient NMR Diffusion and TEM Methods. *Soft Matter* **2011**, *7*, 5711–5716, DOI: 10.1039/c1sm05070b.

(479) Schauser, N. S.; Sanoja, G. E.; Bartels, J. M.; Jain, S. K.; Hu, J. G.; Han, S. I.; Walker, L. M.; Helgeson, M. E.; Seshadri, R.; Segalman, R. A. Decoupling Bulk Mechanics and Mono- and Multivalent Ion Transport in Polymers Based on Metal–Ligand Coordination. *Chem. Mater.* **2018**, *30*, 5759–5769, DOI: 10.1021/acs.chemmater.8b02633.

(480) Johnson, C. S. Diffusion Ordered Nuclear Magnetic Resonance Spectroscopy: Principles and Applications. *Prog. Nucl. Magn. Reson. Spectrosc.* **1999**, *34*, 203–256, DOI: 10.1016/S0079-6565(99)00003-5.

(481) Li, W. B.; Chung, H. Y.; Daeffler, C.; Johnson, J. A.; Grubbs, R. H. Application of H-1 DOSY for Facile Measurement of Polymer Molecular Weights. *Macromolecules* **2012**, *45*, 9595–9603, DOI: 10.1021/ma301666x.

(482) Vieville, J.; Tanty, M.; Delsuc, M. A. Polydispersity Index of Polymers revealed by DOSY NMR. *J. Magn. Reson.* **2011**, *212*, 169–173, DOI: 10.1016/j.jmr.2011.06.020.

(483) Gu, K. C.; Onorato, J.; Xiao, S. S. Y. S.; Luscombe, C. K.; Loo, Y. L.

Determination of the Molecular Weight of Conjugated Polymers with Diffusion-Ordered NMR Spectroscopy. *Chem. Mater.* **2018**, *30*, 570–576, DOI: 10.1021/acs.chemmater.7b05063.

(484) Kamiguchi, K.; Kuroki, S.; Satoh, M.; Ando, I. Diffusion of Probe Polystyrenes with Different Molecular Weights in Poly(methyl methacrylate) Gels and Inhomogeneity of the Network Structure as Studied by Time-Dependent Diffusion NMR Spectroscopy. *Polymer* **2005**, *46*, 11470–11475, DOI: 10.1016/j.polymer.2005.10.045.

(485) Gosecka, M.; Gosecki, M.; Kazmierski, S. DOSY NMR as a Tool for Predicting Optimal Conditions for Hydrogel Formation: The Case of a Hyperbranched Polyglycidol Cross-linked with Boronic Acids. *J. Polym. Sci., Part B: Polym. Phys.* **2016**, *54*, 2171–2178, DOI: 10.1002/polb.24126.

(486) Nonappa,; Saman, D.; Kolehmainen, E. Studies on Supramolecular Gel Formation using DOSY NMR. *Magn. Reson. Chem.* **2015**, *53*, 256–260, DOI: 10.1002/mrc.4185.

(487) Wiesner, B.; Kohn, B.; Mende, M.; Scheler, U. Polymer Chain Mobility under Shear—A Rheo-NMR Investigation. *Polymers* **2018**, *10*, DOI: 10.3390/polym10111231.

(488) Ratzsch, K. F.; Friedrich, C.; Wilhelm, M. Low-Field Rheo-NMR: A Novel Combination of NMR Relaxometry with High End Shear Rheology. *J. Rheol.* **2017**, *61*, 905–917, DOI: 10.1122/1.4991513.

(489) Rantzsch, V.; Ratzsch, K. F.; Guthausen, G.; Schlabach, S.; Wilhelm, M. Molecular Dynamics of Polymer Composites Using Rheology and Combined RheoNMR on the Example of TiO2-Filled Poly(n-Alkyl Methacrylates) and Trans-1,4-Polyisoprene. *Soft Mater.* **2014**, *12*, S4–S13, DOI: 10.1080/1539445x.2014.930045.

(490) Callaghan, P. T.; Gil, A. M. *Magnetic Resonance in Food Science*; 2001; pp 29–42, DOI: 10.1039/9781847551252-00029.

(491) Roe, R. J. *Methods of X-Ray and Neutron Scattering in Polymer Science*; Topics in Polymer Science; Oxford University Press: New York, 2000.

(492) Mezei, F. Neutron Spin-Echo—New Concept in Polarized Thermal-Neutron Techniques. *Z. Phys.* **1972**, *255*, 146–160, DOI: 10.1007/Bf01394523.

(493) Rao, A.; Yao, H.; Olsen, B. D. Regimes of Anomalous Diffusion in Associative Protein Hydrogels. *Submitted* **2020**,

(494) Richter, D.; Butera, R.; Fetters, L. J.; Huang, J. S.; Farago, B.; Ewen, B. Entanglement Constraints in Polymer Melts—a Neutron Spin-Echo Study. *Macromolecules* **1992**, *25*, 6156–6164, DOI: 10.1021/ma00049a011.

(495) Wischnewski, A.; Monkenbusch, M.; Willner, L.; Richter, D.; Likhtman, A. E.; McLeish, T. C. B.; Farago, B. Molecular Observation of Contour-Length Fluctuations Limiting Topological Confinement in Polymer Melts. *Phys. Rev. Lett.* **2002**, *88*, 058301, DOI: 10.1103/PhysRevLett.88.058301.

(496) Richter, D. Neutron Spin-Echo for the Exploration of Large Scale Macromolecular Dynamics. *J. Phys. Soc. Jpn.* **2006**, *75*, 111004, DOI: 10.1143/Jpsj.75.111004.

(497) Richter, D.; Farago, B.; Ewen, B.; Oeser, R. The Fluctuations of Cross-Links in a Rubber—a Neutron Spin-Echo Study. *Physica B* **1989**, *156*, 426–429, DOI: 10.1016/0921-4526(89)90696-0.

(498) Oeser, R.; Ewen, B.; Richter, D.; Farago, B. Dynamic Fluctuations of Crosslinks in a Rubber—a Neutron-Spin-Echo Study. *Phys. Rev. Lett.* **1988**, *60*, 1041–1044, DOI: 10.1103/PhysRevLett.60.1041.

(499) Holler, S.; Moreno, A. J.; Zamponi, M.; Bacova, P.; Willner, L.; Iatrou, H.; Falus, P.; Richtert, D. The Role of the Functionality in the Branch Point Motion in Symmetric Star Polymers: A Combined Study by Simulations and Neutron Spin Echo Spectroscopy. *Macromolecules* **2018**, *51*, 242–253, DOI: 10.1021/acs.macromol.7b01579.

(500) Lee, S.; Tirumala, V. R.; Nagao, M.; Tominaga, T.; Lin, E. K.; Gong, J. P.; Wu, W. L. Dynamics in Multicomponent Polyelectrolyte Solutions. *Macromolecules* **2009**, *42*, 1293–1299, DOI: 10.1021/ma802217m.

(501) Sakai, T.; Matsunaga, T.; Yamamoto, Y.; Ito, C.; Yoshida, R.; Suzuki, S.; Sasaki, N.; Shibayama, M.; Chung, U. I. Design and Fabrication of a High-Strength Hydrogel with Ideally Homogeneous Network Structure from Tetrahedron-like Macromonomers. *Macromolecules* **2008**, *41*, 5379–5384, DOI: 10.1021/ma800476x.

(502) Kawecki, M.; Adlmann, F. A.; Gutfreund, P.; Falus, P.; Uhrig, D.; Gupta, S.; Farago, B.; Zolnierczuk, P.; Cochran, M.; Wolff, M. Direct Measurement of Topological Interactions in Polymers under Shear using Neutron Spin-Echo Spectroscopy. *Sci. Rep.* **2019**, *9*, 2823, DOI: 10.1038/s41598-019-39437-2.

(503) Lodge, T.; Chapman, B. Applications of Forced Rayleigh Scattering to Diffusion in Polymeric Fluids. *Trends Polym. Sci.* **1997**, *5*, 122–128.

(504) Schartl, W. *Soft Matter Characterization*; 2008; pp 678–701.

(505) Wesson, J. A.; Takezoe, H.; Yu, H.; Chen, S. P. Dye Diffusion in Swollen Gels by Forced Rayleigh-Scattering. *J. Appl. Phys.* **1982**, *53*, 6513–6519, DOI: 10.1063/1.330077.

(506) Antonietti, M.; Sillescu, H. Self-Diffusion of Polystyrene Chains in Networks. *Macromolecules* **1985**, *18*, 1162–1166, DOI: 10.1021/ma00148a021.

(507) Dalvi, M. C.; Lodge, T. P. Parallel and Perpendicular Chain Diffusion in a Lamellar Block Copolymer. *Macromolecules* **1993**, *26*, 859–861, DOI: 10.1021/ma00056a046.

(508) Urbach, W.; Hervet, H.; Rondelez, F. On the Application of Forced Rayleigh Light Scattering to Mass Diffusion Measurements. *J. Chem. Phys.* **1985**, *83*, 1877–1887, DOI: 10.1063/1.449853.

(509) Wang, M. Dynamics of Rod-Coil Block Copolymers. Thesis, 2015.

(510) Tang, S. Dynamics and Mechanics of Associating Polymer Networks. Thesis, 2016.

(511) Tang, S. C.; Wang, M. Z.; Olsen, B. D. Anomalous Self-Diffusion and Sticky Rouse Dynamics in Associative Protein Hydrogels. *J. Am. Chem. Soc.* **2015**, *137*, 3946–3957, DOI: 10.1021/jacs.5b00722.

(512) Tang, S. C.; Habicht, A.; Li, S. L.; Seiffert, S.; Olsen, B. D. Self-Diffusion of Associating Star-Shaped Polymers. *Macromolecules* **2016**, *49*, 5599–5608, DOI: 10.1021/acs.macromol.6b00959.

(513) Ramirez, J.; Dursch, T. J.; Olsen, B. D. A Molecular Explanation for Anomalous Diffusion in Supramolecular Polymer Networks. *Macromolecules* **2018**, *51*, 2517–2525, DOI: 10.1021/acs.macromol.7b02465.

(514) Hedvig, P. *Dielectric Spectroscopy of Polymers*; Wiley: New York, 1977; p 430.

(515) Havriliak, S.; Negami, S. A Complex Plane Representation of Dielectric and Mechanical Relaxation Processes in Some Polymers. *Polymer* **1967**, *8*, 161–210, DOI: 10.1016/0032-3861(67)90021-3.

(516) Linares, A.; Nogales, A.; Sanz, A.; Ezquerra, T. A.; Pieruccini, M. Restricted Dynamics in Oriented Semicrystalline Polymers: Poly(vinilydene fluoride). *Phys. Rev. E* **2010**, *82*, DOI: 10.1103/PhysRevE.82.031802.

(517) Kremer, F.; Schönhals, A. *Broadband Dielectric Spectroscopy*; Springer: Berlin, 2003; p 729.

(518) Kannurpatti, A. R.; Bowman, C. N. Structural Evolution of Dimethacrylate Networks Studied by Dielectric Spectroscopy. *Macromolecules* **1998**, *31*, 3311–3316, DOI: 10.1021/ma970721r.

(519) Fitz, B. D.; Mijovic, J. Segmental Dynamics and Density Fluctuations in Polymer Networks During Chemical Vitrification. *Macromolecules* **1999**, *32*, 4134–4140, DOI: 10.1021/ma981435y.

(520) Karabanova, L.; Pissis, P.; Kanapitsas, A.; Lutsyk, E. Thermodynamic State, Temperature Transitions, and Broadband Dielectric Relaxation Behavior in Gradient Interpenetrating Polymer Networks. *J. Appl. Polym. Sci.* **1998**, *68*, 161–171, DOI: 10.1002/(SICI)1097-4628(19980404)68.

(521) Fitz, B. D.; Mijovic, J. Segmental Dynamics in Poly(methylphenylsiloxane) Networks by Dielectric Relaxation Spectroscopy. *Macromolecules* **1999**, *32*, 3518–3527, DOI: 10.1021/ma981937b.

(522) Kalakkunnath, S.; Kalika, D. S.; Lin, H. Q.; Raharjo, R. D.; Freeman, B. D. Molecular Dynamics of Poly(ethylene glycol) and Poly(propylene glycol) Copolymer Networks by Broadband Dielectric Spectroscopy. *Macromolecules* **2007**, *40*, 2773–2781, DOI: 10.1021/ma070016a.

(523) Hernandez, M.; Grande, A. M.; van der Zwaag, S.; Garcia, S. J. Monitoring Network and Interfacial Healing Processes by Broadband Dielectric Spectroscopy: A Case Study on Natural Rubber. *ACS Appl. Mater. Interfaces* **2016**, *8*, 10647–10656, DOI: 10.1021/acsami.6b02259.

(524) Carretero-Gonzalez, J.; Retsos, H.; Verdejo, R.; Toki, S.; Hsiao, B. S.; Giannelis, E. P.; Lopez-Manchado, M. A. Effect of Nanoclay on Natural Rubber Microstructure. *Macromolecules* **2008**, *41*, 6763–6772, DOI: 10.1021/ma800893x.

(525) Hernandez, M.; Valentin, J. L.; Lopez-Manchado, M. A.; Ezquerra, T. A. Influence of the Vulcanization System on the Dynamics and Structure of Natural Rubber: Comparative Study by Means of Broadband Dielectric Spectroscopy and Solid-State NMR Spectroscopy. *Eur. Polym. J.* **2015**, *68*, 90–103, DOI: 10.1016/j.eurpolymj.2015.04.021.

(526) Carretero-Gonzalez, J.; Ezquerra, T. A.; Amnuaypornsri, S.; Toki, S.; Verdejo, R.; Sanz, A.; Sakdapipanich, J.; Hsiao, B. S.; Lopez-Manchado, M. A. Molecular Dynamics of Natural Rubber as Revealed by Dielectric Spectroscopy: The Role of Natural Cross-Linking. *Soft Matter* **2010**, *6*, 3636–3642, DOI: 10.1039/c003087b.

(527) Hernandez, M.; Ezquerra, T. A.; Verdejo, R.; Lopez-Manchado, M. A. Role of Vulcanizing Additives on the Segmental Dynamics of Natural Rubber. *Macromolecules* **2012**, *45*, 1070–1075, DOI: 10.1021/ma202325k.

(528) Liu, J.; Wu, S. W.; Tang, Z. H.; Lin, T. F.; Guo, B. C.; Huang, G. S. New Evidence Disclosed for Networking in Natural Rubber by Dielectric Relaxation Spectroscopy. *Soft Matter* **2015**, *11*, 2290–2299, DOI: 10.1039/c4sm02521k.

(529) Runt, J. P.; Fitzgerald, J. J. *Dielectric Spectroscopy of Polymeric Materials : Fundamentals and Applications*; American Chemical Society: Washington, DC, 1997; p 461.

(530) Bratton, A. F.; Kim, S. S.; Ellison, C. J.; Miller, K. M. Thermomechanical and Conductive Properties of Thiol-Ene Poly(ionic liquid) Networks Containing Backbone and Pendant lmidazolium Groups. *Ind. Eng. Chem. Res.* **2018**, *57*, 16526–16536, DOI: 10.1021/acs.iecr.8b04720.

(531) Bartels, J.; Sanoja, G. E.; Evans, C. M.; Segalman, R. A.; Helgeson, M. E. Decoupling Mechanical and Conductive Dynamics of Polymeric Ionic Liquids via a Trivalent Anion Additive. *Macromolecules* **2017**, *50*, 8979–8987, DOI: 10.1021/acs.macromol.7b01351.

(532) Sanoja, G. E.; Schauser, N. S.; Bartels, J. M.; Evans, C. M.; Helgeson, M. E.; Seshadri, R.; Segalman, R. A. Ion Transport in Dynamic Polymer Networks Based on Metal-Ligand Coordination: Effect of Cross-Linker Concentration. *Macromolecules* **2018**, *51*, 2017–2026, DOI: 10.1021/acs.macromol.7b02141.

(533) Schauser, N. S.; Grzetic, D. J.; Tabassum, T.; Kliegle, G. A.; Le, M. L.; Susca, E. M.; Antoine, S.; Keller, T. J.; Delaney, K. T.; Han, S.; Seshadri, R.; Fredrickson, G. H.; Segalman, R. A. The Role of Backbone Polarity on Aggregation and Conduction of Ions in Polymer Electrolytes. *J. Am. Chem. Soc.* **2020**, *142*, 7055–7065, DOI: 10.1021/jacs.0c00587.

(534) Jones, S. D.; Schauser, N. S.; Fredrickson, G. H.; Segalman, R. A. The Role of Polymer–Ion Interaction Strength on the Viscoelasticity and Conductivity of Solvent-Free Polymer Electrolytes. *Macromolecules* **2020**, DOI: 10.1021/acs.macromol.0c02233.

(535) Frenkel, D.; Smit, B. *Understanding Molecular Simulation: from Algorithms to Applications*; Academic Press: San Diego, 1996; p 443.

(536) Binder, K. *Monte Carlo and Molecular Dynamics Simulations in Polymer Sciences*; Oxford University Press: New York, 1995; p 587.

(537) Tamai, Y.; Tanaka, H.; Nakanishi, K. Molecular Dynamics Study of Polymer–Water Interaction in Hydrogels .I. Hydrogen-Bond Structure. *Macromolecules* **1996**, *29*, 6750–6760, DOI: 10.1021/ma951635z.

(538) Pavlov, A. S.; Khalatur, P. G. Filler Reinforcement in Cross-Linked Elastomer Nanocomposites: Insights from Fully-Atomistic Molecular-Dynamics Simulation. *Soft Matter* **2016**, *12*, 5402–5419, DOI: 10.1039/c6sm00543h.

(539) Kallivokas, S. V.; Sgouros, A. P.; Theodorou, D. N. Molecular Dynamics Simulations of EPON-862/DETDA Epoxy Networks: Structure, Topology, Elastic Constants, and Local Dynamics. *Soft Matter* **2019**, *15*, 721–733, DOI: 10.1039/c8sm02071j.

(540) Heine, D. R.; Grest, G. S.; Lorenz, C. D.; Tsige, M.; Stevens, M. J. Atomistic Simulations of End-Linked Poly(dimethylsiloxane) Networks: Structure and Relaxation. *Macromolecules* **2004**, *37*, 3857–3864, DOI: 10.1021/ma035760j.

(541) Grest, G. S.; Kremer, K. Molecular-Dynamics Simulation for Polymers in the Presence of a Heat Bath. *Phys. Rev. A* **1986**, *33*, 3628–3631, DOI: 10.1103/PhysRevA.33.3628.

(542) Kremer, K.; Grest, G. S. Dynamics of Entangled Linear Polymer Melts—a Molecular-Dynamics Simulation. *J. Chem. Phys.* **1990**, *92*, 5057–5086, DOI: 10.1063/1.458541.

(543) Everaers, R.; Karimi-Varzaneh, H. A.; Fleck, F.; Hojdis, N.; Svaneborg, C. Kremer–Grest Models for Commodity Polymer Melts: Linking Theory, Experiment, and Simulation at the Kuhn Scale. *Macromolecules* **2020**, *53*, 1901–1916, DOI: 10.1021/acs.macromol.9b02428.

(544) Jang, S. S.; Goddard, W. A.; Kalani, M. Y. S. Mechanical and Transport Properties of the Poly(ethylene oxide)-Poly(acrylic acid) Double Network Hydrogel from Molecular Dynamic Simulations. *J. Phys. Chem. B* **2007**, *111*, 1729–1737, DOI: 10.1021/jp0656330.

(545) Everaers, R. Entanglement Effects in Defect-Free Model Polymer Networks. *New J. Phys.* **1999**, *1*, DOI: 10.1088/1367-2630/1/1/312.

(546) Grest, G. S.; Kremer, K. Statistical Properties of Random Cross-Linked Rubbers. *Macromolecules* **1990**, *23*, 4994–5000, DOI: 10.1021/ma00225a020.

(547) Auhl, R.; Everaers, R.; Grest, G. S.; Kremer, K.; Plimpton, S. J. Equilibration of Long Chain Polymer Melts in Computer Simulations. *J. Chem. Phys.* **2003**, *119*, 12718–12728, DOI: 10.1063/1.1628670.

(548) Ahlrichs, P.; Everaers, R.; Dunweg, B. Screening of Hydrodynamic Interactions in Semidilute Polymer Solutions: A Computer Simulation Study. *Phys. Rev. E* **2001**, *64*, 040501, DOI: 10.1103/PhysRevE.64.040501.

(549) Uchidaa, N.; Grest, G. S.; Everaers, R. Viscoelasticity and Primitive Path Analysis of Entangled Polymer Liquids: From F-Actin to Polyethylene. *J. Chem. Phys.* **2008**, *128*, 044902, DOI: 10.1063/1.2825597.

(550) Duering, E. R.; Kremer, K.; Grest, G. S. Structure and Relaxation of End-Linked Polymer Networks. *J. Chem. Phys.* **1994**, *101*, 8169–8192, DOI: 10.1063/1.468202.

(551) Torres-Knoop, A.; Kryven, I.; Schamboeck, V.; Iedema, P. D. Modeling the Free-Radical Polymerization of Hexanediol Diacrylate (HDDA): a Molecular Dynamics and Graph Theory Approach. *Soft Matter* **2018**, *14*, 3404–3414, DOI: 10.1039/c8sm00451j.

(552) Hosono, N.; Masubuchi, Y.; Furukawa, H.; Watanabe, T. A Molecular Dynamics Simulation Study on Polymer Networks of End-Linked Flexible or Rigid Chains. *J. Chem. Phys.* **2007**, *127*, DOI: 10.1063/1.2790007.

(553) Adhikari, R.; Makarov, D. E. Mechanochemical Kinetics in Elastomeric Polymer Networks: Heterogeneity of Local Forces Results in Non-Exponential Kinetics. *J. Phys. Chem. B* **2017**, *121*, 2359–2365, DOI: 10.1021/acs.jpcb.6b12758.

(554) Higuchi, Y.; Saito, K.; Sakai, T.; Gong, J. P.; Kubo, M. Fracture Process of Double-Network Gels by Coarse-Grained Molecular Dynamics Simulation. *Macromolecules* **2018**, *51*, 3075–3087, DOI: 10.1021/acs.macromol.8b00124.

(555) Triandafilidi, V.; Hatzikiriakos, S. G.; Rottler, J. Poisson–Boltzmann Modeling and Molecular Dynamics Simulations of Polyelectrolyte Gel Diodes in the Static Regime. *Soft Matter* **2020**, *16*, 1091–1101, DOI: 10.1039/c9sm02232e.

(556) Escobedo, F. A.; de Pablo, J. J. Molecular Simulation of Polymeric Networks and Gels: Phase Behavior and Swelling. *Phys. Rep.* **1999**, *318*, 86–112, DOI: 10.1016/S0370-1573(99)00012-5.

(557) Svaneborg, C.; Grest, G. S.; Everaers, R. Strain-Dependent Localization, Microscopic Deformations, and Macroscopic Normal Tensions in Model Polymer Networks. *Phys. Rev. Lett.* **2004**, *93*, 257801, DOI: 10.1103/PhysRevLett.93.257801.

(558) Rottach, D. R.; Curro, J. G.; Budzien, J.; Grest, G. S.; Svaneborg, C.; Everaers, R. Permanent Set of Cross-Linking Networks: Comparison of Theory with Molecular Dynamics Simulations. *Macromolecules* **2006**, *39*, 5521–5530, DOI: 10.1021/ma060767x.

(559) Grest, G. S.; Kremer, K.; Duering, E. R. Kinetics and Relaxation of End Cross-Linked Polymer Networks. *Phys. A* **1993**, *194*, 330–337, DOI: 10.1016/0378-4371(93)90366-C.

(560) Duering, E. R.; Kremer, K.; Grest, G. S. Dynamics of Model Networks — the Role of the Melt Entanglement Length. *Macromolecules* **1993**, *26*, 3241–3244, DOI: 10.1021/ma00064a045.

(561) Zidek, J.; Milchev, A.; Jancar, J.; Vilgis, T. A. Deformation-Induced Damage and Recovery in Model Hydrogels — A Molecular Dynamics Simulation. *J. Mech. Phys. Solids* **2016**, *94*, 372–387, DOI: 10.1016/j.jmps.2016.05.013.

(562) Gartner, T. E.; Jayaraman, A. Modeling and Simulations of Polymers: A Roadmap. *Macromolecules* **2019**, *52*, 755–786, DOI: 10.1021/acs.macromol.8b01836.

(563) Sides, S. W.; Grest, G. S.; Stevens, M. J.; Plimpton, S. J. Effect of End-Tethered Polymers on Surface Adhesion of Glassy Polymers. *J. Polym. Sci., Part B: Polym. Phys.* **2004**, *42*, 199–208, DOI: 10.1002/polb.10672.

(564) Svaneborg, C.; Karimi-Varzaneh, H. A.; Hojdis, N.; Fleck, F.; Everaers, R. Multiscale Approach to Equilibrating Model Polymer Melts. *Phys. Rev. E* **2016**, *94*, DOI: 10.1103/PhysRevE.94.032502.

(565) Escobedo, F. A.; de Pablo, J. J. Simulation and Theory of the Swelling of Athermal Gels. *J. Chem. Phys.* **1997**, *106*, 793–810, DOI: 10.1063/1.473166.

(566) Mann, B. A.; Kremer, K.; Holm, C. The Swelling Behavior of Charged Hydrogels. *Macromol. Symp.* **2006**, *237*, 90–107, DOI: 10.1002/masy.200650511.

(567) Schneider, S.; Linse, P. Swelling of Cross-Linked Polyelectrolyte Gels. *Eur. Phys. J. E: Soft Matter Biol. Phys.* **2002**, *8*, 457–460, DOI: 10.1140/epje/i2002-10043-y.

(568) Trautenberg, H. L.; Sommer, J. U.; Goritz, D. Structure and Swelling of End-Linked Model Networks. *J. Chem. Soc. Faraday Trans.* **1995**, *91*, 2649–2653, DOI: 10.1039/ft9959102649.

(569) Lang, M.; Muller, T. Analysis of the Gel Point of Polymer Model Networks by Computer Simulations. *Macromolecules* **2020**, *53*, 498–512, DOI: 10.1021/acs.macromol.9b02217.

(570) Leung, Y. K.; Eichinger, B. E. Computer-Simulation of End-Linked Elastomers .I. Trifunctional Networks Cured in the Bulk. *J. Chem. Phys.* **1984**, *80*, 3877–3884, DOI: 10.1063/1.447169.

(571) Thompson, A. P.; Plimpton, S. J.; Mattson, W. General Formulation of Pressure and Stress Tensor for Arbitrary Many-Body Interaction Potentials Under Periodic Boundary Conditions. *J. Chem. Phys.* **2009**, *131*, 154107, DOI: 10.1063/1.3245303.

(572) Svaneborg, C.; Grest, G. S.; Everaers, R. Disorder Effects on the Strain Response of Model Polymer Networks. *Polymer* **2005**, *46*, 4283–4295, DOI: 10.1016/j.polymer.2005.03.008.

(573) Harmandaris, V. A.; Mavrantzas, V. G.; Theodorou, D. N. Atomistic Molecular Dynamics Simulation of Stress Relaxation upon Cessation of Steady-State Uniaxial Elongational Flow. *Macromolecules* **2000**, *33*, 8062–8076, DOI: 10.1021/ma9918598.

(574) Lee, W. B.; Kremer, K. Entangled Polymer Melts: Relation between Plateau Modulus and Stress Autocorrelation Function. *Macromolecules* **2009**, *42*, 6270–6276, DOI: 10.1021/ma9008498.

(575) Allen, M. P.; Tildesley, D. J. *Computer Simulation of Liquids*; Oxford Science publications; Oxford University Press: Oxford, 2017; p 385.

(576) Kamerlin, N.; Elvingson, C. Tracer Diffusion in a Polymer Gel: Simulations of Static and Dynamic 3D Networks Using Spherical Boundary Conditions. *J. Phys.: Condens. Matter* **2016**, *28*, 475101, DOI: 10.1088/0953-8984/28/47/475101.

(577) Netz, P. A.; Dorfmuller, T. Computer-Simulation Studies of Anomalous Diffusion in Gels — Structural-Properties and Probe-Size Dependence. *J. Chem. Phys.* **1995**, *103*, 9074–9082, DOI: 10.1063/1.470018.

(578) Cai, L. H.; Panyukov, S.; Rubinstein, M. Hopping Diffusion of Nanoparticles in Polymer Matrices. *Macromolecules* **2015**, *48*, 847–862, DOI: 10.1021/ma501608x.

(579) Fredrickson, G. H. *The Equilibrium Theory of Inhomogeneous Polymers*; Oxford University Press, 2006.

(580) Delaney, K. T.; Fredrickson, G. H. Recent Developments in Fully Fluctuating Field-Theoretic Simulations of Polymer Melts and Solutions. *J. Phys. Chem. B* **2016**, *120*, 7615–34, DOI: 10.1021/acs.jpcb.6b05704.

(581) Lee, W. B.; Elliott, R.; Katsov, K.; Fredrickson, G. H. Phase Morphologies in Reversibly Bonding Supramolecular Triblock Copolymer Blends. *Macromolecules* **2007**, *40*, 8445–8454, DOI: 10.1021/ma071714y.

(582) Hoy, R. S.; Fredrickson, G. H. Thermoreversible Associating Polymer Networks. I. Interplay of Thermodynamics, Chemical Kinetics, and Polymer Physics. *J. Chem. Phys.* **2009**, *131*, 224902, DOI: 10.1063/1.3268777.

(583) Mohan, A.; Elliot, R.; Fredrickson, G. H. Field-Theoretic Model of Inhomogeneous Supramolecular Polymer Networks and Gels. *J. Chem. Phys.* **2010**, *133*, 174903, DOI: 10.1063/1.3497038.

(584) Mester, Z.; Mohan, A.; Fredrickson, G. H. Macro- and Microphase Separation in Multifunctional Supramolecular Polymer Networks. *Macromolecules* **2011**, *44*, 9411–9423, DOI: 10.1021/ma201551c.

(585) Schmid, F. Self-Consistent Field Approach for Cross-Linked Copolymer Materials. *Phys. Rev. Lett.* **2013**, *111*, DOI: 10.1103/PhysRevLett.111.028303.

(586) Man, X.; Delaney, K. T.; Villet, M. C.; Orland, H.; Fredrickson, G. H. Coherent States Formulation of Polymer Field Theory. *J. Chem. Phys.* **2014**, *140*, 024905, DOI: 10.1063/1.4860978.

(587) Fredrickson, G. H.; Delaney, K. T. Coherent States Field Theory in Supramolecular Polymer Physics. *J. Chem. Phys.* **2018**, *148*, 204904, DOI: 10.1063/1.5027582.

(588) Vigil, D. L.; Garcia-Cervera, C. J.; Delaney, K. T.; Fredrickson, G. H. Linear Scaling Self-Consistent Field Theory with Spectral Contour Accuracy. *ACS Macro Lett.* **2019**, *8*, DOI: 10.1021/acsmacrolett.9b00632.

(589) Tito, N. B.; Storm, C.; Ellenbroek, W. G. Self-Consistent Field Lattice Model for Polymer Networks. *Macromolecules* **2017**, *50*, 9788–9795, DOI: 10.1021/acs.macromol.7b01284.

(590) Yang, W.; Suo, Z.; Shih, C. F. Mechanics of Dynamic Debonding. *Proc. R. Soc. London, Ser. A* **1991**, *433*, 679–697, DOI: 10.1098/rspa.1991.0070.

(591) Sha, Y.; Hui, C. Y.; Ruina, A.; Kramer, E. J. Continuum and Discrete Modeling of Craze Failure at a Crack-Tip in a Glassy Polymer. *Macromolecules* **1995**, *28*, 2450–2459, DOI: 10.1021/ma00111a044.

(592) Hui, C. Y.; Muralidharan, V. Gel Mechanics: A Comparison of the Theories of Biot and Tanaka, Hocker, and Benedek. *J. Chem. Phys.* **2005**, *123*, 154905, DOI: 10.1063/1.2061987.

(593) Hong, W.; Zhao, X. H.; Zhou, J. X.; Suo, Z. G. A Theory of Coupled Diffusion and Large Deformation in Polymeric Gels. *J. Mech. Phys. Solids* **2008**, *56*, 1779–1793, DOI: 10.1016/j.jmps.2007.11.010.

(594) Kundu, S.; Crosby, A. J. Cavitation and Fracture Behavior of Polyacrylamide Hydrogels. *Soft Matter* **2009**, *5*, 3963–3968, DOI: 10.1039/b909237d.

(595) Zhang, J. P.; Zhao, X. H.; Suo, Z. G.; Jiang, H. Q. A Finite Element Method for Transient Analysis of Concurrent Large Deformation and Mass Transport in Gels. *J. Appl. Phys.* **2009**, *105*, 093522, DOI: 10.1063/1.3106628.

(596) Hong, W.; Zhao, X. H.; Suo, Z. G. Large Deformation and Electrochemistry of Polyelectrolyte Gels. *J. Mech. Phys. Solids* **2010**, *58*, 558–577, DOI: 10.1016/j.jmps.2010.01.005.

(597) Long, R.; Mayumi, K.; Creton, C.; Narita, T.; Hui, C. Y. Time Dependent Behavior of a Dual Cross-Link Self-Healing Gel: Theory and Experiments. *Macromolecules* **2014**, *47*, 7243–7250, DOI: 10.1021/ma501290h.

(598) Hui, C. Y.; Long, R. A Constitutive Model for the Large Deformation of a Self-Healing Gel. *Soft Matter* **2012**, *8*, 8209–8216, DOI: 10.1039/c2sm25367d.

(599) Bouklas, N.; Landis, C. M.; Huang, R. A Nonlinear, Transient Finite Element Method for Coupled Solvent Diffusion and Large Deformation of Hydrogels. *J. Mech. Phys. Solids* **2015**, *79*, 21–43, DOI: 10.1016/j.jmps.2015.03.004.

(600) Long, R.; Hui, C. Y. Crack Tip Fields in Soft Elastic Solids Subjected to Large Quasi-Static Deformation — A Review. *Extreme Mech. Lett.* **2015**, *4*, 131–155, DOI: 10.1016/j.eml.2015.06.002.

(601) Guo, J. Y.; Long, R.; Mayumi, K.; Hui, C. Y. Mechanics of a Dual Cross-Link Gel with Dynamic Bonds: Steady State Kinetics and Large Deformation Effects. *Macromolecules* **2016**, *49*, 3497–3507, DOI: 10.1021/acs.macromol.6b00421.

(602) Creton, C.; Ciccotti, M. Fracture and Adhesion of Soft Materials: a Review. *Rep. Prog. Phys.* **2016**, *79*, 046601, DOI: 10.1088/0034-4885/79/4/046601.

(603) Creton, C. 50th Anniversary Perspective: Networks and Gels: Soft but Dynamic and Tough. *Macromolecules* **2017**, *50*, 8297–8316, DOI: 10.1021/acs.macromol.7b01698.

(604) Liu, Z. Z.; Jagota, A.; Hui, C. Y. Modeling of Surface Mechanical Behaviors of Soft Elastic Solids: Theory and Examples. *Soft Matter* **2020**, *16*, 6875–6889, DOI: 10.1039/d0sm00556h.

(605) Jackson, N. E.; Webb, M. A.; de Pablo, J. J. Recent Advances in Machine Learning Towards Multiscale Soft Materials Design. *Curr. Opin. Chem. Eng.* **2019**, *23*, 106–114, DOI: 10.1016/j.coche.2019.03.005.

(606) de Pablo, J. J. et al. New Frontiers for the Materials Genome Initiative. *NPJ Comput. Mater.* **2019**, *5*, DOI: 10.1038/s41524-019-0173-4.

(607) Webb, M. A.; Jackson, N. E.; Gil, P. S.; de Pablo, J. J. Targeted Sequence Design within the Coarse-Grained Poly-

mer Genome. *Sci. Adv.* **2020**, *6*, DOI: 10.1126/sciadv.abc6216.

(608) Audus, D. J.; de Pablo, J. J. Polymer Informatics: Opportunities and Challenges. *ACS Macro Lett.* **2017**, *6*, 1078–1082, DOI: 10.1021/acsmacrolett.7b00228.

(609) Lin, T. S.; Coley, C. W.; Mochigase, H.; Beech, H. K.; Wang, W. C.; Wang, Z.; Woods, E.; Craig, S. L.; Johnson, J. A.; Kalow, J. A.; Jensen, K. F.; Olsen, B. D. BigSMILES: A Structurally-Based Line Notation for Describing Macromolecules. *ACS Cent. Sci.* **2019**, *5*, 1523–1531, DOI: 10.1021/acscentsci.9b00476.

For Table of Contents Only